Test of Thermobattrie heat storage module

Dannemand, Mark; Furbo, Simon

Publication date:
2014

Document Version
Publisher's PDF, also known as Version of record

Test of Thermobattrie heat storage module

Mark Dannemand
Simon Furbo

Report

Department of Civil Engineering
2014

DTU Civil Engineering-Report R 308 (UK)
April 2014

DTU Civil Engineering
Department of Civil Engineering

Contents

List of symbols: 3
1. Introduction 5
2. Method 7
2.1 Charge and discharge 7
2.2 Heat loss coefficient 7
2.3 Energy content 7
2.4 Heat exchange capacity rate 7
2.5 Heat of fusion 8
2.5.1 Compound theory 8
2.5.2 Incongruently melting theory 9
2.6 Theoretical properties of Thermobatterie: 12
2.6.1 Heat capacity 12
2.6.2 Heat loss coefficient 12
2.7 Measurements 14
2.7.1 Measurement equipment: 14
3. Results 15
3.1 Test with Water: 15
3.1.1 Test cycle 1 with water: 15
3.1.2 Summary of test with water 22
3.2 Tests with a sodium acetate water mixture 25
3.2.1 Measurement overview. 25
3.2.2 Test cycle 2: 27
3.2.3 Test cycle 9: 35
3.3 Summary and discussion of test with sodium acetate water mixture 44
4. Conclusion 50
5. References 52
6. Acknowledgement 52
7. Appendix A – Tests with water 53
8. Appendix B – Tests with sodium acetate water mixture 78

List of symbols:

C_{tank}: heat capacity of storage tank material excluding primary heat storage medium [kJ/K]

$C_{storage}$: heat capacity of storage tank including water [kJ/K]

C_{water}: heat capacity of water in storage [kJ/K]

C_{mat}: heat capacity of storage material [kJ/K]

C_p: Specific heat capacity [J/kgK]

d_y: outer diameter of storage tank including insulation [m]

E_{charge}: thermal energy charged to the storage [kJ]

$E_{discharge}$: thermal energy discharged from the storage [kJ]

E_{start}: heat/thermal energy content at start condition [kJ]

E_{end}: heat/thermal energy content at end condition [kJ]

E_{max}: heat content at maximum storage temperature. [kJ]

E_{super} : heat content at supercooled state. [kJ]

E(t): change in heat content for the time period *t* [kJ]

e_s: thickness of insulation on side [m]

e_t: thickness of insulation on top [m]

e_b: thickness of insulation on bottom [m]

H_{side}: heat loss coefficient from the side of the storage tank [W/Km]

H_{top}: heat loss coefficient from the top of the storage tank [W/K]

H_{bottom}: heat loss coefficient from the bottom of the storage tank [W/K]

H_{loss}: the total heat loss coefficient from the storage tank [W/K]

H: heat exchange capacity rate [W/K]

m: mass [kg]

Q_{charge}: charge power [W]

$Q_{discharge}$: discharge power [W]

T_{end}: end mean storage temperature [°C]

T_i: inlet temperature [°C]

T_o: outlet temperature [°C]

T_{max}: maximum mean storage temperature [°C]

T_{melt}: melting temperature of sodium acetate –water mixture [58°C]

T_{start}: start mean storage temperature [°C]

T_s: mean storage temperature [°C]

T_{amb}: ambient temperature [°C]

dT: temperature change [K]

t: time [hr]

V: volume flow rate [m^3/s]

ρ: density [kg/m^3]

k: thermal conductivity [W/mK]

L: latent heat of fusion [kJ/kg]

Sa(t): temperature dependent solubility of anhydrous salt in water [

Fsol(t): fraction of solid phase sodium acetate trihydrate in salt water mixture based on weight at temperature t. [-]

Subscript:

exp: experimental

theo: theoretical

incon: incongruent melting theory

com: compound theory

s: solid

l: liquid

1. Introduction

Tests were carried out on a “Thermobatterie” heat storage module developed by H.M. Heizkörper GmbH & Co. KG. The Thermobatterie is a thermal energy storage utilizing stable supercooling of a sodium acetate water mixture. The performance of the heat storage module has been evaluated based on laboratory tests where the storage module was connected to an electric heating unit for charging and a cooling unit for discharging the storage module.

The storage material used in the heat storage is the salt hydrate, sodium acetate trihydrate which has a melting temperature of 58°C. The relevant temperatures, when considering solar heating systems, domestic hot water preparation and space heating, is in the range from 10°C to 99°C. In this temperature range the sodium acetate trihydrate will be in solid or liquid state. The energy required to melt the material or change the phase from solid to liquid is known as the latent heat of fusion. The latent heat of fusion takes up a significant amount of energy when considering the relevant temperature interval. Furthermore the material has the ability to supercool. Supercooling is when a liquid material cools down below its melting temperature without solidifying, hence without releasing the latent heat of fusion. The supercooled salt hydrate can be stored at ambient temperature without further heat loss and can later solidify and release the latent heat of fusion. Letting melted sodium acetate trihydrate rest at ambient temperature in supercooled state makes long term heat storage possible.

The following investigations and measurements were carried on the “Thermobatterie” developed by H.M. Heizkörper. The tested model was with two inspection windows installed in the side of the tank. The inspection windows cause a thermal bridge in the insulation which was sought covered with additional insulation to reduce this additional heat loss from the tank. The test results of the model with inspection windows may deviate from the model without inspection windows.

Figure 1a and 1b. The Thermobatterie test setup and tank with inspection windows.

The Thermobatterie is a vertical cylindrical container made of stainless steel. The height of the stainless steel cylinder is 150 cm and the diameter 30 cm. A layer of EPP insulation covers the cylinder making the total height of the Thermobatterie without stand 160 cm and the diameter 38 cm. The Thermobatterie module contained approximately 116 kg of sodium acetate – water mixture. This leaves an air volume in the top of the tank of approximately 10% of the total volume. The water content was increased from 39.7% of the trihydrate composition to 43.5% in the tested sodium acetate water mixture to reduce the problem with phase separation of the incongruently melting salt hydrate by the extra water principle (Furbo, 1982). The heat exchanger consists of 16 stainless steel pipes located in a circular formation with thin aluminum plates attached to increase the heat transfer area. Manifolds are located on the top and bottom of the cylinder. The distance between the aluminum plates is approximately 0.5 - 1 cm. Pictures of the heat exchanger are shown in Fig. 2a and 2b. The module was heated and cooled with water as the heat transfer fluid. The flow direction was from bottom to top.

The main cylinder of the Thermobatterie was connected to a cylindrical expansion tank to reduce the pressure in the main module caused by the expansion of air and salt water mixture in the closed system when heating up the module. High pressure may cause deformation or moving parts inside the module that work as mechanical triggering of the supercooled salt water mixture, similar to the metallic disk trigger in the hand warmer heat packs, and therefore problems with the stability of the supercooling (Rogerson & Cardoso, 2003).

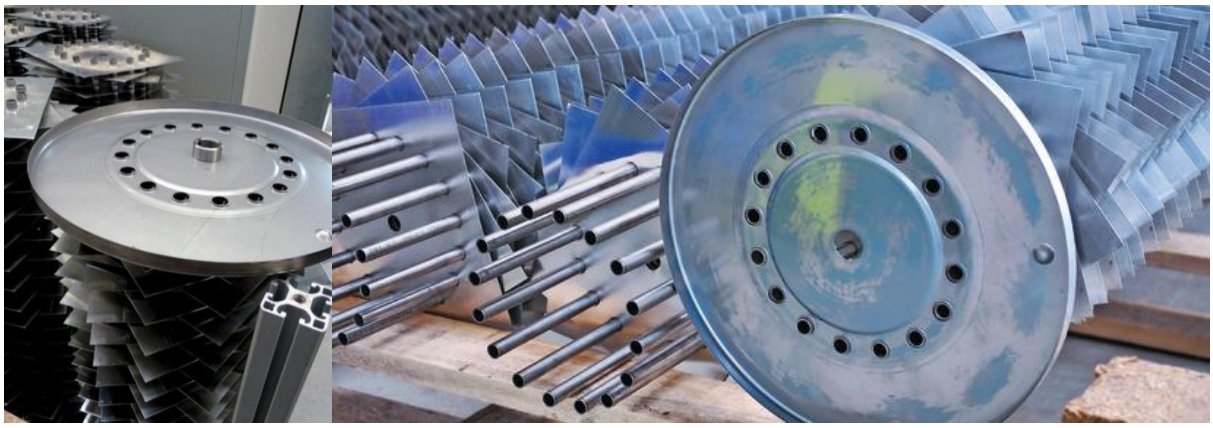

Figure 2a and 2b. Heat exchanger of Thermobatterie (source: www.industrieanzeiger.de, www.blechnet.com).

Test of the Thermobatterie was carried out in the heat storage testing facility of the Technical University of Denmark, Department of Civil Engineering.

2. Method

The following sections describe how relevant parameters, used to determine the performance of the storage were measured and calculated. When showing analyzed measurement results in figures values for power, heat exchange capacity rate and flow rate are averaged over a 5 to 9 minute period to avoid large fluctuations caused by measurement uncertainties and the hysteresis of the heating element.

2.1 Charge and discharge

The charge and discharge powers of the storage were determined by:

$$Q_{charge} = V \cdot C_p \cdot \rho \cdot (T_i - T_o)$$

$$Q_{discharge} = V \cdot C_p \cdot \rho \cdot (T_i - T_o)$$

where, T_i is the inlet temperature, T_o is the return temperature, V is the volume flow rate of the heat transfer fluid measured at the inlet, C_p is the specific heat capacity of the heat transfer fluid at mean temperature between T_i and T_o, ρ is the density of the heat transfer fluid at T_i.

During charge periods the power is considered as positive and for the discharge the power is considered as negative.

2.2 Heat loss coefficient

The heat loss coefficient of the storage was measured by heating the module to a stable temperature over a long period where no additional energy is stored in the heat storage. The energy balance of the system was used to determine the heat loss experimentally e.g. the energy added to the system is equal to the heat loss when the storage temperature is stable over a period. In this way a simplified heat loss coefficient with a constant value was determined. In reality the heat loss coefficient will be influenced by the temperature level of the storage and ambient.

$$H_{loss,exp} = Q_{charge}/(T_s - T_{amb})$$

Where T_s is the mean storage temperature and T_{amb} is the ambient temperature. The heat loss coefficient for the storage module is used when calculating energy content of the storage based on the measured data.

2.3 Energy content

The change of heat content in the storage module over a specific time period during a charge is determined by:

$$E(t) = \int_0^t Q_{charge} - H_{loss,exp} \cdot (T_s - T_{amb})dt$$

At the maximum storage temperature T_{max} the experimentally determined heat content of the storage is $E_{charge,exp}$ for the respective test cycles.

2.4 Heat exchange capacity rate

The heat exchange capacity rate is an expression related to how fast heat is transferred between the heat transfer fluid and the heat storage material in the heat storage. It indicates how well the heat exchanger of

the storage works. The heat exchange capacity rate is a function of the power, the storage temperatures, the flow rate, the heat storage design and material properties. A high heat exchange capacity rate is desired to be able to charge the storage fast when solar energy is available and to discharge the energy from the storage fast enough to meet the demand. The heat exchange capacity rate is expressed by the following equation which can be derived from the heat transfer rate and log mean temperature difference (Cengel, 2003)(Furbo, 2005):

$$H = -V \cdot C_p \cdot \rho \cdot ln\left(1 - \frac{T_i - T_o}{T_i - T_s}\right)$$

where T_s is the storage mean temperature.

2.5 Heat of fusion

The measured thermal energy content of the storage was compared to the theoretical thermal energy content. The measurements were compared to two different theories. To get a rough estimation of the energy difference from cold solid to hot melted state and the energy content in supercooled state a simple compound theory was used describing melting at a specific temperature. To get a more realistic theoretical correlation between the storage temperature and energy content of the storage during charge, the melting behavior was considered by using the theory of incongruently melting salt hydrates. The incongruently melting sodium acetate water mixture changes phase over a temperature range due to the temperature dependent solubility of the anhydrate salt in water.

2.5.1 Compound theory

The following theory explains the theoretical thermal energy content of the sodium acetate water mixture in a simplified way as if the salt water mixture behaves as an ideal compound which changes from solid to liquid phase at a specific melting temperature. The following simplification is for this report referred to as the “simple ideal melting theory” or “compound theory”.

The following equations show the theoretical change of thermal energy in the heat storage tank for a charge and a discharge for the compound theory.

$$E_{charge,com} = m \cdot \Big((T_{melt} - T_{start}) \cdot C_p(s) + L + (T_{max} - T_{melt}) \cdot C_p(l)\Big) + C_{tank} \cdot (T_{max} - T_{start})$$

$$E_{discharge,com} = m \cdot \Big((T_{max} - T_{melt}) \cdot C_p(l) + L + (T_{melt} - T_{end}) \cdot C_p(s)\Big) + C_{tank} \cdot (T_{max} - T_{end})$$

where m is the mass of the salt water mixture, T_{melt} is the melting temperature of the sodium acetate water mixture of 58°C, T_{start} is the mean storage temperature at the start of the charge, $C_p(s)$ is the specific heat of the sodium acetate water mixture in solid phase, $C_p(l)$ is the specific heat of the sodium acetate water mixture in liquid phase, L is the latent heat of fusion, C_{tank} is the heat capacity of the tank material, T_{max} is the mean maximum temperature the heat storage reaches during charge, T_{end} is the mean temperature the heat storage reaches after the discharge.

When the heat storage cools down to T_{end} without crystalizing, assuming that the specific heat of the supercooled sodium water mixture has the same properties as the liquid sodium acetate water mixture, then the stored thermal energy at supercooled state is:

$$E_{super,com} = E_{charge} - (T_{max} - T_{end}) \cdot (m \cdot C_p(l) + C_{tank})$$

If the start temperature and end temperature are equal, then the energy charged and discharged from storage excluding the heat losses also equal.

$$T_{start} = T_{end} \Rightarrow E_{charge} = E_{discharge}$$

The thermal energy stored at supercooled state is therefore:

$$E_{super,com} = m \cdot L - m \cdot (T_{melt} - T_{end}) \cdot (C_p(l) - C_p(s))$$

The following material properties were used for the sodium acetate water mixture.

The theoretical specific heat for solid and liquid phase material of the salt water mixture was determined using the theory of Araki (Araki, Futamura, Makino, & Shibata, 1995). Non temperature dependent heat capacities for the solid and liquid phase sodium acetate water mixture were determined based on an average over the relevant temperature interval. The latent heat of fusion was by the theory of Araki determined to 205 kJ/kg for the 43.5 % water 56.5 % sodium acetate mixture. The experiments showed that the value was slightly higher and 215 kJ/kg was used to get a better fir between measurement and theory. Values are listed in the Tab. 1.

Table 1. Material properties for sodium acetate water mixture for 43.5 % water 56.5 % sodium acetate based on Araki 1995 for compound approximation.

$C_p(s)$	$C_p(l)$	L
2.1 kJ/kgK	3.2 kJ/kgK	215 kJ/kg (205 kJ/kg)

2.5.2 Incongruently melting theory

The following theory describes the theoretical energy content of the salt water mixture based on the theory of incongruently melting salt water mixtures explained in the report “Heat storage in solar heating system using salt hydrates” (Furbo and Svendsen, 1980). The theory used in this report is a simplification of Furbo’s theory. Here non temperature dependent specific heats for the salt water mixture were used. Same values for specific heats as in Table 1 were used.

In short the theory states that the latent heat of fusion of the salt hydrate in a salt water mixture is released over a temperature range due to the temperature dependent solubility of the anhydrous salt in water and not at a specific temperature as for the compound in the simple ideal melting theory. Figure 3 shows the temperature dependent solubility of anhydrous sodium acetate in water. Based on the solubility a temperature dependent relation of the fraction of solid phase salt hydrate in the salt water mixture Fsol(t) was calculated based on the actual water content of the mixture and the water content of the pure salt hydrate. This basically describes that as the temperature increases more salt will be dissolved in the extra water.

$$Fsol(t) = \frac{56.5\% - S_a(t)}{60.3\% - S_a(t)}$$

Where 56.5% is the sodium acetate content of the used salt water mixture, 60.3% is the sodium acetate content of the sodium acetate trihydrate and $S_a(t)$ is the temperature dependent solubility of the anhydrous salt in water. Fig. 3 shows that even at low temperatures a part of the salt water mixture is in liquid state hence some of the latent heat is already released. At a temperature of approximately 50°C does the liquid fraction start to increase rapidly until 58°C where it is fully liquid. The latent heat is released as the liquid fraction increases. For this theory a latent heat of fusion of L = 250 kJ/kg was used. This corresponds well with the value of L = 215 kJ/kg for the simple compound theory as at a starting point of 20°C 86% of the salt water mixture is already in liquid phase according to the theory.

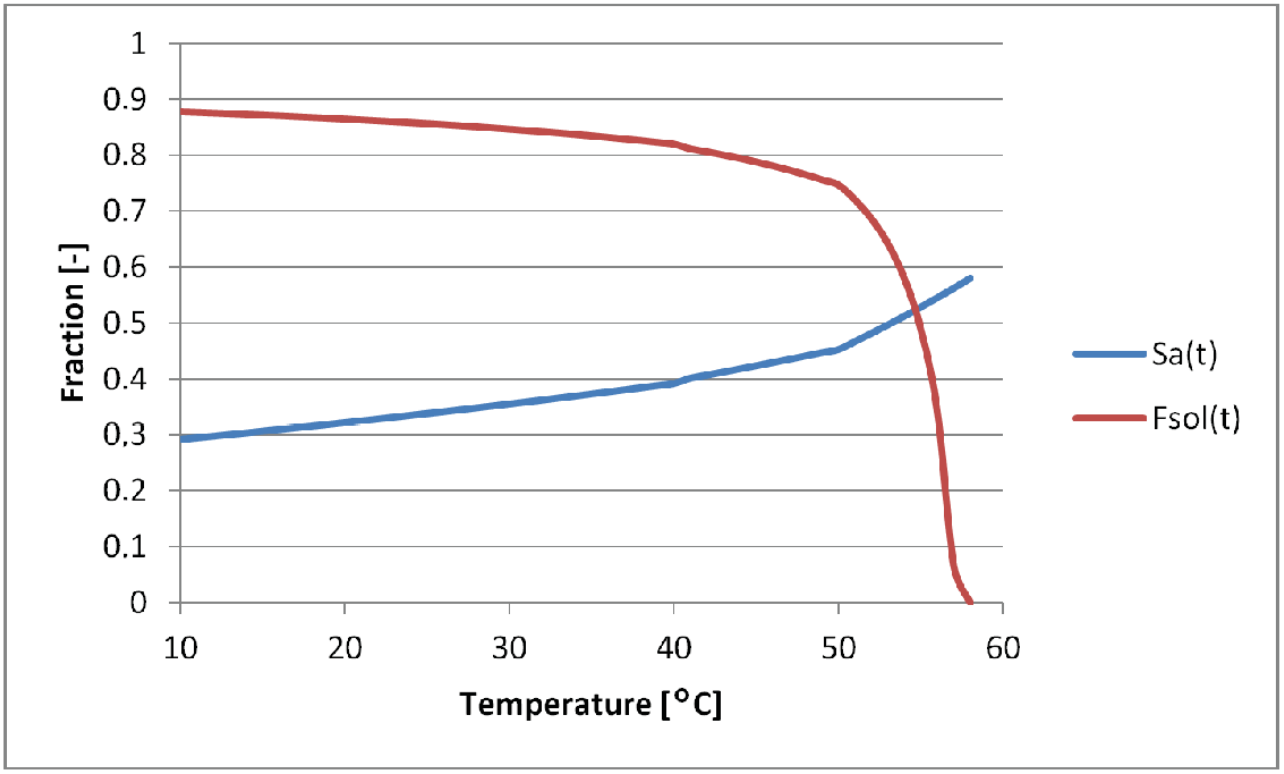

Figure 3. Solubility of anhydrous salt in water and fraction of solid phase salt hydrate in 43.5 % water and 56.5% sodium acetate mixture.

The energy content of the salt water mixture based on the theory of incongruently melting salt water mixtures is:

$$E_{charge,incon} = m \cdot \left((T_{melt} - T_{start}) \cdot C_p(s) + L \cdot F_{sol}(T_{start}) + (T_{max} - T_{melt}) \cdot C_p(l)\right) + C_{tank} \cdot (T_{max} - T_{start})$$

The energy content at supercooled state for this theory is calculated by extrapolating the straight line representing the energy content in the fully melted state down to ambient temperature without the release of latent heat. This is in principle the same way as for the simple compound theory where the salt water mixture cools down below the melting point without releasing the latent heat of fusion but heat is released based on the specific heat of the liquid phase salt water mixture, see Fig 4.

The energy content of the salt water mixture at supercooled state based on the theory of incongruently melting salt water mixtures is:

$$E_{super,incon} = m \cdot L \cdot F_{sol}(T_{end}) - m \cdot (T_{melt} - T_{end}) \cdot (C_p(l) - C_p(s))$$

Fig. 4 shows the theoretical energy content of the salt water mixture as a function of the temperature of the material above 20 °C for the two different theories.

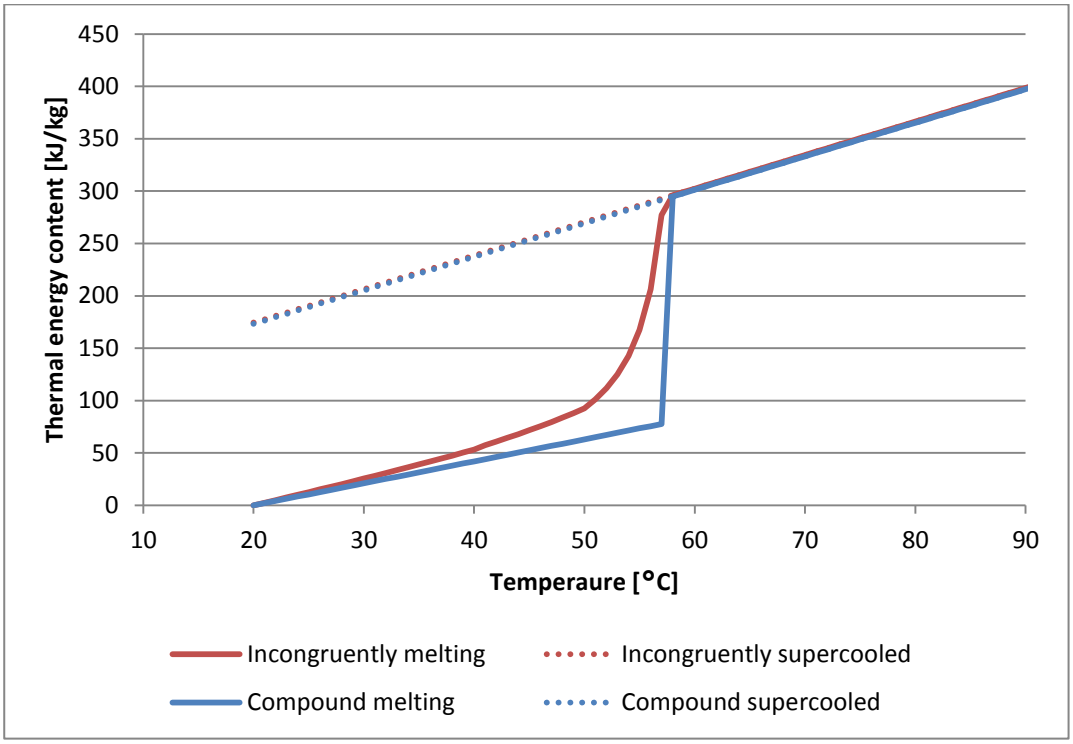

Figure 4. Thermal energy content of salt water mixture based on compound theory and incongruently melting salt theory.

To compare the measured thermal energy content of the heat storage with the theoretical, the mean storage temperature at the starting point of the test cycle was selected as the reference point. The reference point varies from 18 to 28°C for the test cycles.

2.6 Theoretical properties of Thermobatterie:

Relevant theoretical properties of the storage module are calculated.

2.6.1 Heat capacity

The theoretical heat capacity of the heat storage material for the heat storage module was determined with the following dimensions and assumptions:

Table 2. Heat storage material mass and specific heat capacity.

Material	Mass	Specific heat capacity
Stainless steel	45 kg	500 J/kgK
Aluminium	10 kg	920 J/kgK
Water in heat exchanger	2 kg	4186 J/kgK

This gives the following theoretical heat capacity for the heat storage material:

$$C_{tank,theo} = 45\ kg\ \cdot 500\frac{J}{kgK} + 10\ kg\ \cdot 920\frac{J}{kgK} + 2kg \cdot 4186\frac{J}{kgK} = 40.1\ kJ/K$$

2.6.2 Heat loss coefficient

The theoretical heat loss coefficient of the Thermobatterie heat storage module was determined.

The heat loss coefficient from the side per meter was calculated based on the following approximated equation (Furbo, 1984):

$$H_{side} = \frac{\pi}{\frac{1}{2k} ln\frac{d_y + 2e_s}{d_y} + \frac{0.13\frac{m^2K}{W}}{d_y + 2e_s}} W/Km$$

The heat loss coefficient from the top and bottom are calculated based on the following approximated equations (Furbo, 1984):

$$H_{top} = \frac{\frac{\pi}{4}\left(d_y + e_s\right)^2}{\frac{e_t}{k} + 0.1\frac{m^2K}{W}} \mathrm{W/K}$$

$$H_{bottom} = \frac{\frac{\pi}{4}\left(d_y + e_s\right)^2}{\frac{e_b}{k} + 0.17\frac{m^2K}{W}} \mathrm{W/K}$$

The total heat loss coefficient was the sum of the above.

$$H_{loss} = H_{side} \cdot h + H_{top} + H_{bottom}$$

where *k* is the thermal conductivity of the insulation material, d_y is the outer diameter of the steel tank, e_s is the thickness of the insulation on the side, e_t is the thickness of the insulation on the top, e_b is the thickness of the insulation on the bottom, 0.1 m^2K/W, 0.13 m^2K/W and 0.17 m^2K/W represents the thermal

resistance between the outer surface of the insulation and the ambient for the respective orientations, h is the height of the tank.

With the thermal conductivity of the insulation material k = 0.043 W/mK (at 80°C) and the dimensions d_y = 0.3 m, e_s = 0.04 m, e_b = 0.05, e_t = 0.03 m, h = 1.50 m, the theoretical heat loss coefficient is:

$$H_{loss,theo} = 1.7\ W/K$$

2.7 Measurements

The Thermobatterie was heated and cooled under controlled conditions to evaluate its performance. The energy transferred to and from the module was measured to evaluate the heat storage capacity, the heat loss coefficient and the heat exchange capacity rate. The heat to charge the module was generated by an electric heating element. Water was used as the heat transfer fluid circulating through the heat exchanger of the Thermobatterie. The set point temperature and the charging power were varied. To simulate a heat demand the module was connected to a cooling unit which supplied an inlet temperature of 18-20°C. The flow rate to the storage module was varied by valves.

2.7.1 Measurement equipment:

A 5 junction thermopile with counter flow sensors inside the inlet and outlet pipes measured the temperatures difference across the inlet and outlet. The absolute flow temperatures were measured with thermocouples type TT. All thermocouples were copper/constantan type TT thermocouples with an accuracy of 0.5 K. The accuracy of the temperature difference measurement by the thermopile is 0.1 K.

Tank temperatures were measured with 1 thermocouple on the bottom outer surface, 5 thermocouples distributed evenly on the outer side of the tank wall inside the insulation and a rod in the center of the tank with 5 thermocouples. One thermocouple measures the ambient temperature.

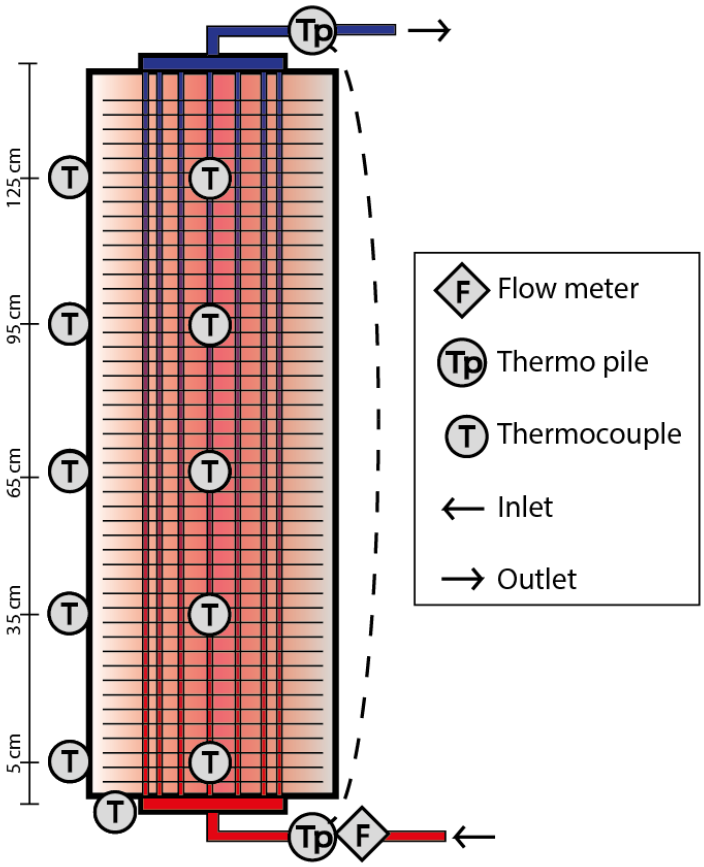

Figure 5. Measurement equipment and placement.

The flow rate was measured at the inlet by a Cloruis flow meter which was calibrated to have an accuracy of ± 1 % in the relevant flow range.

All data was logged on a PC using Impview.

3. Results

Initially tests were carries out with water filled into the storage module instead of the salt water mixture. Afterwards the water was emptied out and the salt water mixture was filled in the module and a series of test were carried out.

3.1 Tests with Water:

The Thermobatterie heat storage module was filled with 91 kg water to reach the same level as when the tank is filled with 115 kg of salt water mixture. The level of water in the tank at 20°C was 15 cm below the top.

The specific heat capacity of the water $C_p = 4186\ J/kgK$ was determined as average from 20°C to 80°C.

This gives a heat capacity for the total mass of the water in the tank:

$$C_{water}: 4186\ J/kgK \cdot 91\ kg = 380926\ J/K = 380.9\ kJ/K$$

This gives a total theoretical heat capacity of the heat storage filled with water:

$$C_{storage,theo} = C_{water} + C_{tank,theo} = 380.9\ kJ/K + 40.1\ kJ/K = 421\ kJ/K$$

A series of 6 heating and cooling cycles with different flow rates and powers during charge and discharge were carried out. One test cycle is explained in detail followed by a summary of the 6 test cycles. Details for the rest of the test cycles are in appendix A.

The heat loss coefficient was determined to $H_{loss,exp} = 1.7\ W/K$ from the measurements in test cycle 2 where stable conditions were obtained. This corresponds well with the theoretically determined value of $H_{loss,theo} = 1.7\ W/K$. The heat loss coefficient of $H_{loss,exp} = 1.7\ W/K$ was used when analyzing the measurements in all test cycles.

The following measurement data is displayed for the heating and cooling cycles.

- Graphs showing the measured temperatures over time along with the flow rate
- The heat content of the storage with the starting temperature condition as reference along with the mean temperature of all measured temperatures of the storage
- The calculated heat exchange capacity rates and the charge and discharge powers as a function of time
- The heat exchange capacity rate as a function of power
- The heat exchange capacity rate as a function of storage temperature

3.1.1 Test cycle 1 with water:

Charge and discharge parameters are listed in Tab 2. The electric heating element was set to a temperature of 90°C which gives an inlet temperature of 84°C - 87°C depending on the flow rate.

Table 3. Power and flow rate.

	Heating element power	Flow rate	Set temperature
Charge	**9 kW**	**7.2 l/min (0.9 l/min)**	**90 °C**
Discharge	**-**	**5.6 l/min**	**18-19 °C**

Fig. 6 shows the measured surface temperatures, inlet temperature, outlet temperature, ambient temperature and the flow rate for the heating and cooling cycle. For this cycle the flow rate was reduced in the fully charged state leading to a slight drop in temperature.

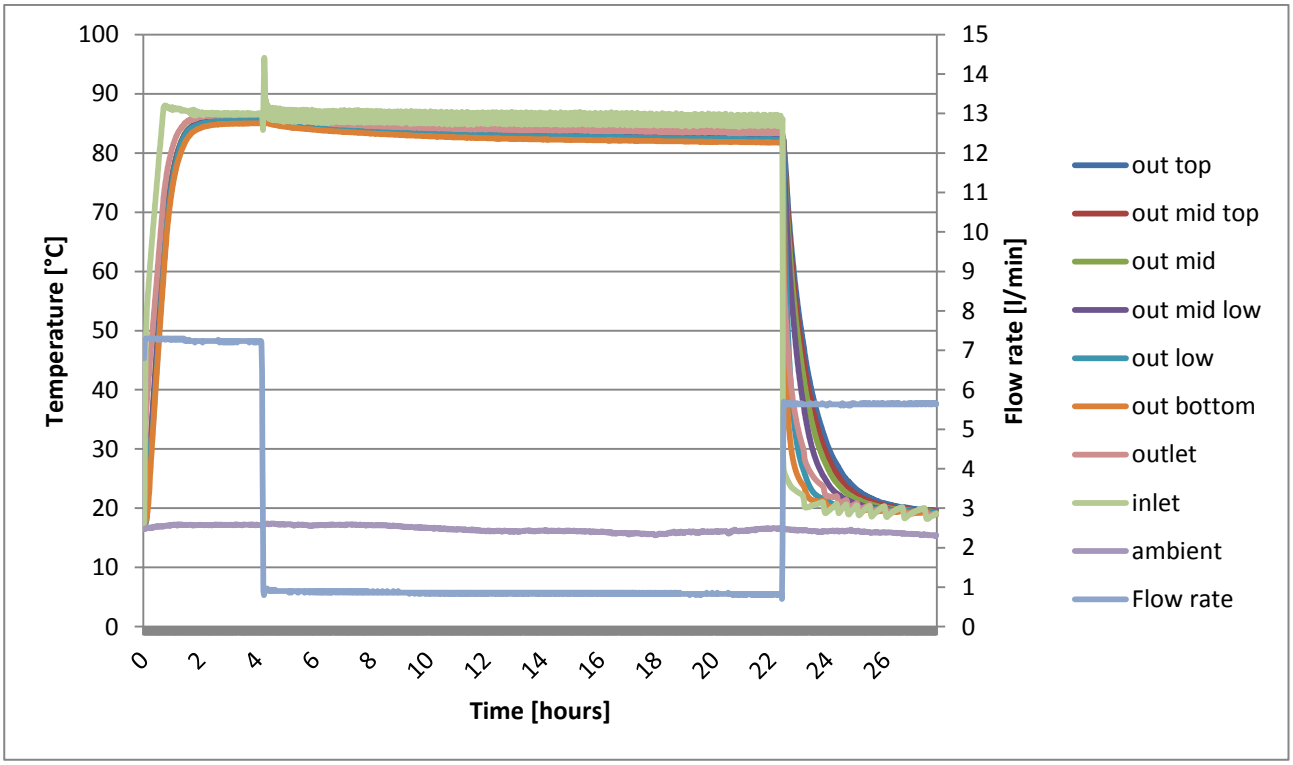

Figure 6. Temperature development and flow rate.

Fig. 7 shows the charge period in detail.

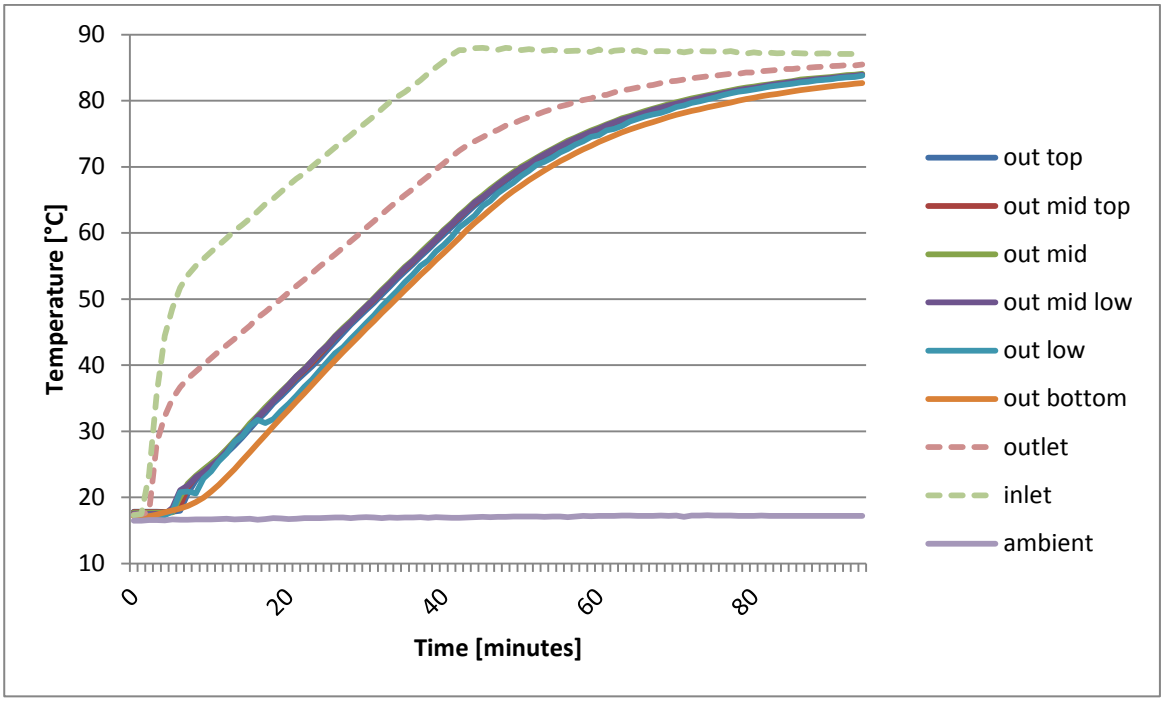

Figure 7. Temperature development for charge period.

From Fig. 7 can be seen that during the charge period the heat storage has low thermal stratification. With the inlet at the bottom of the storage module the flow direction and the naturel forces works for heating the module with a relatively uniform temperature distribution in the vertical direction. This indicates the upwards flow direction is beneficial when a certain minimum temperature for all parts of the storage has to be reached.

Fig. 8 displays the discharge period in details.

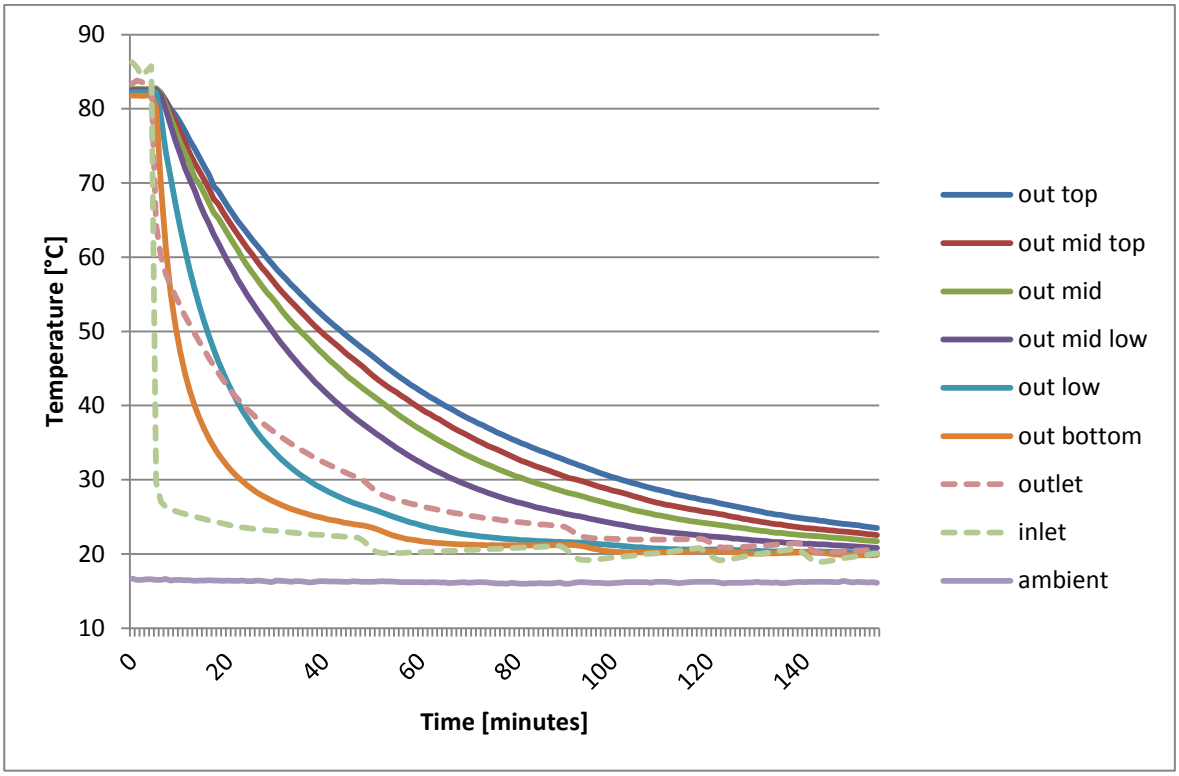

Figure 8. Temperature development for discharge period.

From Fig. 8 can be seen that during discharge the tank gets a high thermal stratification. The upwards flow direction was beneficial for the development of this thermal stratification. This indicates that the heat from the storage module will be discharged at a higher temperature over a shorter period compared to a downwards flow direction where more mixing will occur.

Tab. 3 summarizes the start, maximum and end temperature of the storage with water.

Table 4. Start temperature, maximum temperature and end temperature of storage.

T_{start}	T_{max}	T_{end}
17.5°C	85.8°C	19.3°C

Fig. 9 displays the measured heat content of the storage above start condition E(t) and the mean temperature of the storage over time. The mean temperature was determined as an average of the 6 external temperatures sensors.

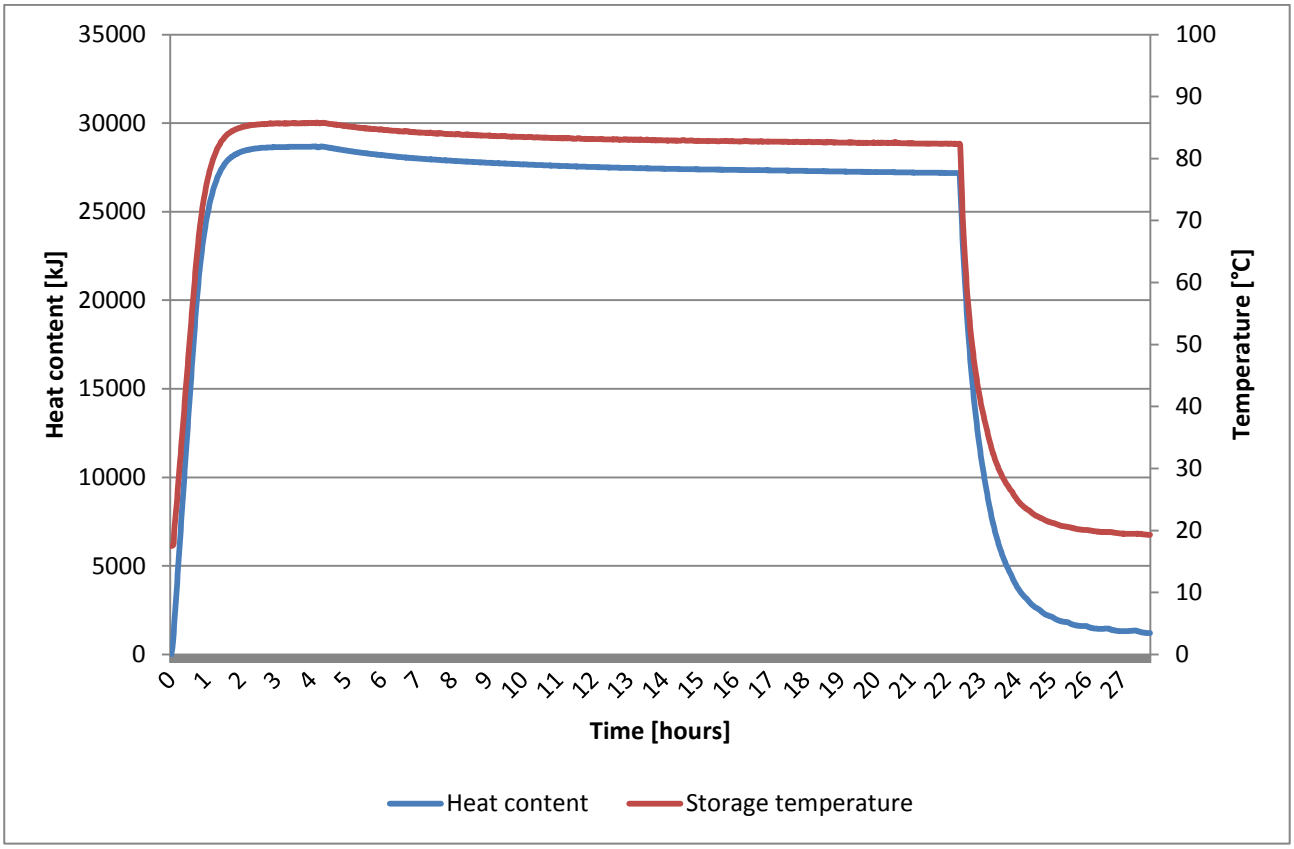

Figure 9. Energy content and mean storage temperature.

The theoretical heat change in the storage from the start temperature to the maximum temperature was determined based on the measured start and maximum temperatures and the theoretical heat storage capacity.

$$E_{charge,theo} = (T_{max} - T_{start}) * C_{storage,theo} = (85.8 - 17.5\ C) * 421\ kJ/K = \ 28754\ kJ$$

The maximum measured heat content of the storage is listed in Tab. 4 along with the theoretical value.

Table 5. Measured and calculated heat contents during the test.

Max measured energy content $E_{charge,exp}$	Theoretical max energy content $E_{charge,theo}$
28900 kJ	28754 kJ

The deviation between the measured energy content and the theoretical energy indicates the uncertainty of the measurements and the used heat loss coefficient. The deviation between the measured and the theoretical energy content at hot state was just 0.5%. This shows that the theoretical calculations and assumptions were consistent with the measurements.

The heat exchange capacity rates for the charge and discharge period are displayed in Fig. 10 and Fig. 11 along with the charge and discharge power over time.

Example of calculation of the heat exchange capacity value after 10 min of charge:

$$H = -V \cdot C_p \cdot \rho \cdot ln\left(1 - \frac{T_i - T_o}{T_i - T_s}\right)$$

$$= -0.000122 \frac{m^3}{s} \cdot 4186 \frac{J}{kgK} \cdot 988 \frac{kg}{m^3} \cdot ln\left(1 - \frac{58.2°C - 42.1°C}{58.1°C - 25.1°C}\right) = 338\ W/K$$

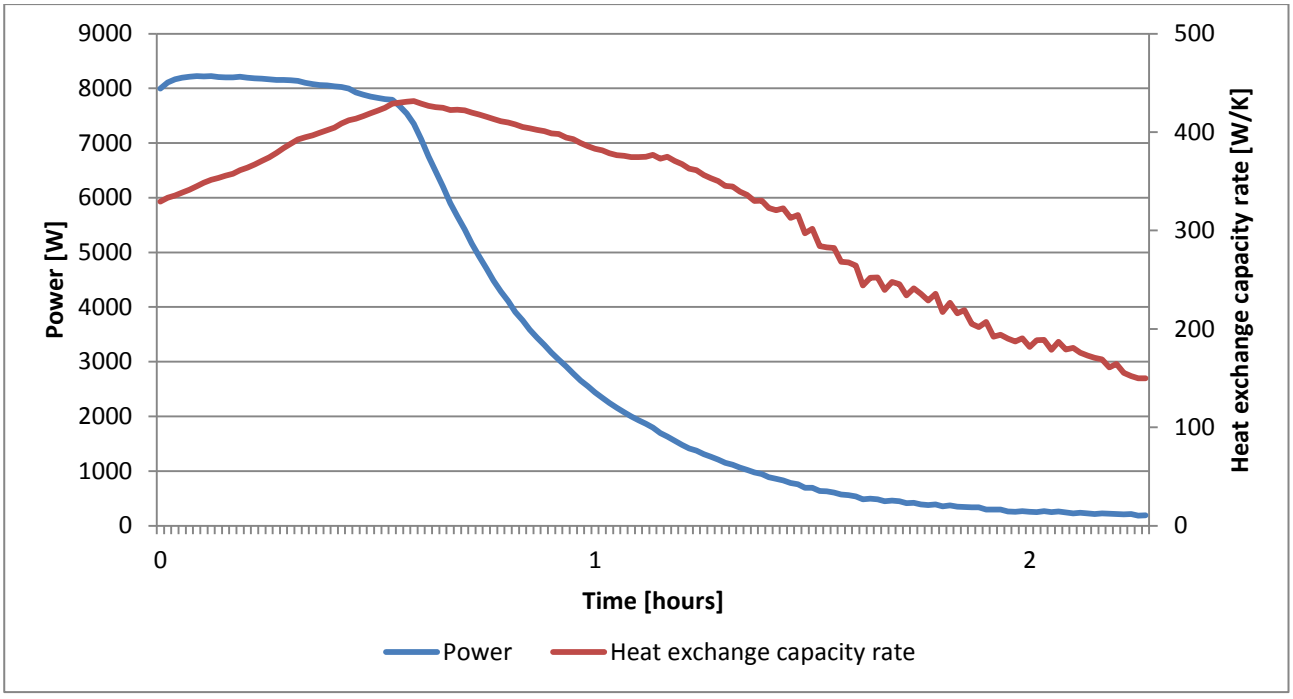

Figure 10. Power and heat exchange capacity rate over time for charge.

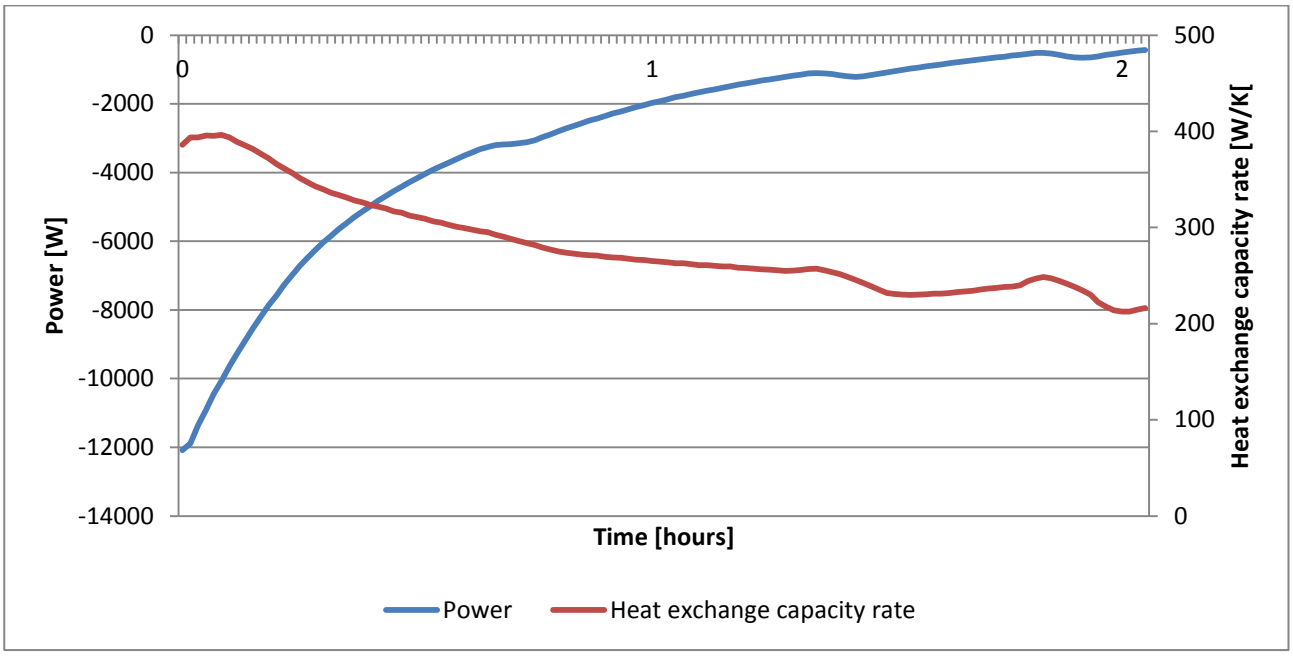

Figure 11. Power and heat exchange capacity rate over time for discharge.

Heat exchange capacity rate is displayed as a function of the mean storage temperature for charge and discharge in Fig. 12.

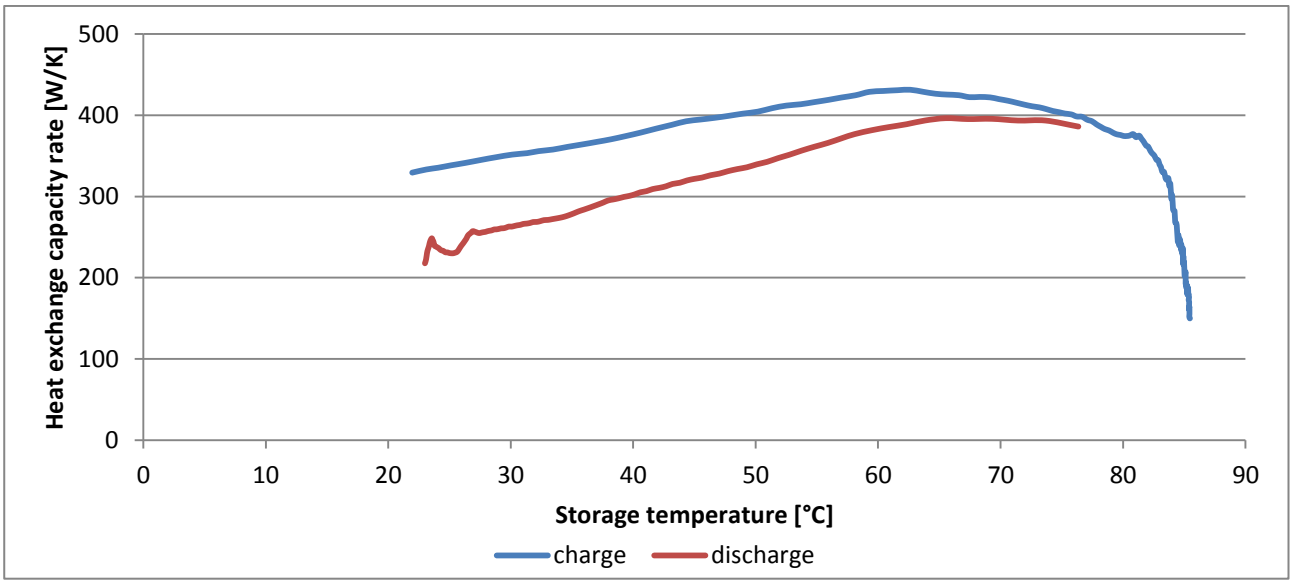

Figure 12. Heat exchange capacity rate as a function of storage temperature.

Heat exchange capacity rate is displayed as a function of the charge and discharge power in Fig. 13.

From Fig. 12 it can be seen that the heat exchange capacity rate was increasing for increasing heat storage temperature until 20 K before the maximum temperature was reached. For the charge this is due to the decreased power supply.

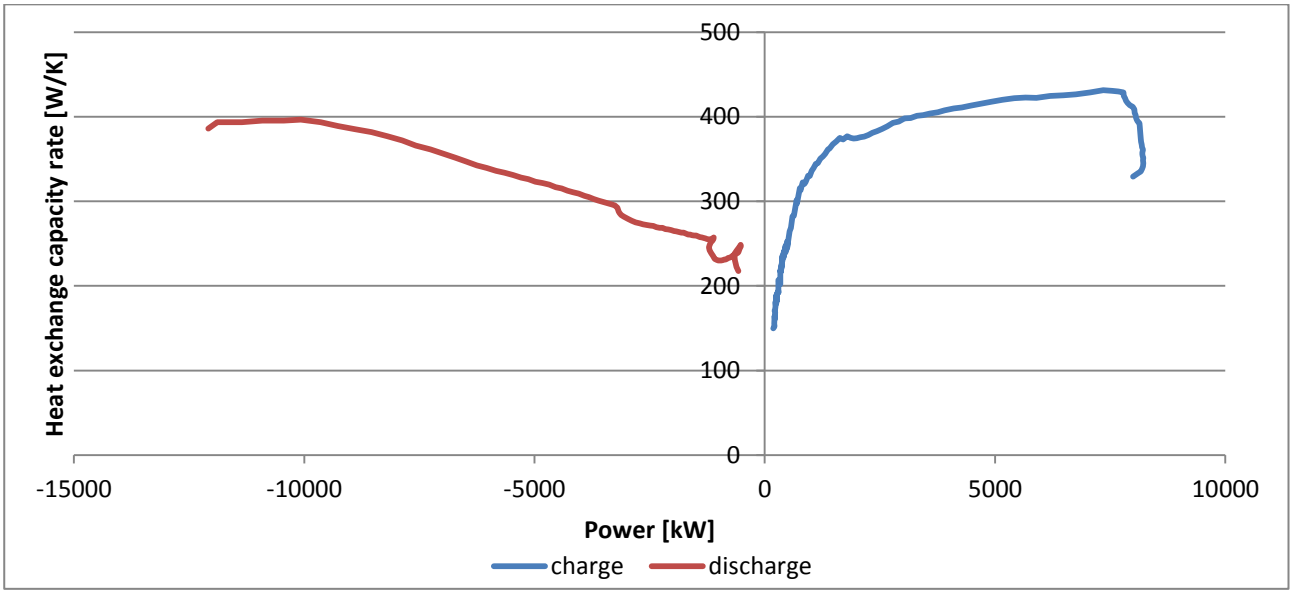

Figure 13. Heat exchange capacity rate as a function of charge and discharge power.

From Fig. 13 it can also be seen that the heat exchange capacity rate is increasing for increasing power transfer. For this test cycle with a flow rate of 5.6 to 7.2 l/min the heat exchange capacity rates was 250 – 400 W/K.

3.1.2 Summary of test with water

Tab. 6 summarizes the main findings of the experimental measurement with water in the Thermobatterie module. 6 test cycles were carried out with different flow rates and different charge powers.

"Max dT" is the temperature difference between maximum storage mean temperatures and the start temperature. "Energy to storage" is the measured energy transferred to the storage reduced by the calculated heat loss based on a heat loss coefficient of $H_{loss,exp}$ = 1.7 W/K. "Flow rate charge" is the flow rate averaged over the period from start to the storage was fully charged. "Set power" was the electric heating element setting. "Charge time" was the time from start of charging to the mean temperature had reached 0.5 K below max temperature. "Discharge time" was measured as from start of discharge to the mean storage has reached 22°C. The heat loss coefficient was determined for the cycles where the storage was kept at a steady hot state for a sufficiently long period.

Table 6. Summary of test with water.

Test cycle	Max dT	Energy to storage E_{charge}	Flow rate charge/ discharge [l/min]	Set power	Charge time	Discharge time	Heat Loss Coefficient $H_{loss,exp}$
1	68.3 K	28900 kJ	7.3 / 5.7	9 kW	2 hr 13 min	139 min	NA
2	63.2 K	26500 kJ	0.8 / 0.9	9 kW	13 hr 31 min	254 min	1.75 W/K
3	60 K	25000kJ	1.4 / 1.6	3 kW	9 hr 22 min	197 min	NA
4	67 K	27900 kJ	5.0 / 5.6	9 kW	2 hr 23 min	135 min	NA
5	65.9 K	27700 kJ	5.5 / 5.6	6 kW	2 hr 50 min	138 min	1.7 W/K
6	66.1 K	27650 kJ	6.1 / 5.7	3 kW	4 hr 34 min	141 min	1.8 W/K

The heat capacity of the storage material in the storage tank excluding the water was determined to be $C_{tank,exp}$ = 39 kJ/K based on an average value for the 6 test cycles with water. The following formula was used where $C_{storege,exp}$ is the measured heat capacity of the storage and C_{water} is the theoretical heat capacity of the specific used mass of water in the tank:

$$C_{tank,exp} = C_{storage} - C_{water}$$

Where

$$C_{storage} = E_{charge}/dT$$

Fig. 14 to Fig. 17 summarize the heat exchange capacity rates for the test cycles as functions of the storage temperature and the power.

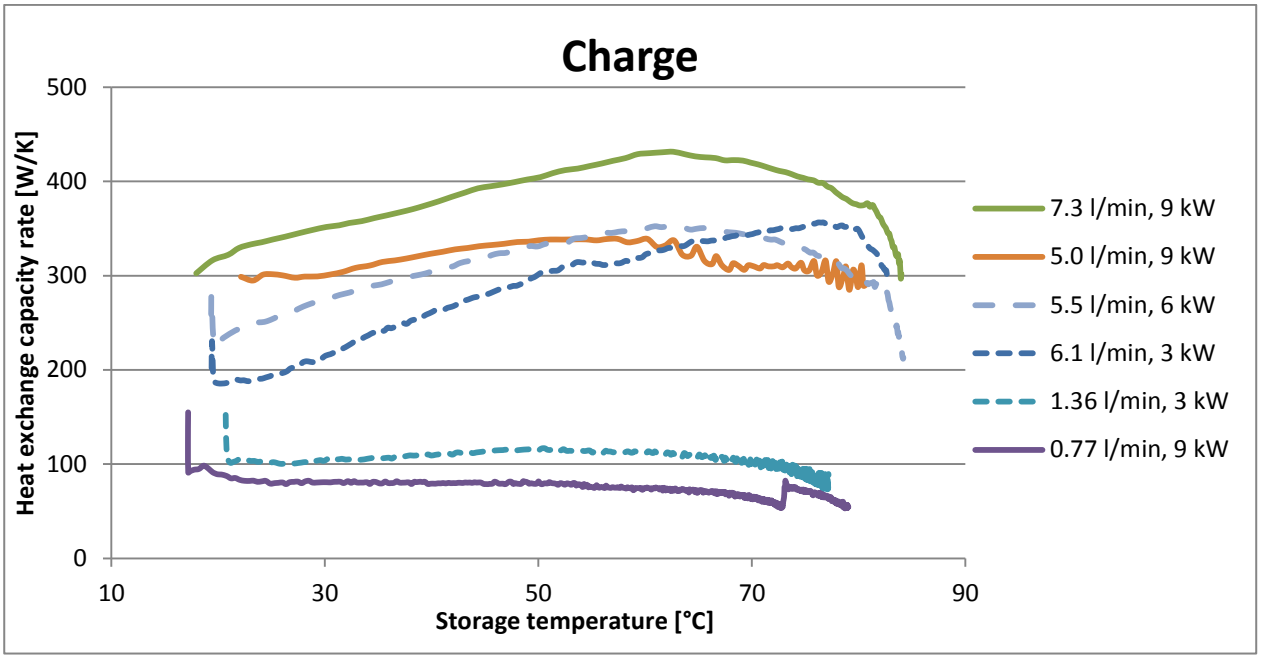

Figure 14. Heat exchange capacity rate as a function of mean storage temperature for 6 charges.

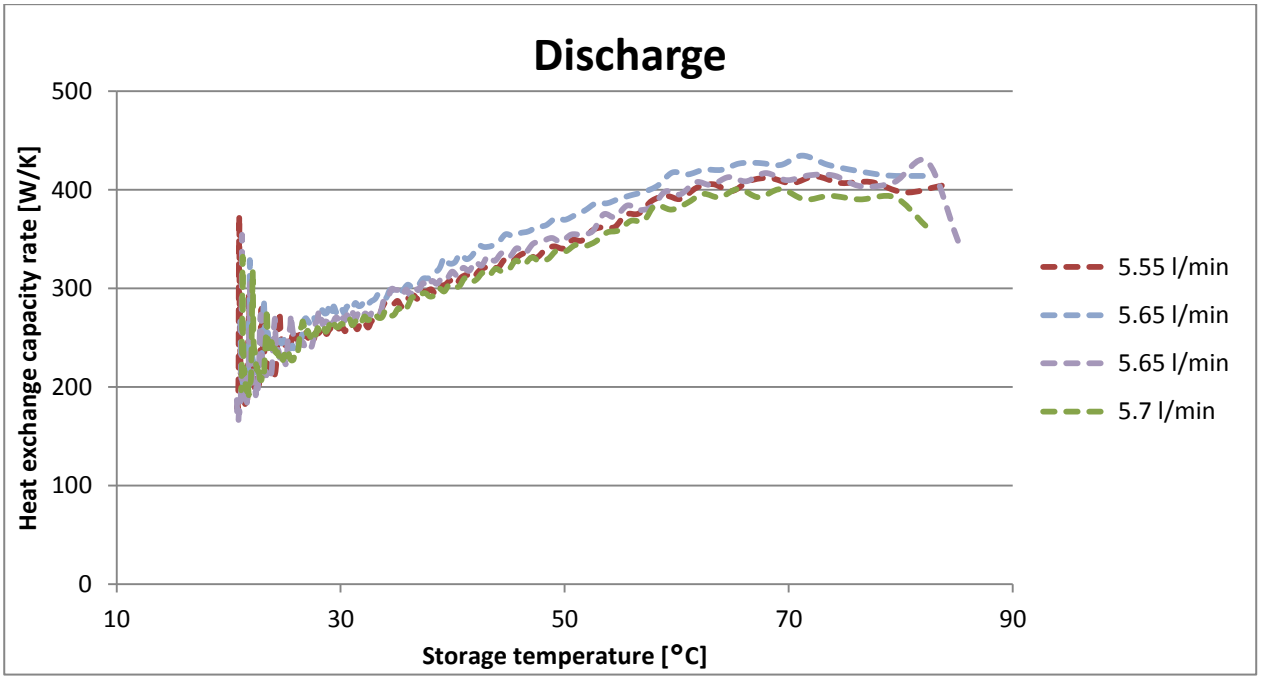

Figure 15. Heat exchange capacity rate as a function of mean storage temperature for 4 discharges.

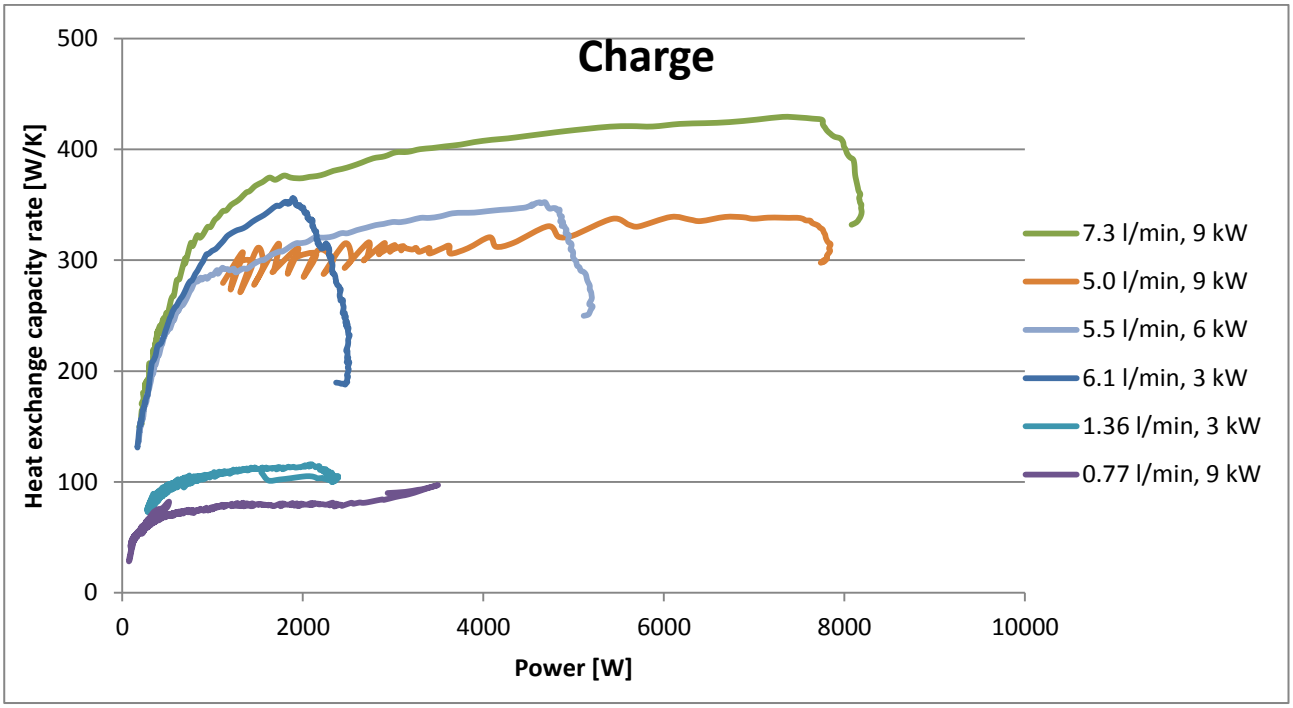

Figure 16. Heat exchange capacity rate as a function of charge power for 6 charges.

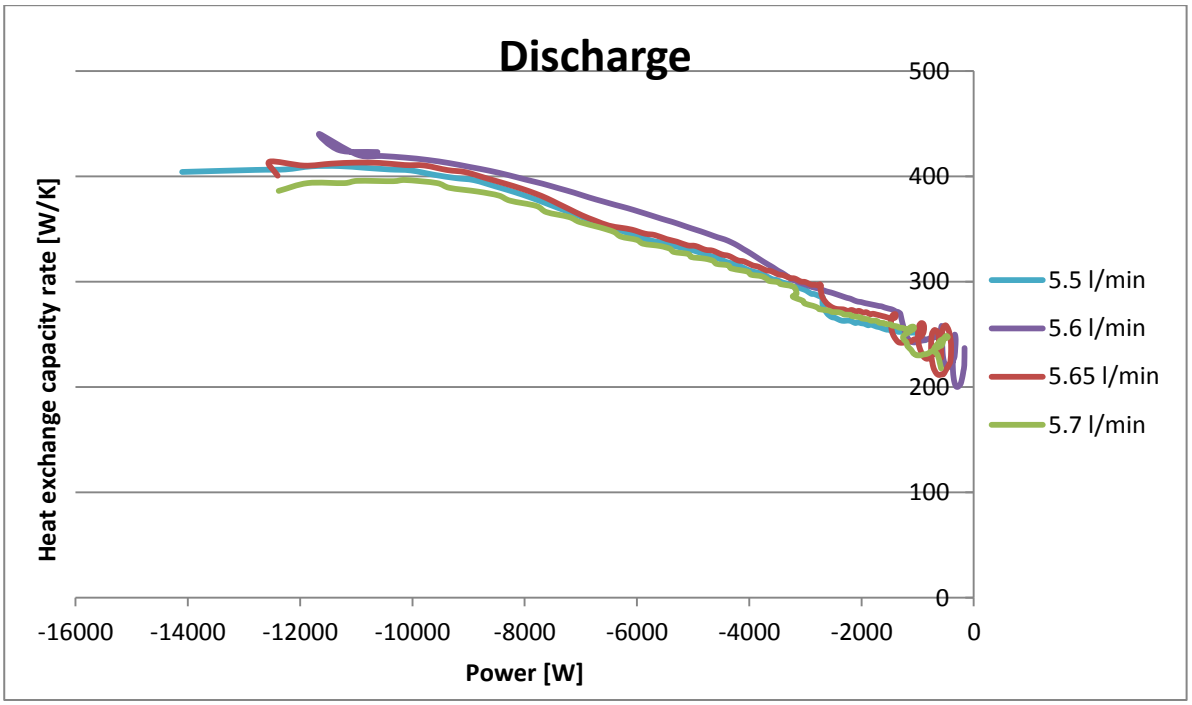

Figure 17. Heat exchange capacity rate as a function of charge power for 4 discharges.

Fig. 14 to Fig. 17 show that the heat exchange capacity rate was strongly influenced by the flow rate, the power and the heat storage temperature. The higher the flow rate, the power and storage temperature, the higher the heat exchange capacity rate will be. The heat exchange capacity rate was up to 450 W/K.

3.2 Tests with a sodium acetate water mixture

The Thermobatterie was filled with 116 kg of sodium acetate water mixture with a composition of approximately 43.5 % water and 56.5% sodium acetate. This corresponds to adding 6.4 % of water to the sodium acetate trihydrate. The top surface of the salt water mixture was approximately 15 cm below the top of the module. The volume above the salt water mixture contained atmospheric air at the start of the testing.

Similar properties for the storage as for the test with water were used for the tank with sodium acetate water mixture. Heat loss coefficient determined experimentally:

$$H_{loss,exp} = 1.7\ W/K$$

The heat capacity of the tank material determined experimentally in previous sections is used:

$$C_{tank,exp} = 39\ kJ/K$$

3.2.1 Measurement overview.

Tab. 7 lists the test cycles carried out with sodium acetate water mixture in the Thermobatterie including the heating element setting, flow rate and comments related supercooling and phase separation.

Table 7. Test cycles

Test cycle	File / date	Included in:	Heating element power / temp set	Flow rate Charge/ Discharge /Activation [l/min]	Supercooling and activation	comments
1	20131122	App B	6 kW / 91°C	1 / 0.6 / 0.6	Reached stable cold. Activated by shaking	Charge started at 28°C
2	20131127	Main report	9 kW 91°C	3.8 / 3.3 / 3.3	Activated spontaneously	Fully solid
3	20131129	App B	9 kW / 91°C	2.2 / 0 / 1.9	Reached stable cold. Activated w hammer	
4a	20131210	App B	9 kW /90°C	7.4 / 0 / 0	Activated spontaneously during passive discharge	Short period charge, liquid layer on top
4b	20131219	App B	9 kW / 90°C	7.4 / 0 / 0	Spontaneous activation during passive discharge	10 cm liquid layer on top
5	20140102	App B	9 kW / 92°C	7.4 / 5.7 / 5.7	Spontaneous during discharge – no supercooling	10 cm liquid layer on top
6	20140106	App B	3 kW / 92°C	2 / 2 / 2	Activated spontaneously	15 cm liquid layer on top

7	20140108	App B	3 kW / 52°C	4 / 4 / NA	Max temp below melting point	15 cm liquid layer on top
8	20140110	App B	3 kW / 90°C	3.9 / 3.7 / 3.7	Reached stable cold. Activated by shaking	15 cm liquid layer on top
9	20140116	Main report	6 kW / 90°C	7.4 / 5.7 / 5.7	Reached stable cold. Activated by shaking	12 cm liquid layer on top
10	20140120	App B	6 kW / 52°C - 74°C - 94°C	4.3 / 3.8 / 3.8	Reached stable cold. Activated by shaking	12 cm liquid layer on top
11	20140127	App B	9 kW / 92°C	7.4 / 5.7 / 5.7	Reached stable cold Activated by shaking	12 cm liquid layer on top
12	20140129	App B	3 kW / 92°C	2.2 / 2.3 /2.3	Spontaneous activation during discharge	
13	20140131	App B	6 kW / 93°C	7.4 / 0 / 0	Spontaneous activation during passive discharge	15 – 20 cm liquid on top
14	20140226	App B	6 kW / 93°C	7.4 / 0 / 0	Spontaneous activation during passive discharge	20 cm liquid on top
15	20140307	App B	6 kW / 93°C	7.4 / 5.7 / 5.7	Reached stable cold Activated by shaking	20 cm liquid on top
16	20140312	App B	6 kW / 93°C	7.4 / 5.7 / 5.7	Spontaneous activation during discharge	20 - 25 cm liquid on top
17	20140314	App B	6 kW / 93°C	7.4 / 5.7 / 5.7	Spontaneous activation during discharge	20 - 25 cm liquid on top

In the following section a detailed description of two test cycles are shown. The details for a number of other test cycles are given in appendix B.

3.2.2 Test cycle 2:

This test cycle was initiated with an average storage temperature of 20°C. Salt water mixture was fully solidified to the top when the test cycle was initiated as seen on figure 18.

Figure 18. Top surface of salt water mixture before test cycle.

Figure 19 shows the temperature development for the inlet, outlet, ambient, surface and internal temperatures as well as the flow rate. The flow rate was 3-4 l/min.

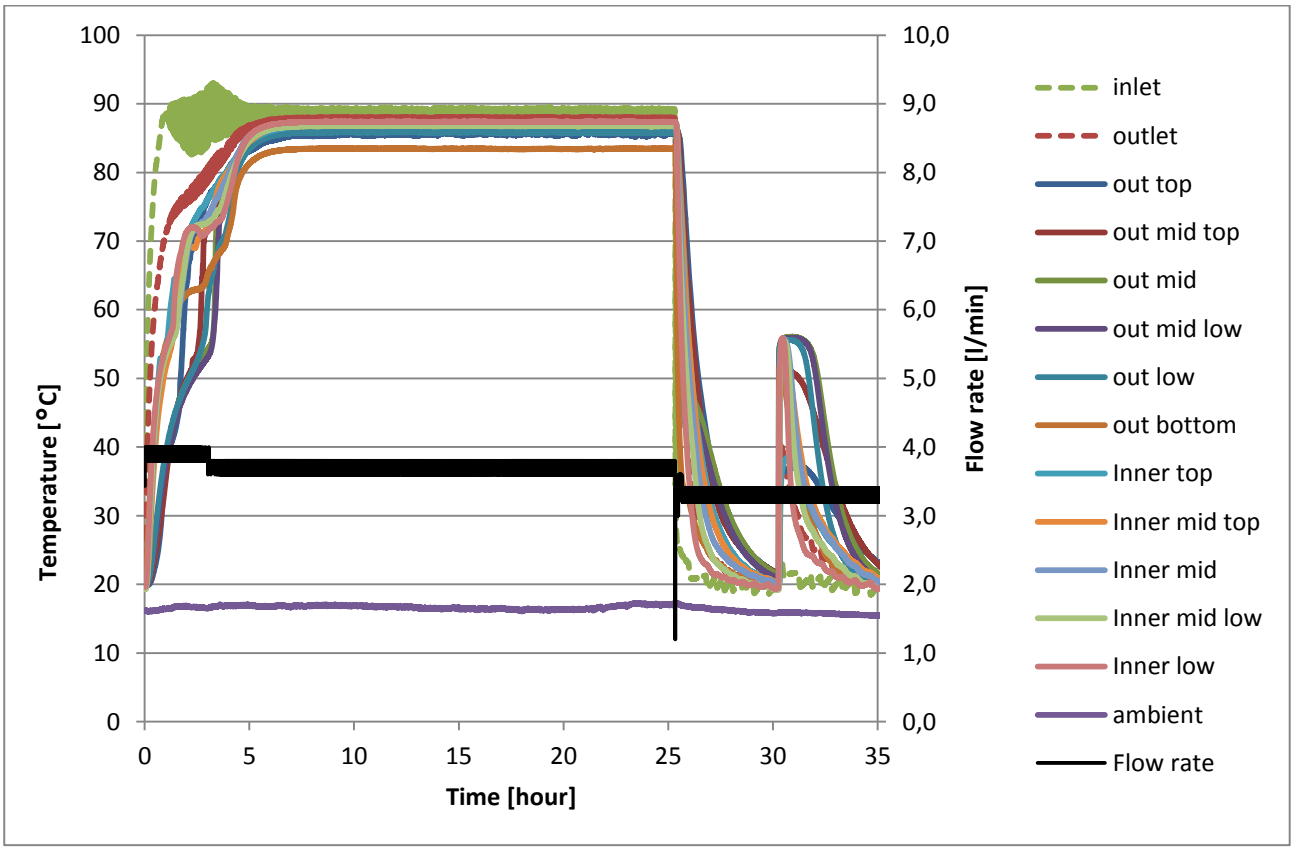

Figure 19. Temperature development and flow rate for test cycle 2.

Fig. 20 shows the temperature development for the charging period in detail. The charge time with this flow rate was 5-6 hours before a stable temperature above 80°C was reached. The inlet temperature fluctuates a lot due to the hysteresis of the heating element.

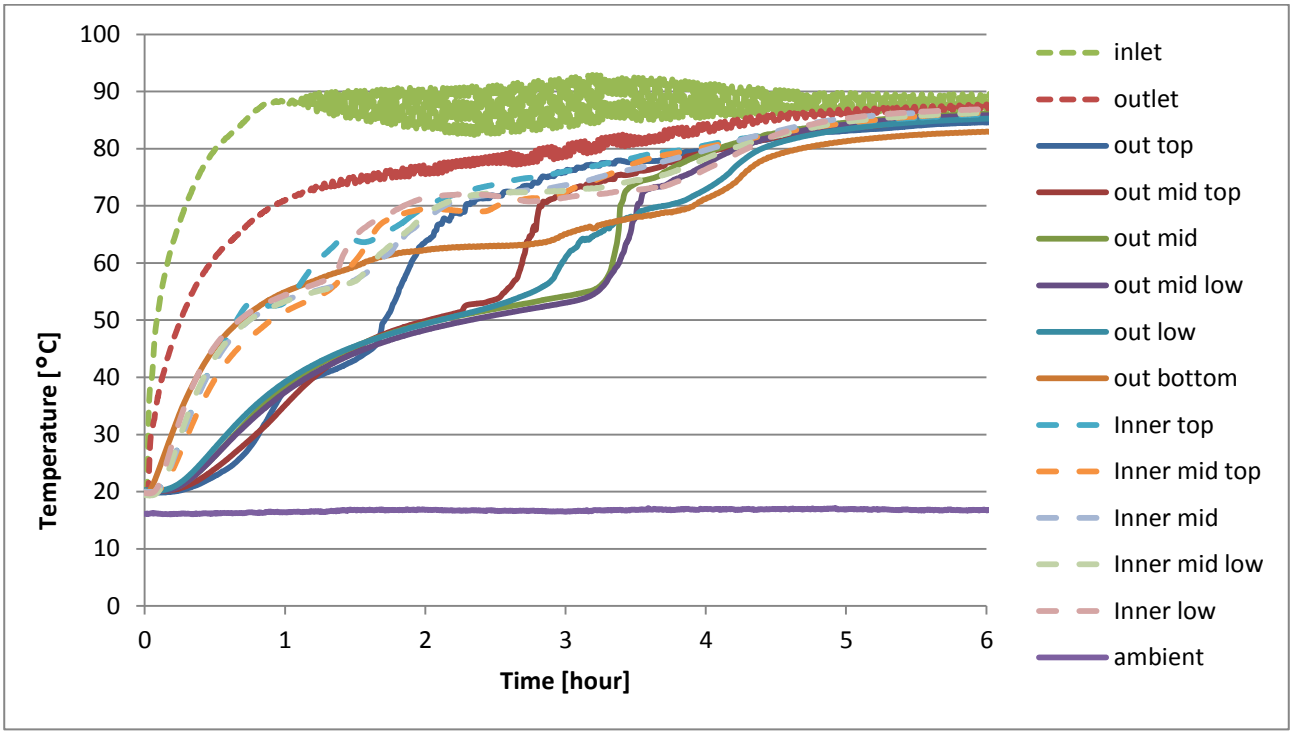

Figure 20. Temperature development during charge.

Fig. 21 shows the discharge to supercooled state and the activations and following discharge in detail. The discharge time after activation was 3-4 hours.

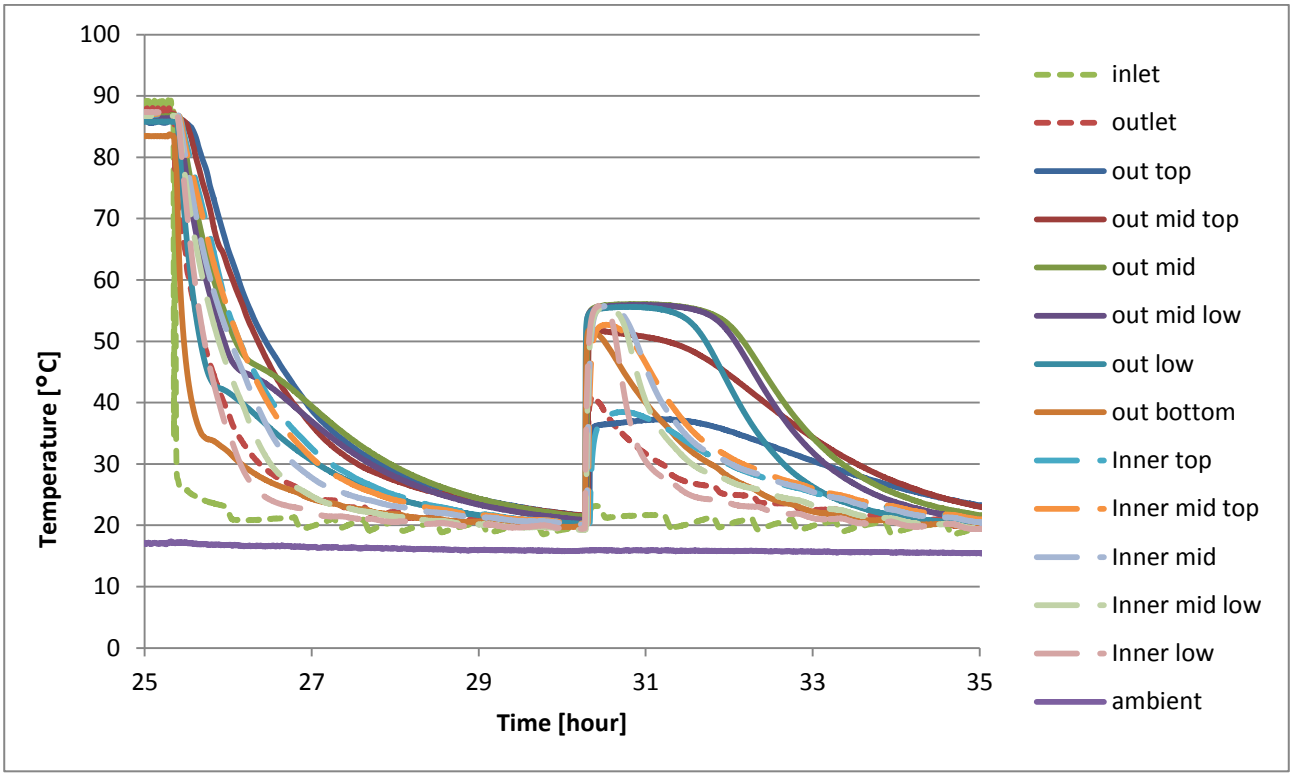

Figure 21. Temperature development for discharge to supercooled state and the following activation and discharge.

The module activated spontaneously just before a stable discharged state was reached. Activation started from the bottom. The top sensors of the module did not reach the same temperature level as elsewhere in the module, which could indicate phase separation.

Fig. 22 shows the mean storage temperature and the thermal energy content of the storage E(t) based on the measurements over the test cycle.

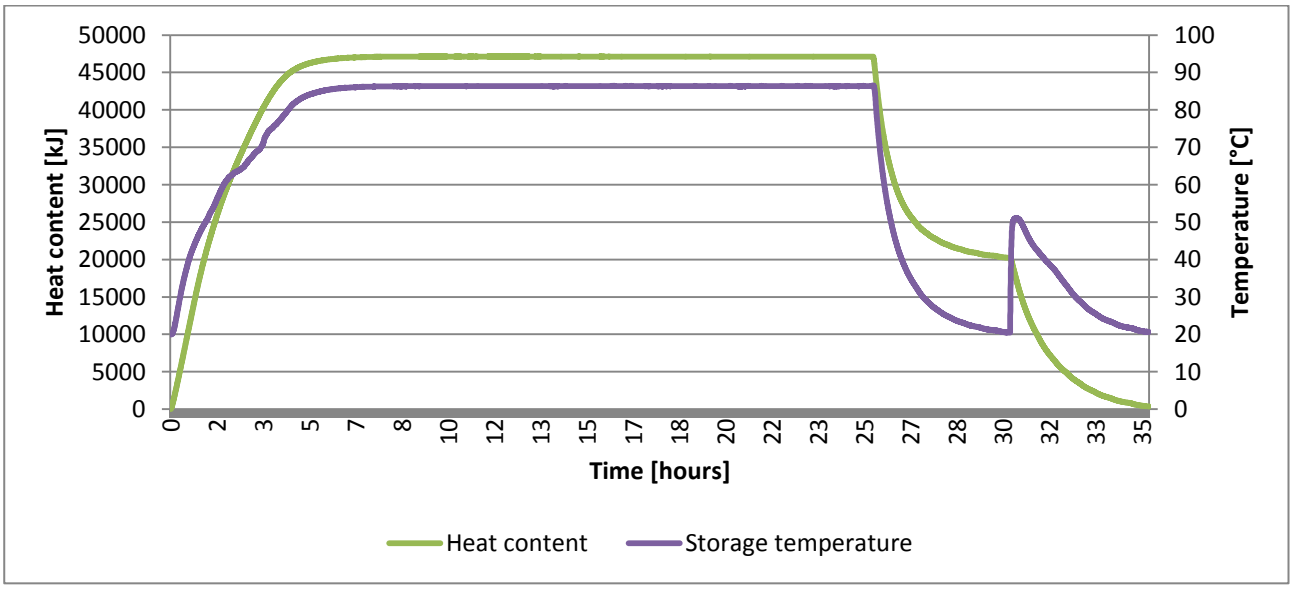

Figure 22. Heat content and storage temperature.

The start and end temperatures were roughly the same. Tab. 8 summarizes the start, maximum and end temperature of the storage for the test cycle.

Table 8. Storage start temperature, maximum temperature and end temperatrure.

T_{start}	20°C
T_{max}	86.5°C
T_{super}	21°C
T_{end}	20.6°C

Measured energy changes:

Tab. 9 lists the thermal energy content $E_{charge,exp}$ determined by the measurements at T_{max} and the enegy content after discharge to supercooled state $E_{super,exp}$ and after the activation and discharge $E_{end,exp}$.

Table 9. Thermal energy content at start, supercooled state and end of test cycle based on measurements.

E_{start}	0 kJ
$E_{charge,exp}$	47150 kJ
$E_{super,exp}$	(20200) kJ
$E_{end,exp}$	370 kJ

The start temperature was the reference temperature for the calculation of the energy content. The thermal energy content in the supercooled state was uncertain and higher than the actual value due to the fact that the storage does not reach a stable supercooled state before activation.

Theoretical energy change:

Based on the compound theory the energy content at the measured temperatures in the heat storage module the theoretical thermal energy change of the storage module is listed in Tab. 10.

Table 10, Thermal energy content based on simple ideal thermal energy content theory.

$E_{start,theo}$	0 kJ
$E_{charge,theo}$	47400 kJ
$E_{super,theo}$	20360 kJ
$E_{end,theo}$	190 kJ

Based on the theory of thermal energy content for incongruently melting salt hydrates the theoretical energy content of the storage at different states are listed in Tab. 11.

Table 11, Thermal energy content based on incongruently melting salt hydrate's thermal energy content.

$E_{start,theo}$	0 kJ
$E_{charege,theo}$	47500 kJ
$E_{super,theo}$	20400 kJ
$E_{end,theo}$	170 kJ

The measured energy content of the storage fits excellent with the theoretical energy content at maximum temperature with a deviation of 1 % in supercooled state.

Figure 23 shows the theoretical and the measured thermal energy content of the salt water mixture per mass unit as a function of the storage temperature. The storage temperature was determined as an average of both inner and outer temperature sensors. The thermal energy content is shown in kJ/kg salt water mixture excluding tank material. The measured thermal energy content was calculated by:

$$C_{salt} = \frac{E_{charge,exp} - C_{tank} \cdot (T_s - T_{start})}{m}$$

Where m is the mass of the salt water mixture.

The mean storage temperature of 20°C at the start of the charging was used as the reference temperature. The measured and the theoretical energy contents are therefore 0 kJ at this temperature. The storage temperature was determined as an average of both inner and outer temperature sensors.

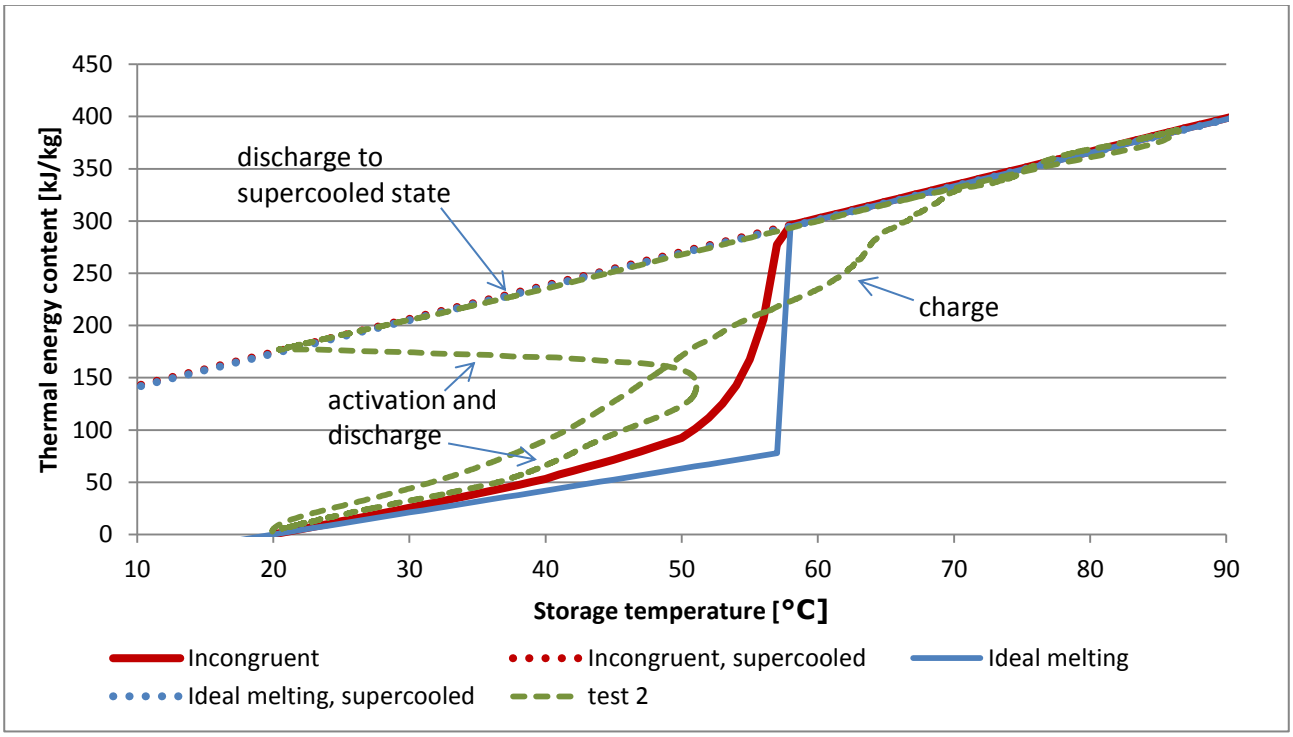

Figure 23. Theoretical and measured thermal energy content of salt water mixture per mass.

In Fig. 23 can be seen that the theoretical predictions fit quite well with the measurements.

Fig. 23 shows that the compound theory had a good agreement with the measured values when considering the start and end condition of the experiment. The theory with the incongruently melting salt hydrate does give a better agreement with the measurement in the temperature interval between the start and end condition. The energy content at the supercooled state does for both theories agree well with the measurements. The deviation between the measurements and the theory was partly due to the delay in the temperature measurements and an uneven temperature in the storage.

Fig. 24 shows the thermal energy content of the salt water mixture as functions of the inner and outer temperature sensors respectively. Here can be seen that the agreement between incongruently melting salt water mixture theory and measurements with the inner temperature sensors fits excellent for charge up to 55°C where after it deviates. For storage temperature above 56°C the outer temperature sensors gives an excellent fit with the theoretical values.

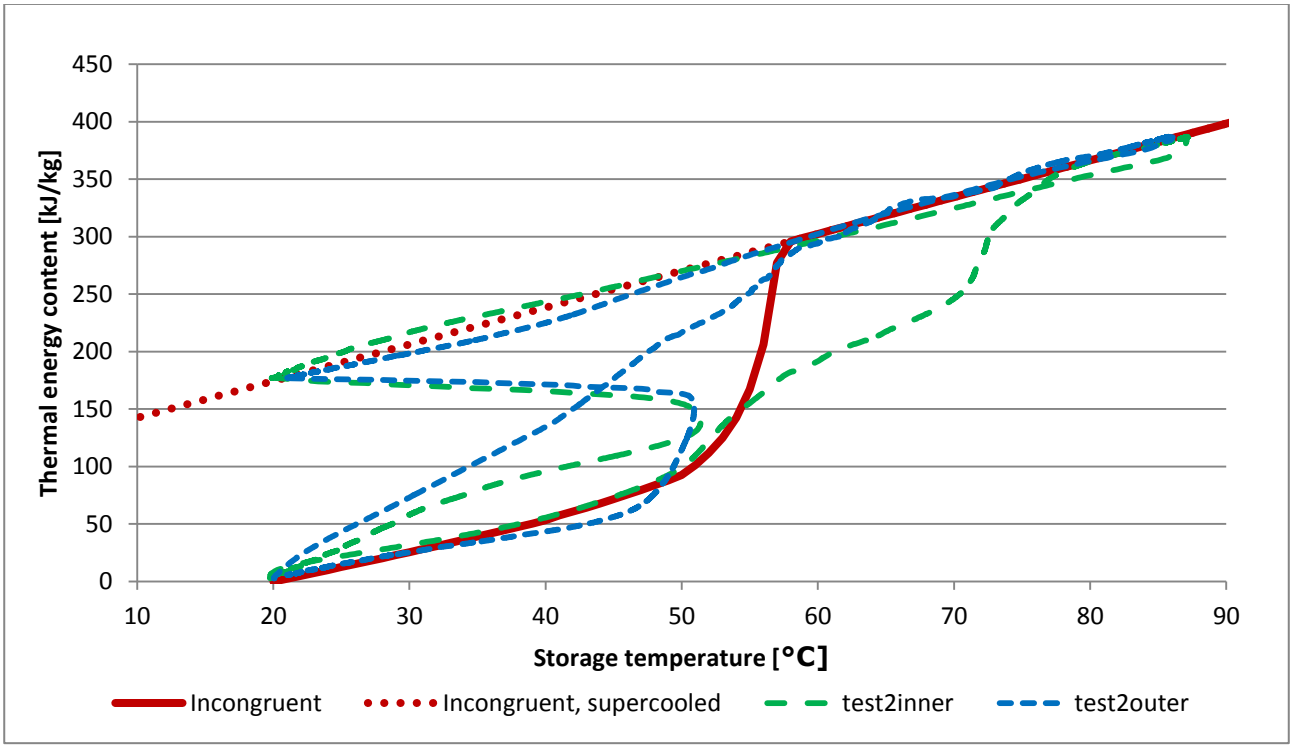

Figure 24. Theoretical and measured thermal energy content of salt water mixture per mass for inner and outer temperature sensors.

The power of the charge is displayed in Fig. 25 along with the heat exchange capacity rate for the same period. The mean storage temperature of both inner and outer sensors was used in the calculation for the heat exchange capacity rate.

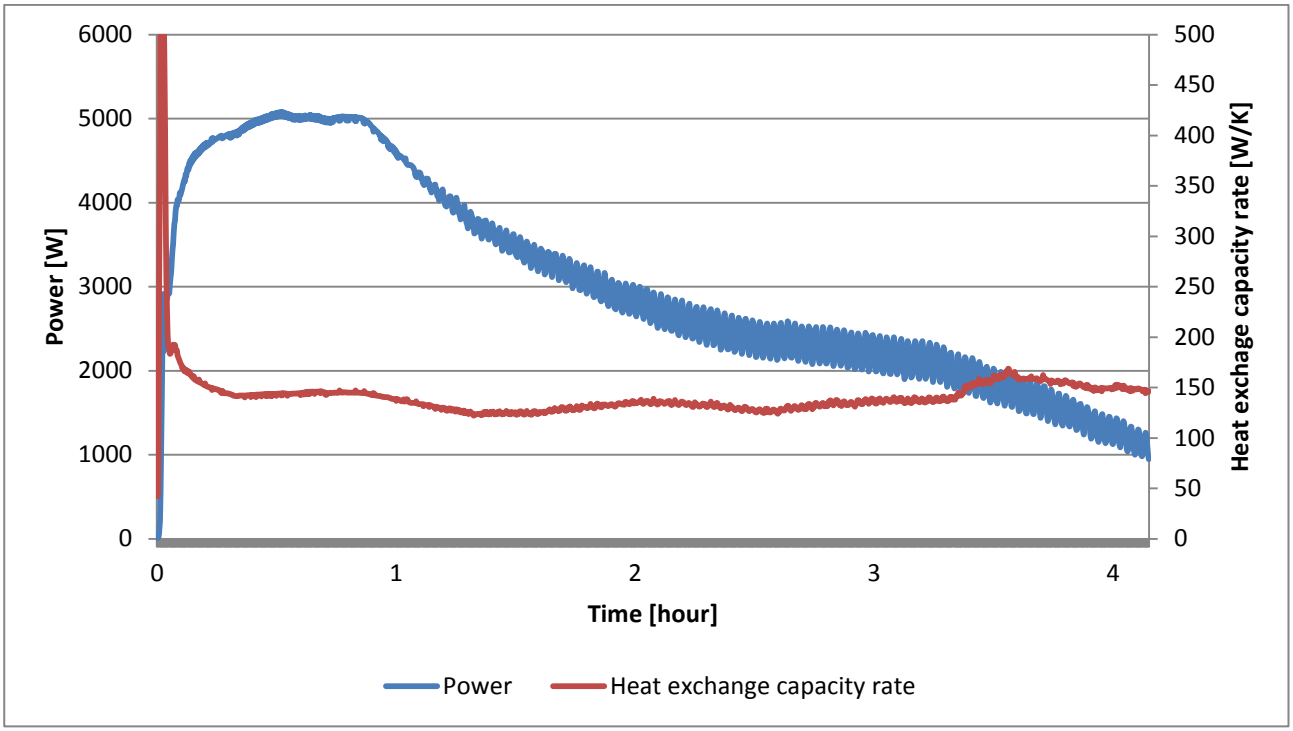

Figure 25. Power and heat exchange capacity rate over time.

The charge power topped at 5 kW and the heat exchange capacity rate was 130 – 150 W/K. The discharge power from T_{max} to supercooled state and the discharge after activation is displayed in Fig. 26.

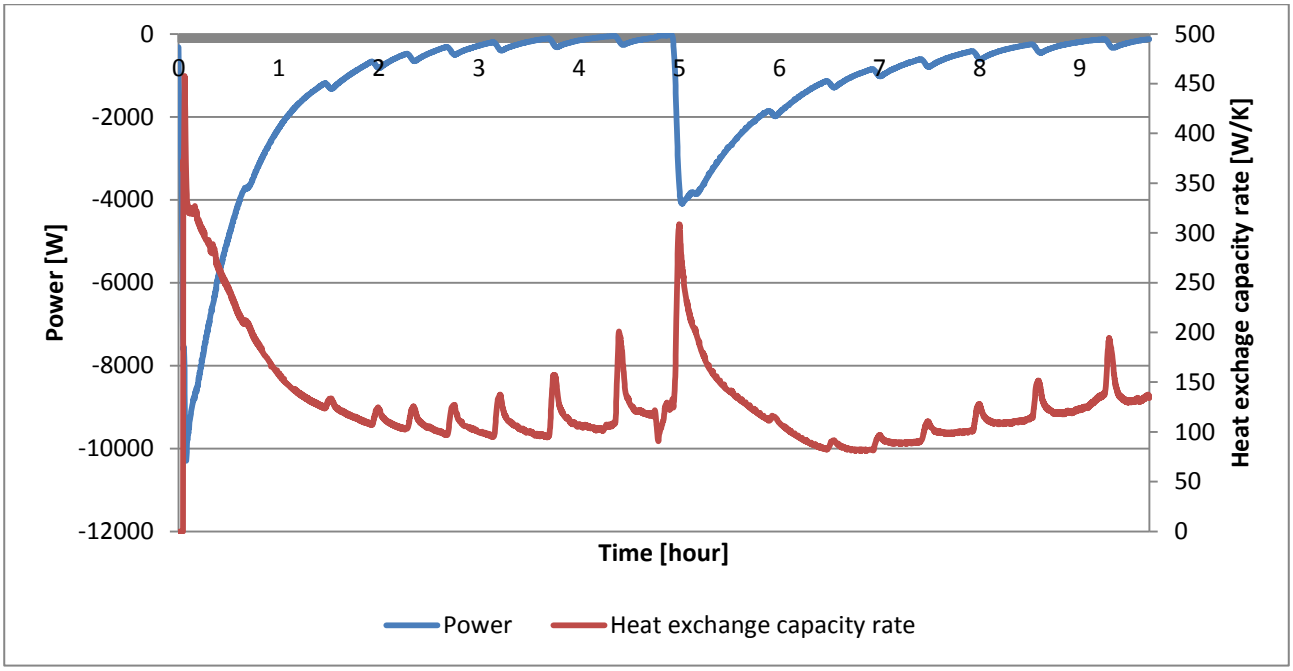

Figure 26. Discharge to supercooled state and discharge after activation.

The discharge power reaches 10 kW initially and 4 kW for the discharge after. The heat exchange capacity rate drops from 400 to 80 W/K for the discharge and activation. Fig. 27 shows the heat exchange capacity rate as a function of storage temperature.

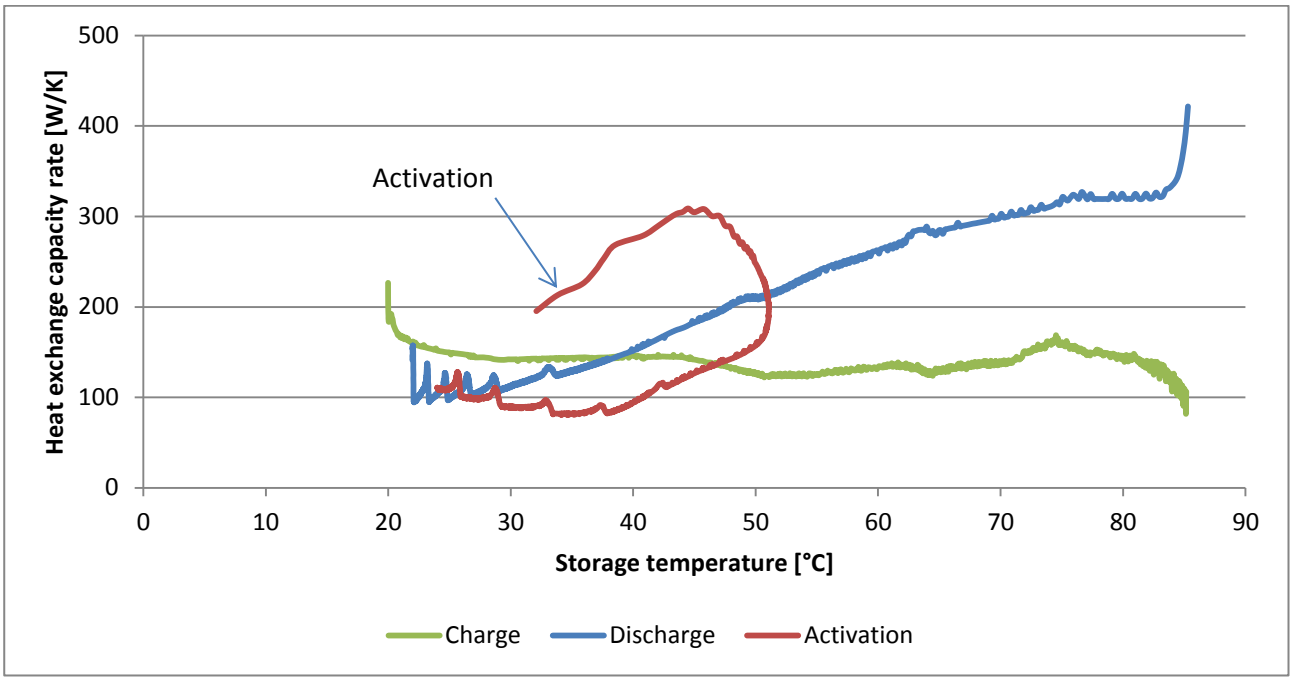

Figure 27. Heat exchange capacity rate as a function of storage temperature for charge discharge to supercooled state and discharge after activation.

Fig. 28 shows the heat exchange capacity rate as a function of the charge power.

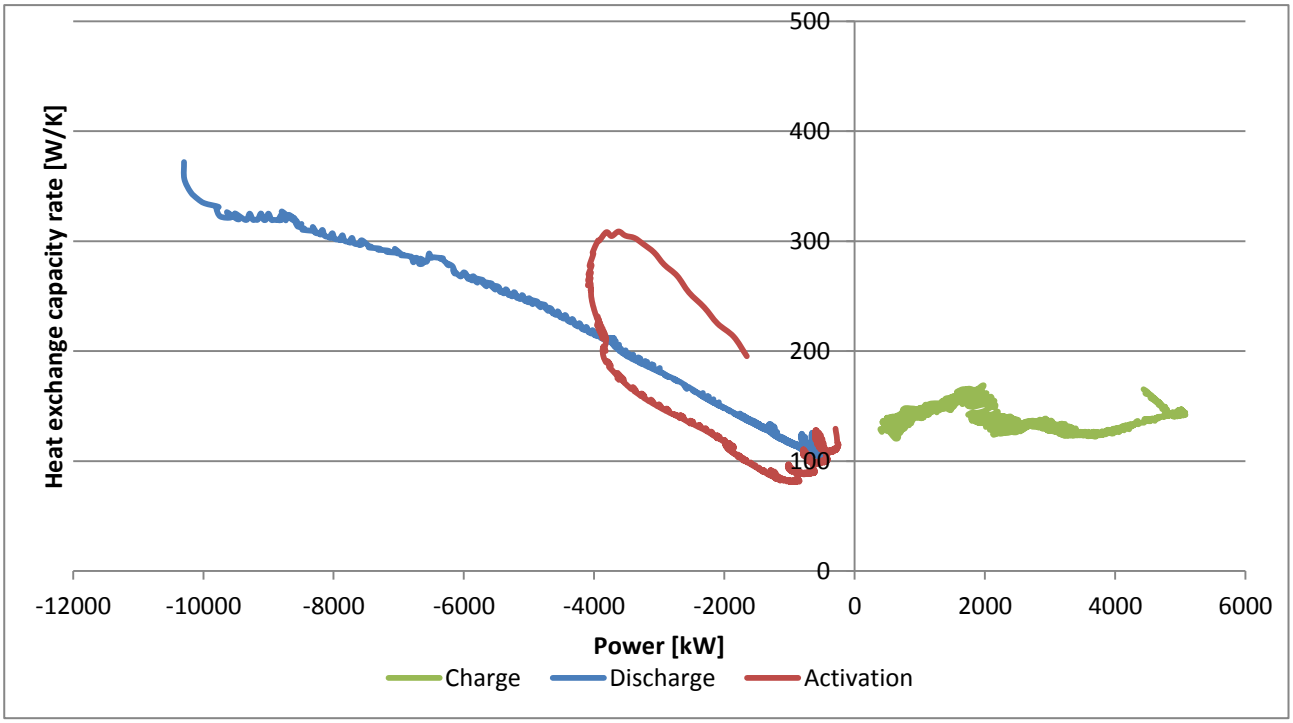

Figure 28. Heat exchange capacity rate as a function of charge power.

3.2.3 Test cycle 9:

The conditions for the 9th test cycles are displayed in Tab. 12. At the start of this test cycle approximately 12 cm of liquid was observed above the solid layer in the top of the storage tank. This shows that the design of the storage tank does not favor the convection and mixing of the salt water mixture that is needed to avoid phase separation when using the extra water principle (Furbo, 1982).

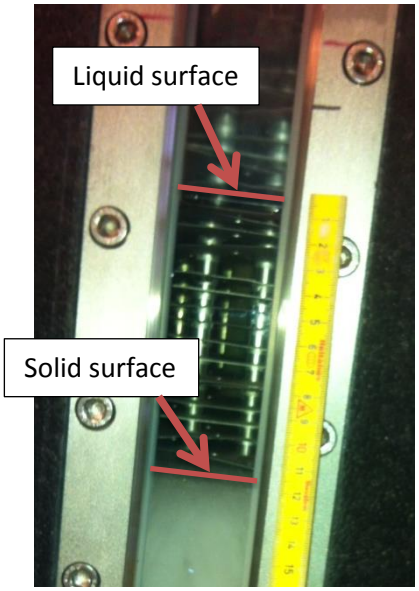

Figure 29. Top surface of salt water mixture before test cycle 9.

The test cycle was initiated with an average storage temperature of 19°C. Fig. 30 shows the temperature development for the sensors measuring inlet, outlet, ambient, surface and internal temperatures as well as the flow rate for the whole test cycle. The flow rate was 7.4 l/min for charge and 5.7 l/min for discharge.

Table 12. Power and flow rate.

	Heating element Power	Flow rate	Set temperature
Charge	**6 kW**	**7.4 l/min**	**90°C**
Discharge	**-**	**5.7 l/min**	**18-20°C**

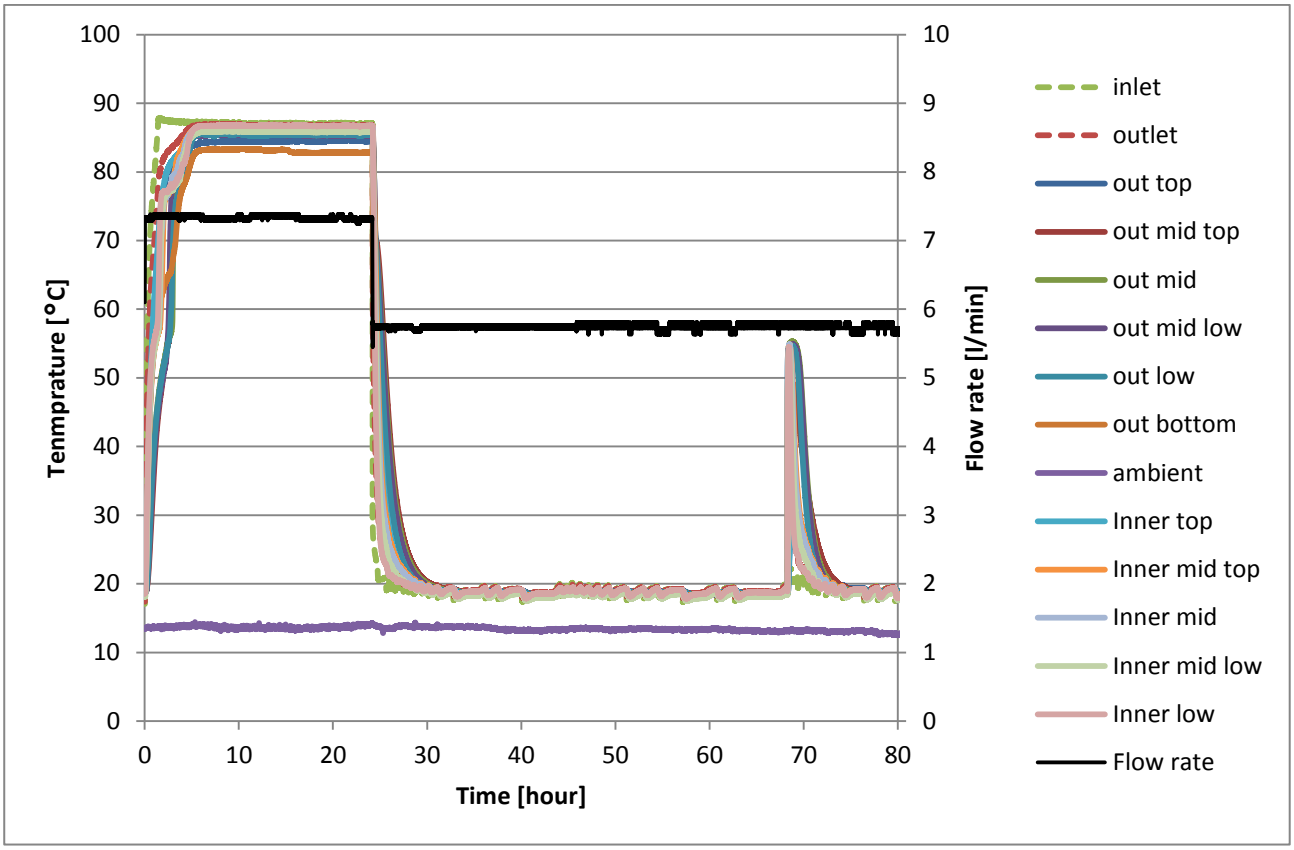

Figure 30. Temperature development and flow rate.

The storage was charged for 24 hours but stable temperatures were reached after 6 hours. The storage module was then actively discharged to supercooled state. The storage module was fully discharged to supercooled state after approximately 6 hours where it was kept for another 38 hours before it was activated. It took another 4-5 hours to fully discharge the module after activation.

Fig. 31 shows the temperature development in the charging period in detail.

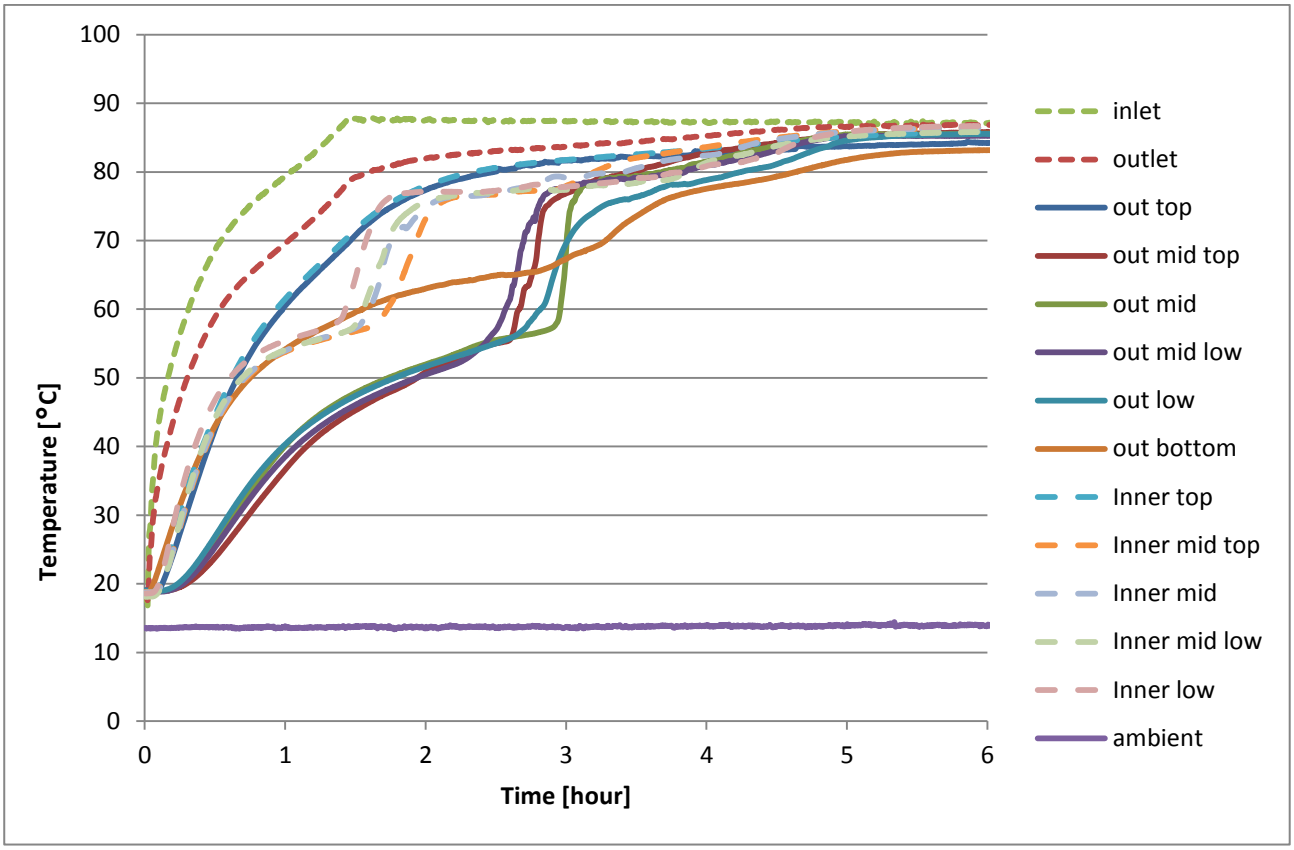

Figure 31. Temperature development during charge.

From Fig. 31 can be seen that the lower part of the storage was the part of the storage that heated up the slowest. The point where the temperature starts to increase rapidly at around 58°C indicates complete phase change. The inner measurement points reacted faster compared to the sensors on the outer surface. The sensors “inner top” and “outer top” did not show the characteristic temperature development for a melting process as the other sensors did but had a more smooth development as for a temperature increase of a material in one phase. This could be because the sensor was located in the liquid layer on top of the solid crystals at the start of the charge. The last sensor to reach the stable state was the sensor on the bottom of the tank. The vertical temperature stratification of the tank was minor according to the inner sensors. There was only a short time delay from the lower sensors to the upper sensors reaching the rapid temperature increase the indicates the fully melted state. The sensors on the outer surface show that the fully melted state is reached in random order.

Fig. 32 shows the discharge to supercooled state in detail.

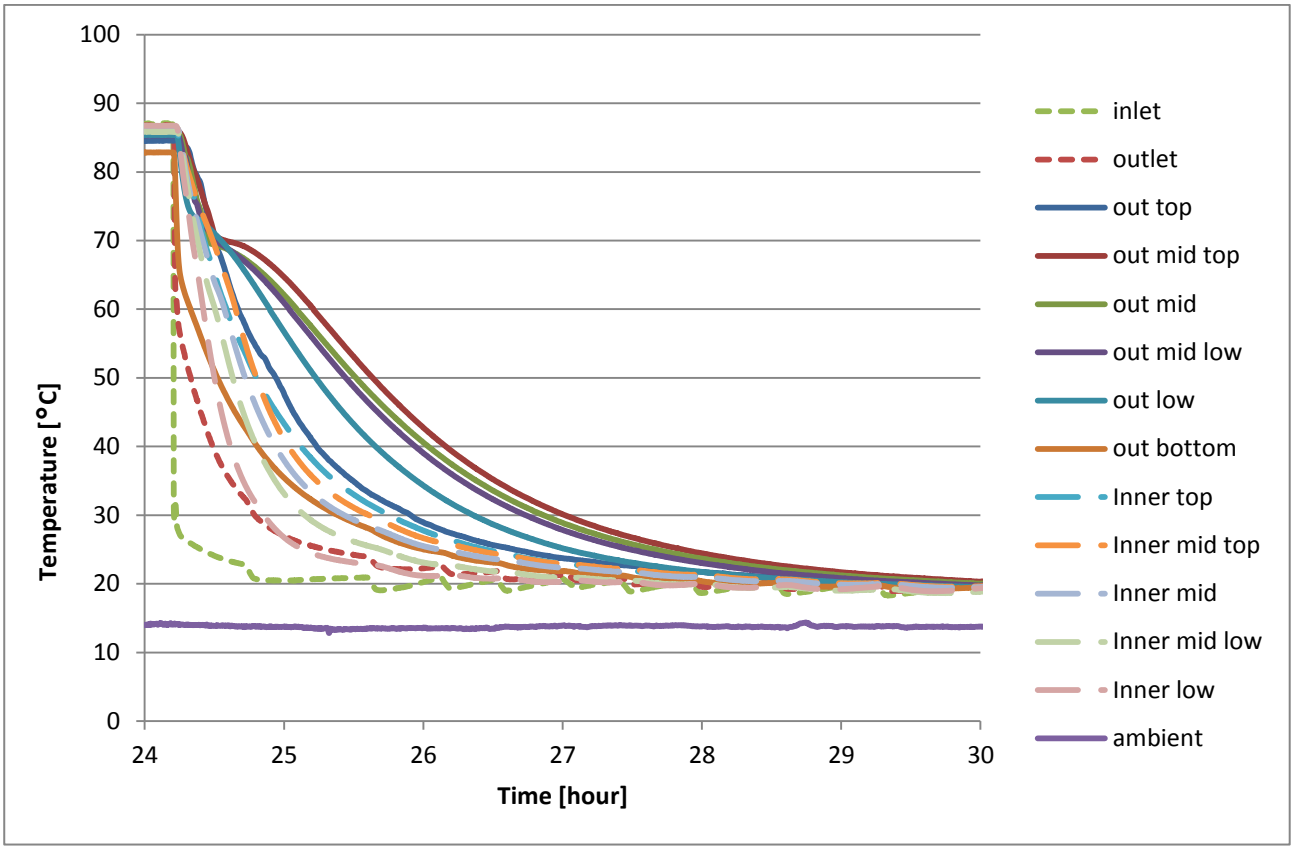

Figure 32. Temperature development for discharge to supercooled state.

Fig. 33 shows the temperature development for the activation and the following discharge.

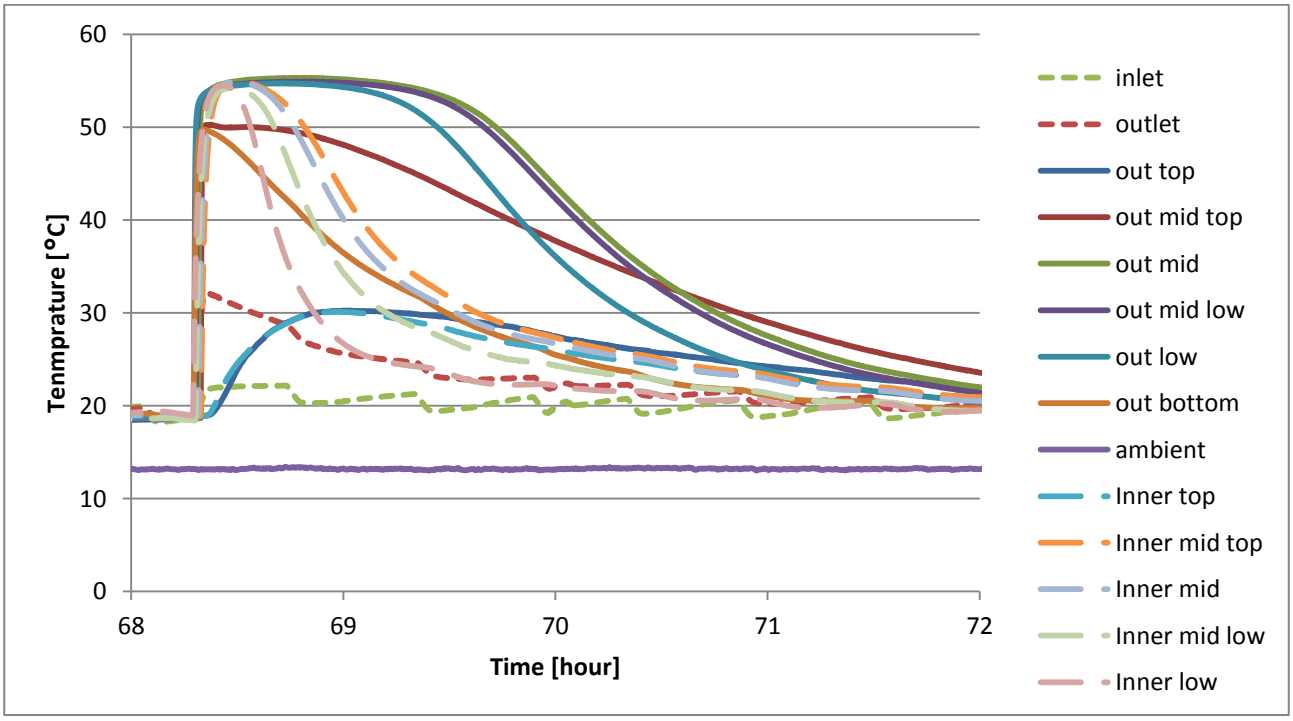

Figure 33. Temperature development for activation and discharge.

Activation started from the bottom initiated by a little shaking of the module. The sensor “out low” was the first to react. The sensors in the top of the module did not reach the same temperature of approximately 55°C after activation as the others did. The sensors “out top” and “inner top” reach just 30°C.

Fig. 34 shows the mean storage temperature and the thermal energy content E(t) of the storage based on the measurements for the test cycle.

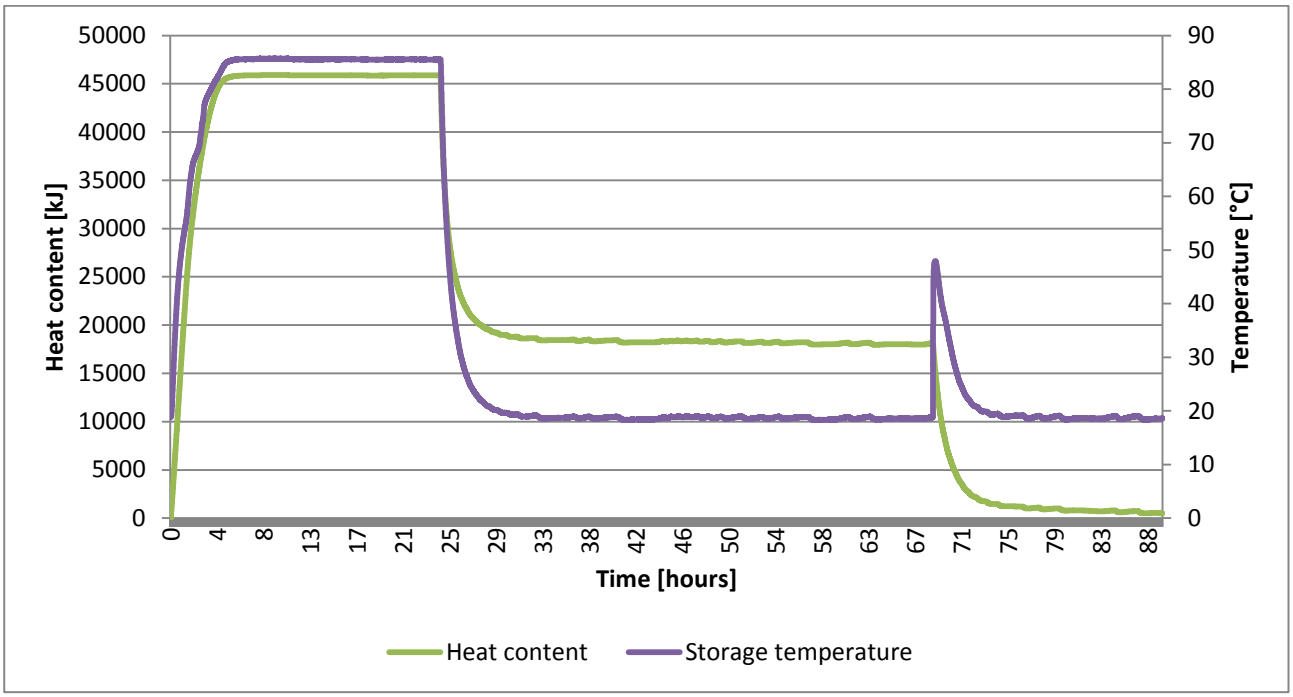

Figure 34. Heat content and storage temperature.

Tab. 13 lists the start, maximum and end temperature of the storage for the test cycle.

Table 13. Storage start temperature, maximum temperature and end temperatrure.

T_{start}	18.8°C
T_{max}	85.7°C
T_{super}	18.6°C
T_{end}	18.6°C

Measured energy changes:

Tab. 14 lists the thermal energy content $E_{charge,exp}$ determined by the measurements at T_{max} after discharge to supercooled state $E_{super,exp}$ and after the activation and discharge $E_{end,exp}$. The start temperature was the reference temperature for the calculation of the energy content.

Table 14. Thermal energy content at start, fully charged, supercooled state and end of test cycle based on measurements.

E_{start}	0 kJ
$E_{charge,exp}$	45900 kJ
$E_{super,exp}$	18000 kJ
$E_{end,exp}$	300 kJ

Theoretical energy change:

Based on the compound theory and the the theoretical thermal energy change of the storage module are listed in Tab. 15.

Table 15, Thermal energy content based on compound theory.

$E_{start,theo}$	0 kJ
$E_{charge,theo}$	47380 kJ
$E_{super,theo}$	20000 kJ
$E_{end,theo}$	30 kJ

Based on the theory of thermal energy content for incongruently melting salt hydrates the theoretical energy content of the storage at the different states are listed in Tab. 16.

Table 16, Thermal energy content based on incongruently melting salt hydrate's thermal energy content.

$E_{start,theo}$	0 kJ
$E_{charge,theo}$	47400 kJ
$E_{super,theo}$	20150 kJ
$E_{end,theo}$	40 kJ

At maximum temperature the measured thermal energy content was 3% lower than the theoretical. At supercooled state the measured content was 2000 kJ or 10% below than the theoretical calculated content.

The mean storage temperature of 18.8°C at the start of the charging was used as the reference temperature. The measured and the theoretical energy contents are therefore 0 kJ at this temperature.

Fig. 35 summarizes the theoretical and the measured thermal energy content of the salt water mixture per mass unit based as function of the mean storage temperature of both inner and outer temperature sensors.

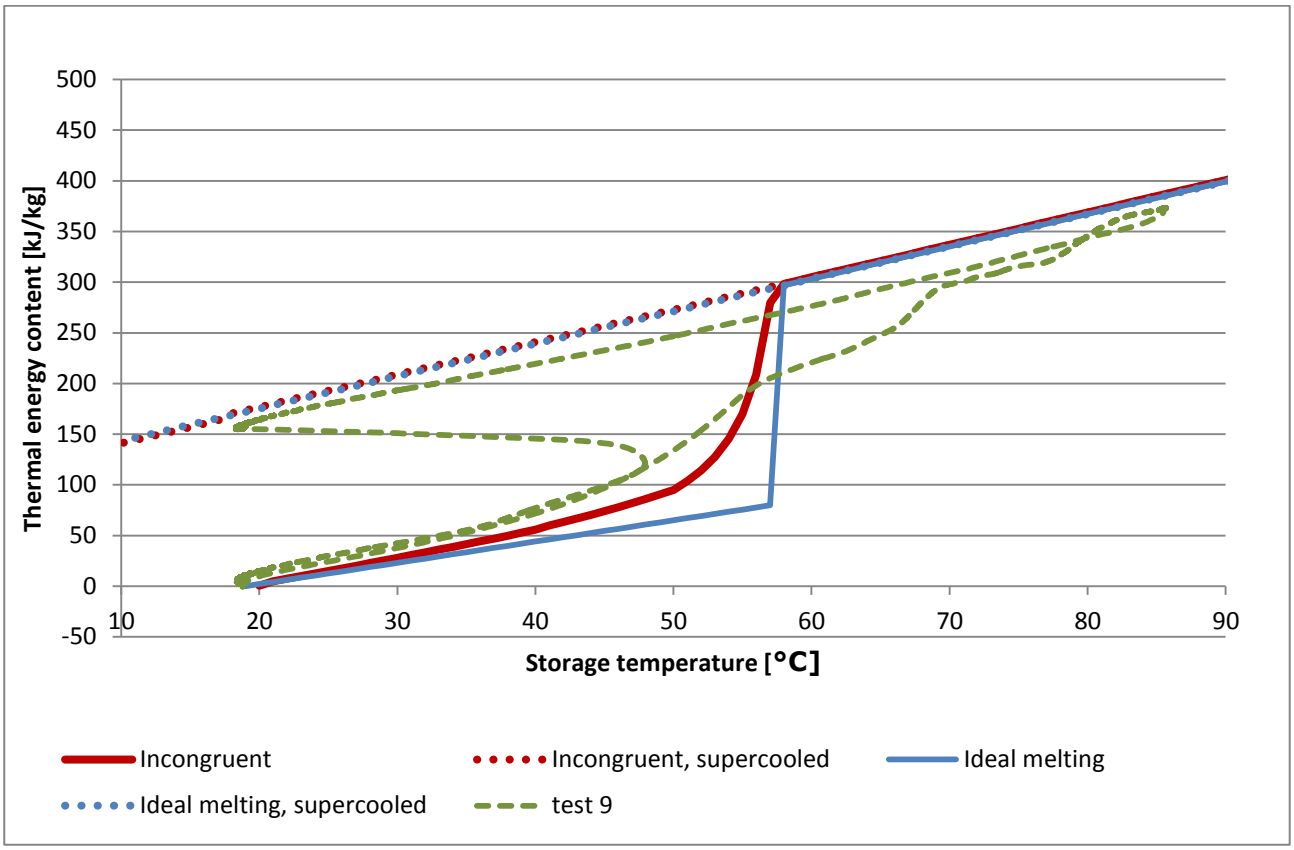

Figure 35. Theoretical and measured thermal energy content of salt water mixture per mass.

From Fig. 35 can be seen that the salt water mixture had a lower thermal energy content compared to the theoretical.

The power of the charge is displayed in Fig. 36 along with the heat exchange capacity rate for the same period. The mean storage temperature of both inner and outer sensors was used in the calculation for the heat exchange capacity rate.

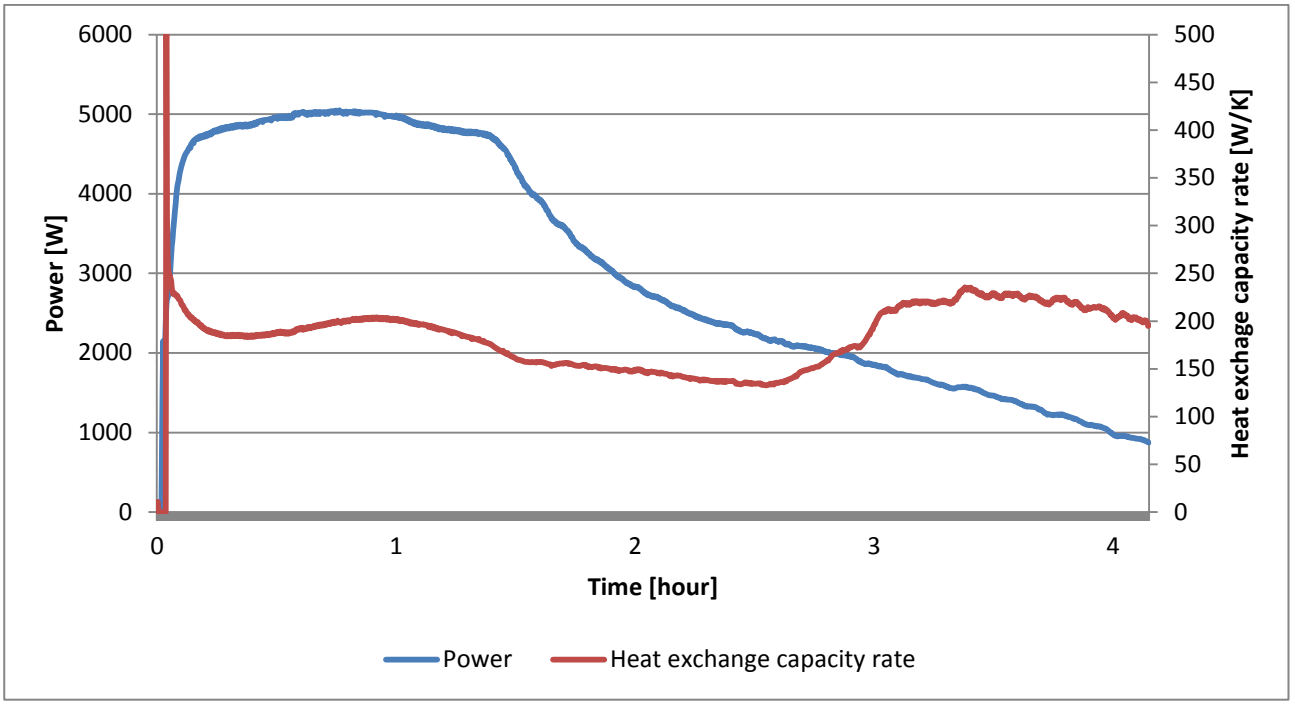

Figure 36. Power and heat exchange capacity rate over time.

The discharge power from T_{max} to supercooled state is displayed in Fig. 37 along with the heat exchange capacity rate.

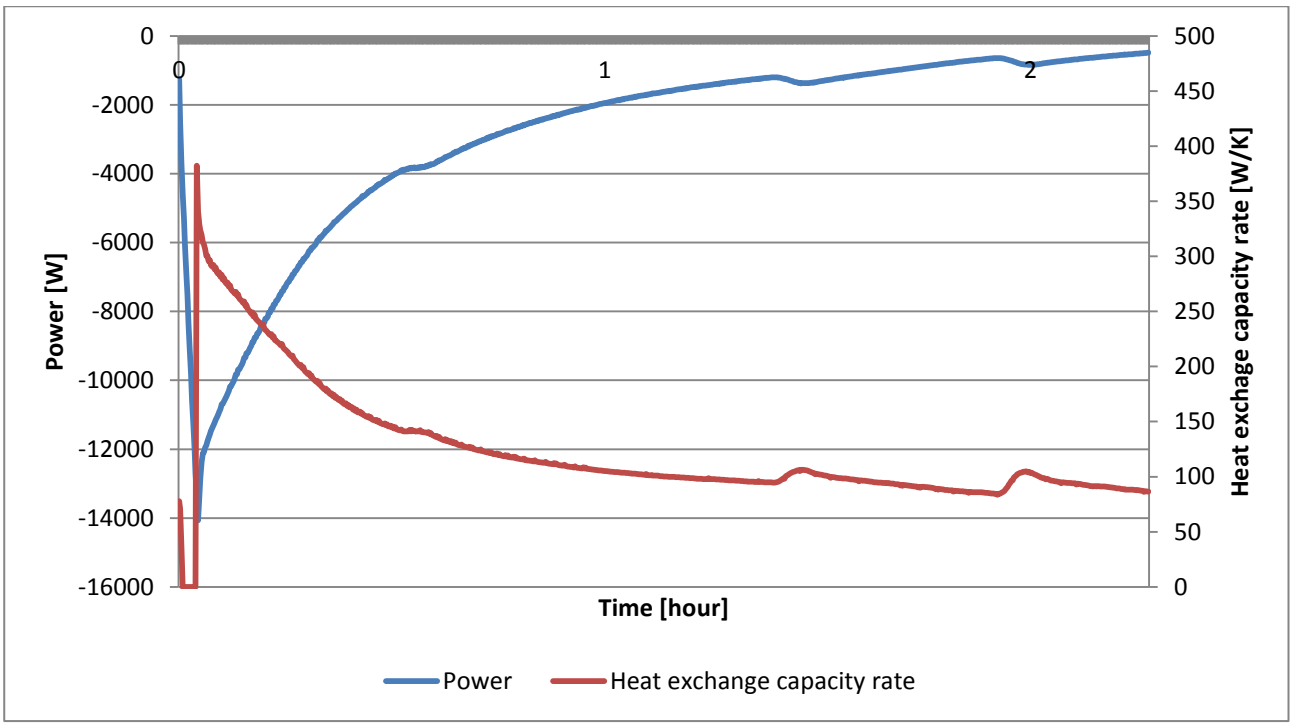

Figure 37. Discharge to supercooled state.

Fig. 38 shows the heat exchange capacity rate as a function of storage temperature.

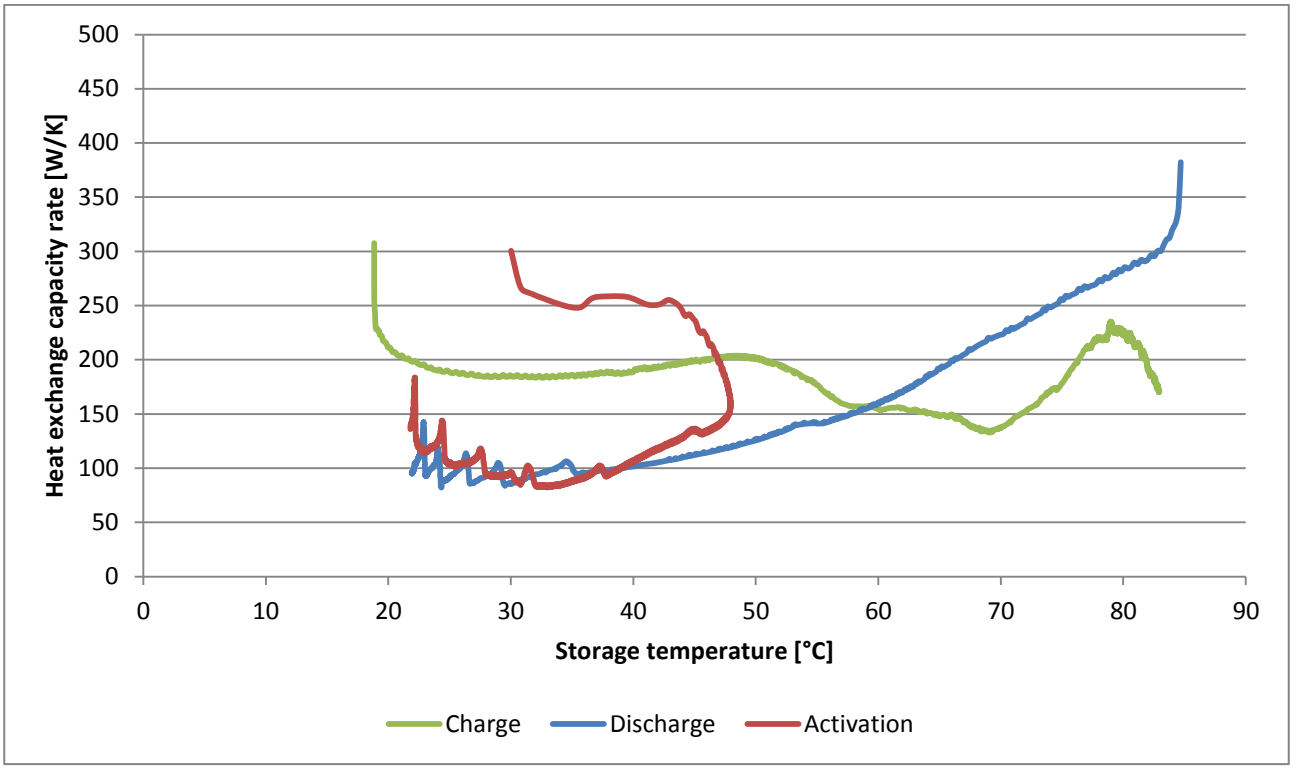

Figure 38. Heat exchange capacity rate as a function of storage temperature.

Fig. 39 shows the heat exchange capacity rate as a function of charge and discharge power.

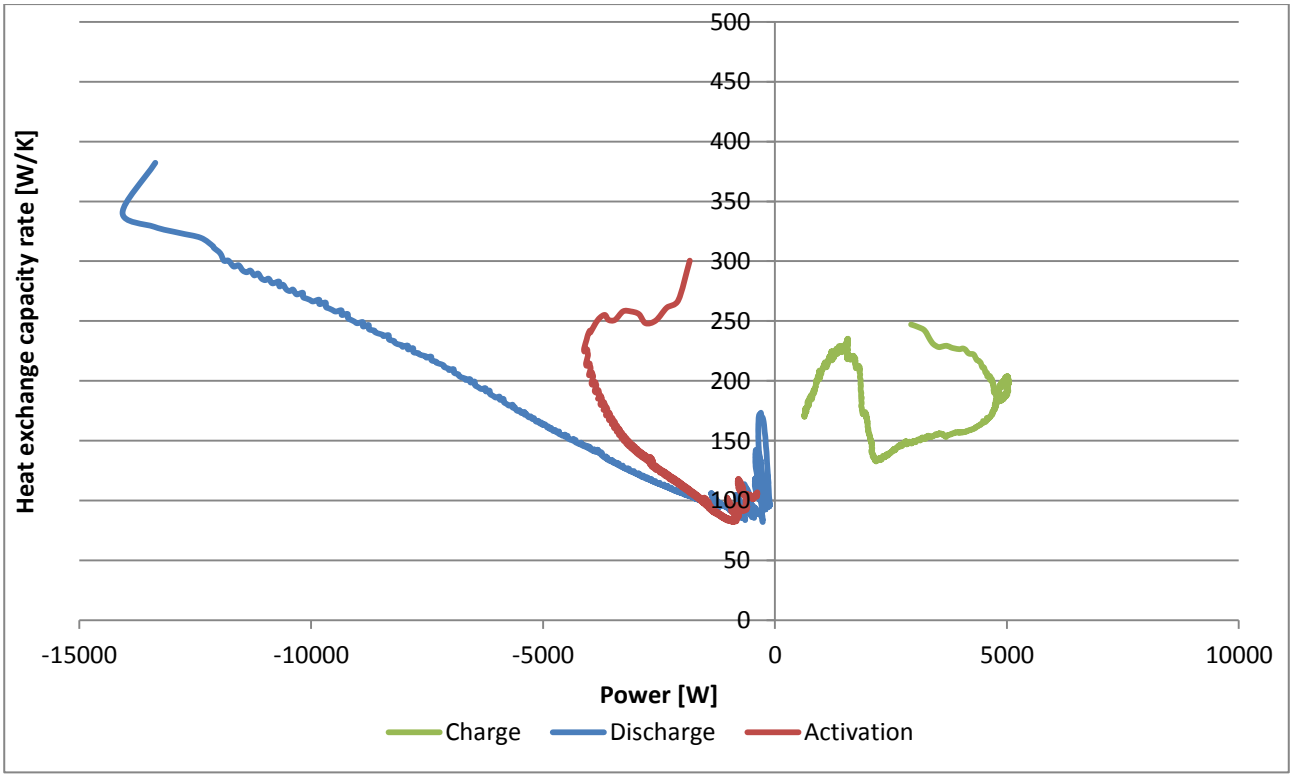

Figure 39. Heat exchange capacity rate as a function of charge and discharge power.

3.3 Summary and discussion of test with sodium acetate water mixture

Fig. 40 shows a summary of heat exchange capacity rate as a function of power for charging for selected test cycles. The mean storage temperature of both inner and outer sensors was used in the calculation for the heat exchange capacity rate. The max power was limited by the heating element power setting of 3, 6, or 9 kW respectively.

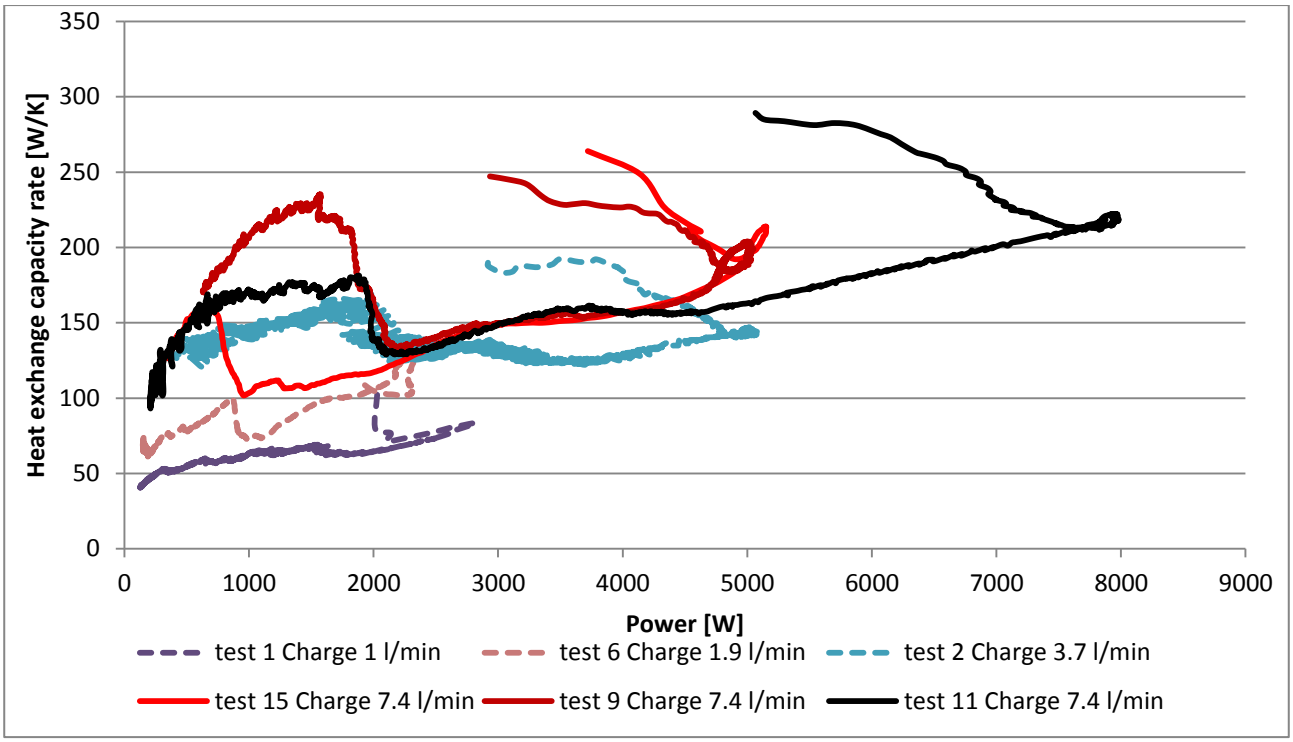

Figure 40. Summary of heat exchange capacity rate as a function of power for charging.

The series of test cycles have shown that the heat exchange capacity rate was 50 – 250 W/K for the charging of the Thermobatterie filled with the salt water mixture. The heat exchange capacity rate was highly depending on the charge power and flow rate. There was a large deviation between the heat exchange capacity rates at low charging power for a flow rate of 7.4 l/min.

Fig. 41 shows a summary of heat exchange capacity rate as a function of storage temperature for charging

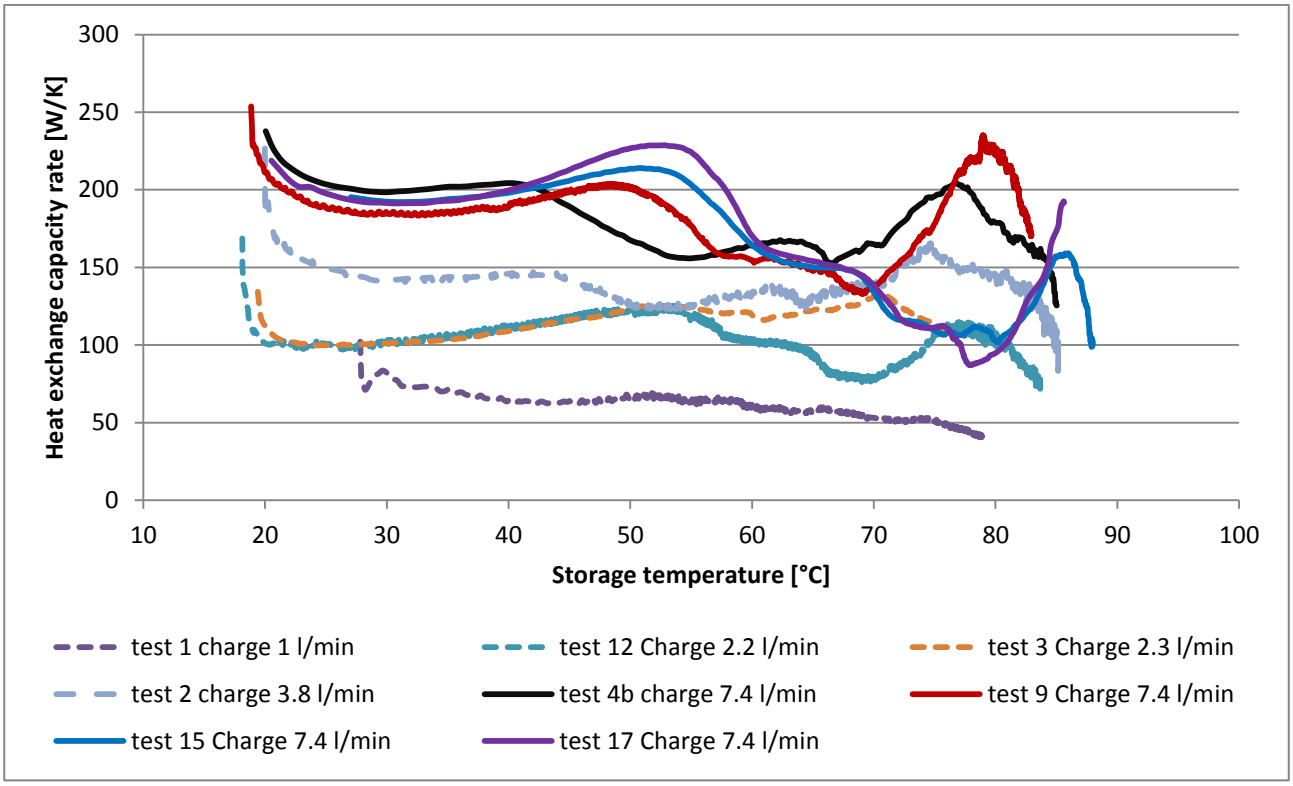

Figure 41. Summary of heat exchange capacity rate as a function of storage temperature for charging.

For charging, the heat exchange capacity rate as a function of temperature seems stable around 200 W/K for temperatures below melting point. During the phase change the heat exchange capacity rate tended to drop to 90 – 150 W/K. The heat exchange capacity tended to increase again at high temperatures when the phase change was complete. There will be some uncertainty in this analysis as the exact temperature of the salt water mixture is determined with some inaccuracy.

For the flow rate of 7.4 l/min the heat exchange capacity rate varied from 90 – 235 W/K.

Fig. 42 shows the heat exchange capacity rates as a function of powers for discharge in selected test cycles.

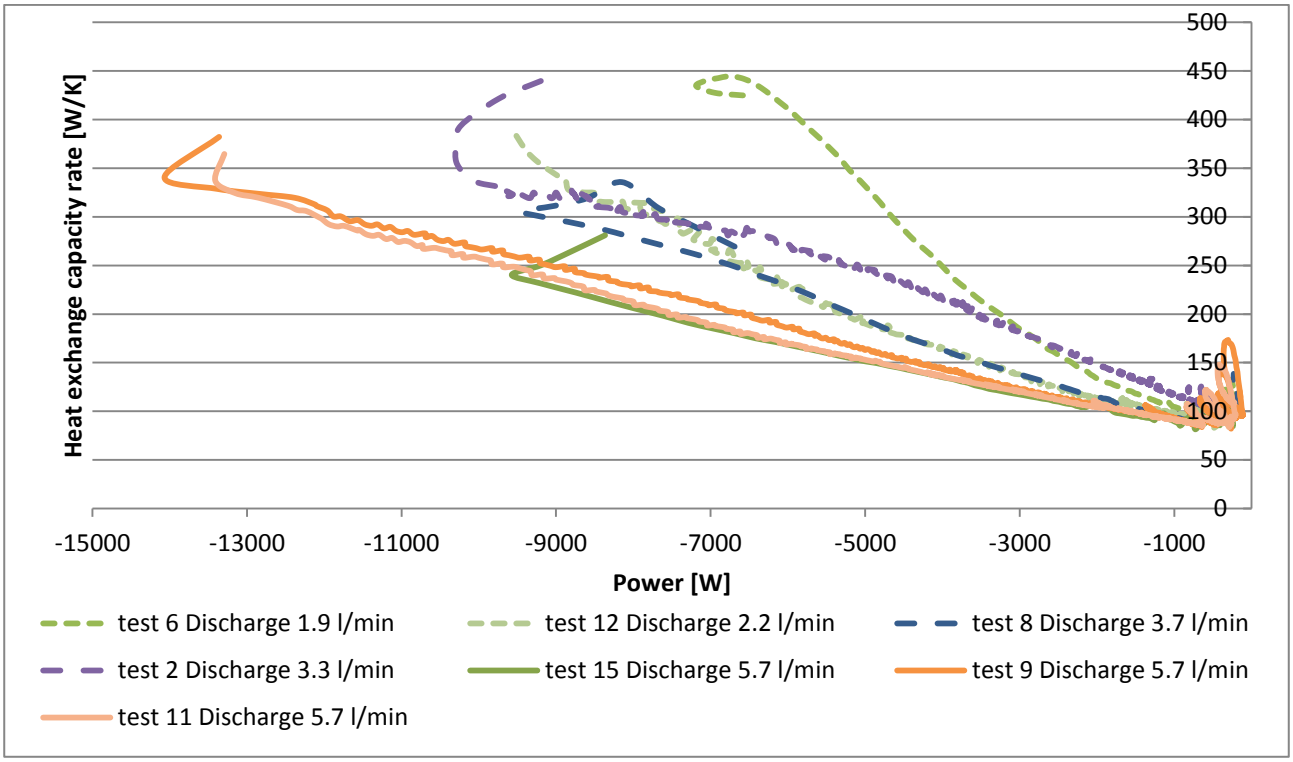

Figure 42. Summary of heat exchange capacity rate as a function of power for discharging.

For discharging to supercooled state with a constant inlet temperature of 20°C the heat exchange capacity rate seem proportional with the discharge power. Lower flow rates appeared to have lower heat exchange capacity rates. With a flow rate of 5.7 l/min the heat exchange capacity rate topped at 350 W/K in the beginning of the discharge with at discharge power of up to 14 kW.

Fig. 43 shows the heat exchange capacity rate as a function of the storage temperature for discharging.

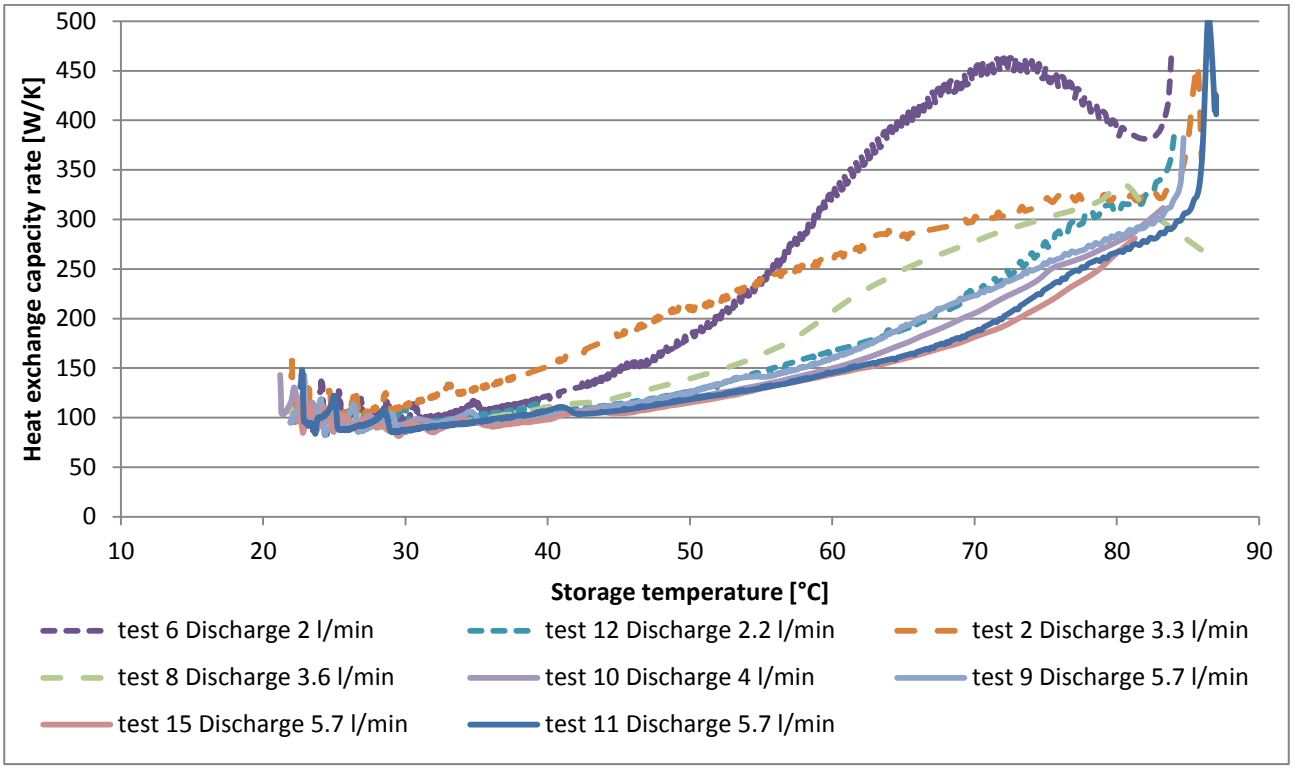

Figure 43. Summary of heat exchange capacity rate as a function of storage temperature for discharging.

The heat exchange capacity rate seems to decrease with decreasing storage temperature.

Fig. 44 shows the heat exchange capacity rate as a function of power for discharging.

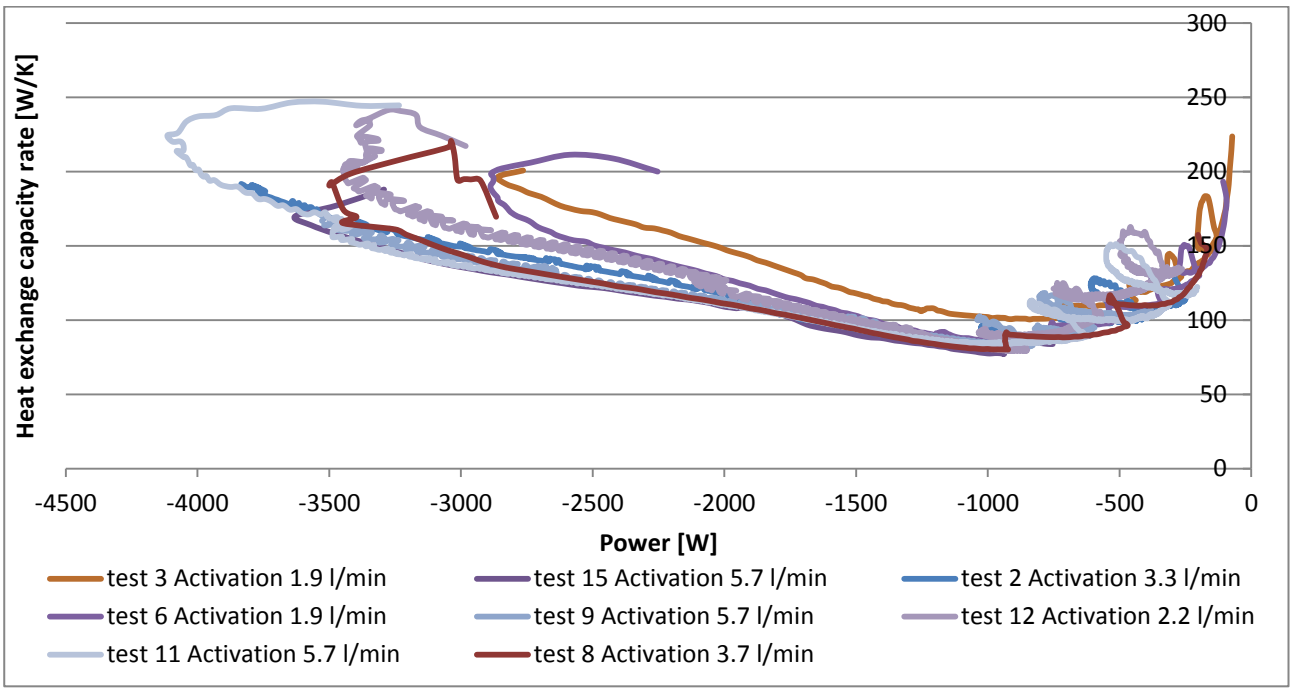

Figure 44. Summary of heat exchange capacity rate as a function of power for discharging after.

For discharge after activation the heat exchange capacity rate starts at 200 – 250 W/K dropping to 80 – 100 W/K during the discharge. Higher flow rates had higher discharge powers. However the heat exchange capacity rate does appear to be in the same interval unaffected of the flow rate.

Fig. 45 shows the heat exchange capacity rate as a function of storage temperature for discharging after activation.

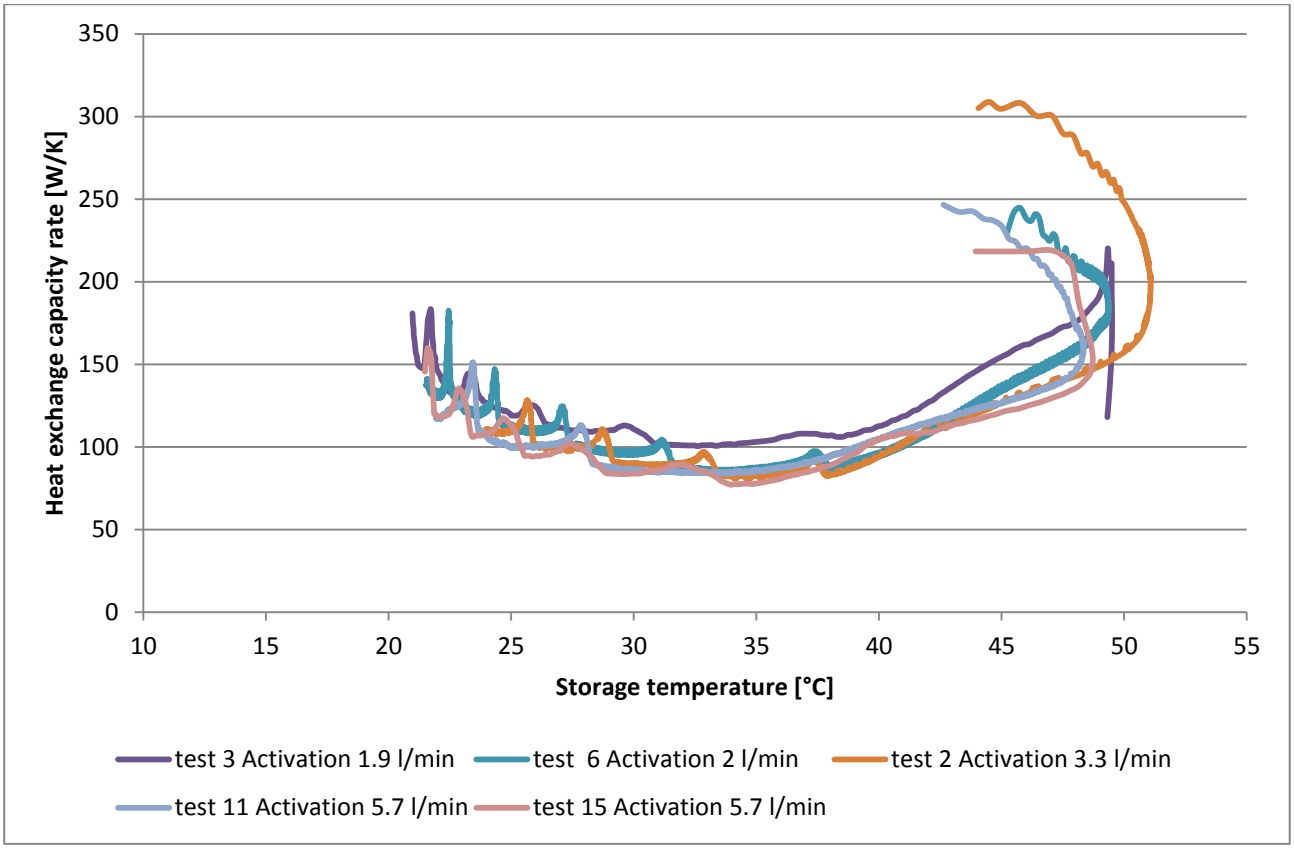

Figure 45. Summary of heat exchange capacity rate as a function of storage temperature for discharging after activation.

It may be seen in Fig. 45 that the heat exchange capacity rate drops over the discharge period as the storage temperature decreases.

Figure 46 show the theoretical energy content per mass of saltwater mixture and the measured heat contents for some selected test cycles. It may be seen that there are some deviations between the test cycles of how much energy is stored and released from the salt water mixture. In the 2nd test cycle the agreement between the measurement and the theoretical predictions is good. For the 12th cycle the energy content at charged and supercooled state are roughly 20 kJ/kg below the theoretical level. For the 15th test cycle the charged energy fits well with the theory but the energy discharged after activation is 35 kJ/kg below the theoretical content.

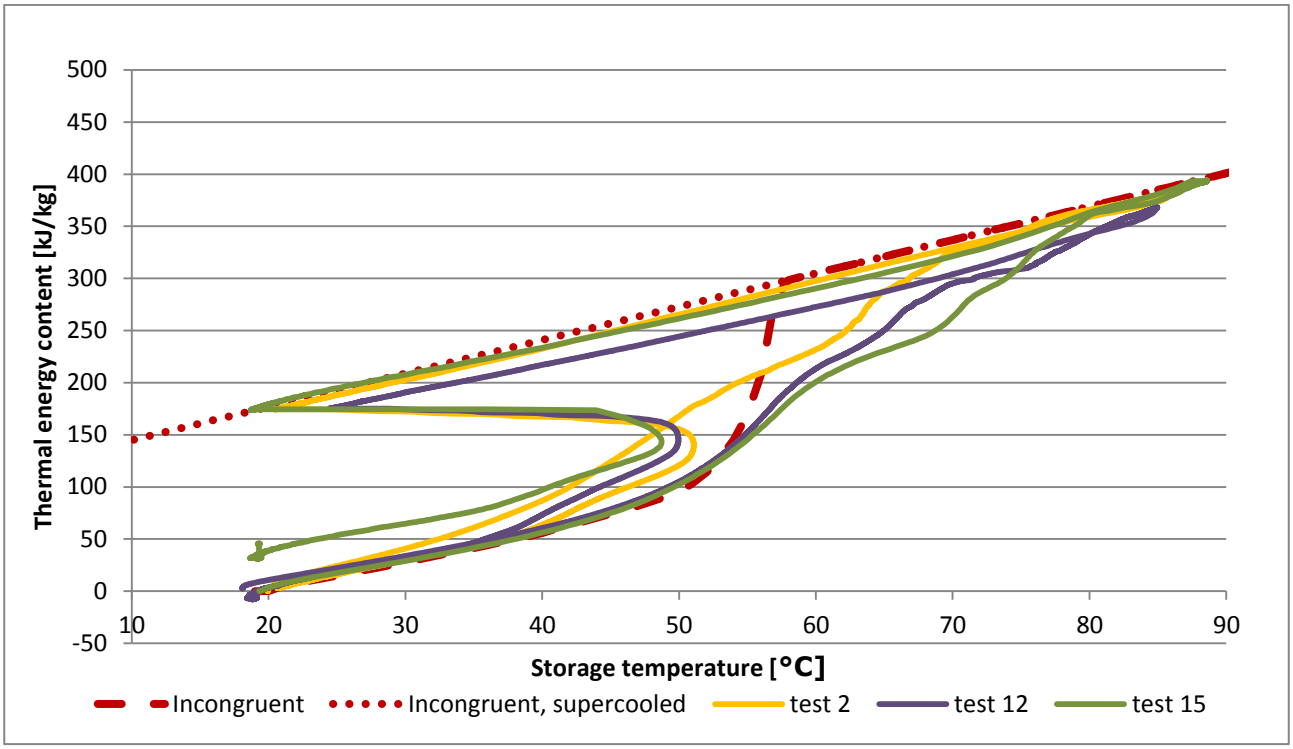

Figure 46. Measured and theoretical thermal energy content of salt water mixture for selected tests.

The test cycles were with relative short storage periods when considering seasonal heat storage. Longer storage periods with the salt water mixture in supercooled state should be investigated as the phase separation effect may worsen over longer time resulting in lower energy discharged after activation.

Of the 17 test cycles the module activated spontaneously 10 times during discharge and supercooled to stable ambient temperature 7 times. The module was activated one time by a hammer on the window frame and 6 times by slight shaking of the module. The crystallization always started form the bottom.

The rod with temperature sensors inserted in the center of the module may cause the instability of the supercooling as a torque by the mounting of the rod may work as a triggering mechanism. Similar cracks or joints inside the storage could also be the unwanted activation mechanism. Spontaneous activation during discharge may be caused by the same problem.

Activating the supercooled salt water mixture and discharging the module, with an inlet temperature of 20°C and a flow rate of 0.6 l/min gave an outlet temperature of 40°C or above for 3 hours. The average discharge power in this case was 1 kW. With a flow rate of 3.3 l/min and an inlet temperature of 20°C, an outlet temperature of 40°C was reached shortly during discharge. The outlet temperature dropped below 30°C after one hour. The discharge power for the first hour was in this case 3 kW on average. Discharging after activation with a flow rate of 5.7 l/min and an inlet temperature of 20°C gave an average discharge power of 2.8 kW with an average outlet temperature of 27°C for the first hour topping at 32°C in the first 10 minutes.

4. Conclusion

Testing the storage module filled with water showed that the heat capacity of the storage material primary stainless steel and aluminum excluding the storage material water or salt water mixture had the specific heat of 39 kJ/K.

The heat exchange capacity rate for the module filled with water was in the interval 200 W/K to 400 W/K for both charge and discharge and a flow rate of 7.4 l/min and 5.7 l/min respectively.

For the module filled with the sodium acetate water mixture the heat exchange capacity rate was in the interval 100 W/K to 250 W/K for charge; 100 W/K to 400 W/K for discharge to supercooled state and 80 W/K to 250 W/K for discharge after activation with a charging flow rate of 7.4 l/min and discharging flow rate of 5.7 l/min.

The measured energy content of the salt water mixture was close to or lower than the theoretical energy content in this application. Some test cycles showed that the discharge of thermal energy after activation from supercooled state was up to 21 % lower than the theoretical energy content in the last stable cycle. The reduction may be due to phase separation of the salt water mixture as a liquid layer was observed in the top of the storage module. The theoretical energy released from the supercooled salt water mixture at 19°C discharged to 19 °C again for the investigated salt water mixture was 177 kJ/kg. The measured energy released after activation varied from 140 – 177 kJ/kg with the lower values in the last cycles.

Fig. 47 shows the measured energy discharged from the module after activation for cycles where the mean storage temperatures before the activation and after are the same. The module was discharged to supercooled state with a temperature of 18.5°C to 21°C; after activation the module was then discharged to the same temperature level. Test cycles where the module activated spontaneously are left blank.

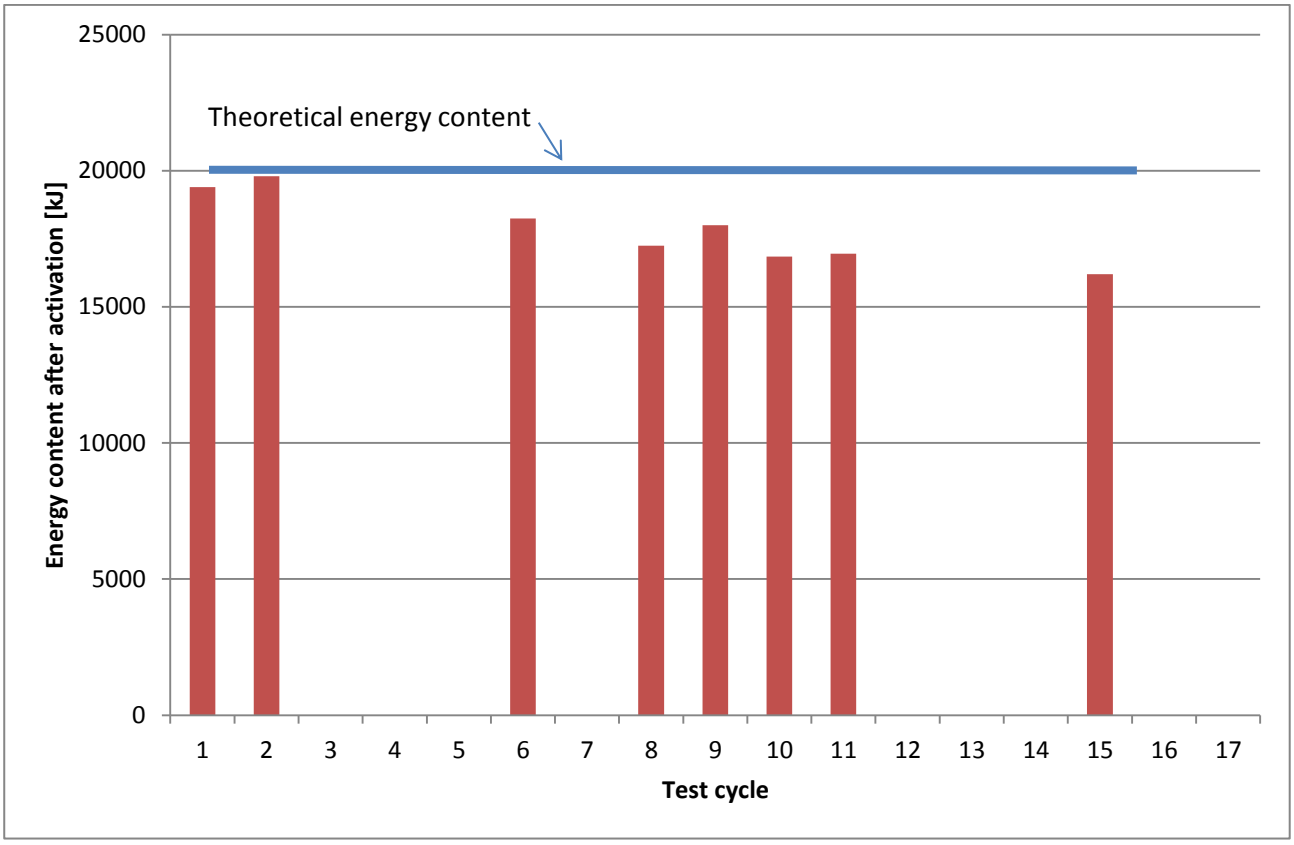

Figure 47. Measured energy content for cycles and theoretical energy content.

The tendency is that the discharged energy after activation was reduced over the cycles. For the 15th test cycle the discharged energy was 20 % below the theoretical energy content and 16 % below the energy discharged after activation in the first test cycle. The reduced energy content over the test cycles is in good agreement with the fact that more and more liquid layer was left in the top of the module after each test cycle. After the 17 test cycles a 20 – 25 cm liquid layer was left in the top of the module. This also showed that in this setup the extra water principle did not solve the problem with phase separation possibly due to lack of mixing by convection in the storage.

The test of heating the module stepwise showed that a value of 2.1 kJ/kgK for the specific heat in the solid state and 3.2 kJ/kgK for the specific heat in the liquid state gives good agreement between measurement and theoretical values. The theory of incongruently melting salt hydrates gave the best agreement between measurement and theoretical energy content in the temperature level below 58°C.

5. References

Araki, N., Futamura, M., Makino, A., & Shibata, H. (1995). Measurements of Thermophysical Properties of Sodium Acetate Hydrate. *Internaltional Journal of Thermophysics*, *16*(6), 1455–1466.

Cengel, Y. A. (2003). *Heat Transfer: A Practical Approach* (2nd ed.).

Furbo, S. (1982). Heat storage units using a salt hydrate as storage medium based on the extra water principle, (I).

Furbo, S. (1984). *Varmelagring til solvarmenalæg*.

Furbo, S. (2005). Heat Storage for Solar Heating Systems. BYG.DTU.

Rogerson, M. A., & Cardoso, S. S. S. (2003). Solidification in Heat Packs : III . Metallic Trigger. *AIChE Journal*, *49*(2).

6. Acknowledgement

Thanks to Christian Muhr and H.M. Heizkörper GmbH & Co. KG for supplying the Thermobatterie for testing at the Department of Civil Engineering at Technical University of Denmark and to Moritz Kuhlencord for delivering it to the test facility. Thanks to the technician Martin Dandanell for help with the installation and to special course student Tamas- Gabor Fulop for carrying out some of the test cycles.

6. Appendix A.

Test cycle 2 with water:

In a similar way as for the first test cycle the measurement data and calculations of heat exchange capacity rate and energy content for the next test cycles are displayed below. Test conditions are summarized in Table 1.

Table 1. Power and flow rate.

	Heating element Power	Flow rate	Set temperature
Charge	**9 kW**	**1.3 l/min -> 0.7 l/min**	**90°C**
Discharge	**-**	**0.95 l/min**	**18-20°C**

Fig. 1 shows the measured surface temperatures, inlet temperature, outlet temperature, ambient temperature and the flow rate for the heating and cooling cycle.

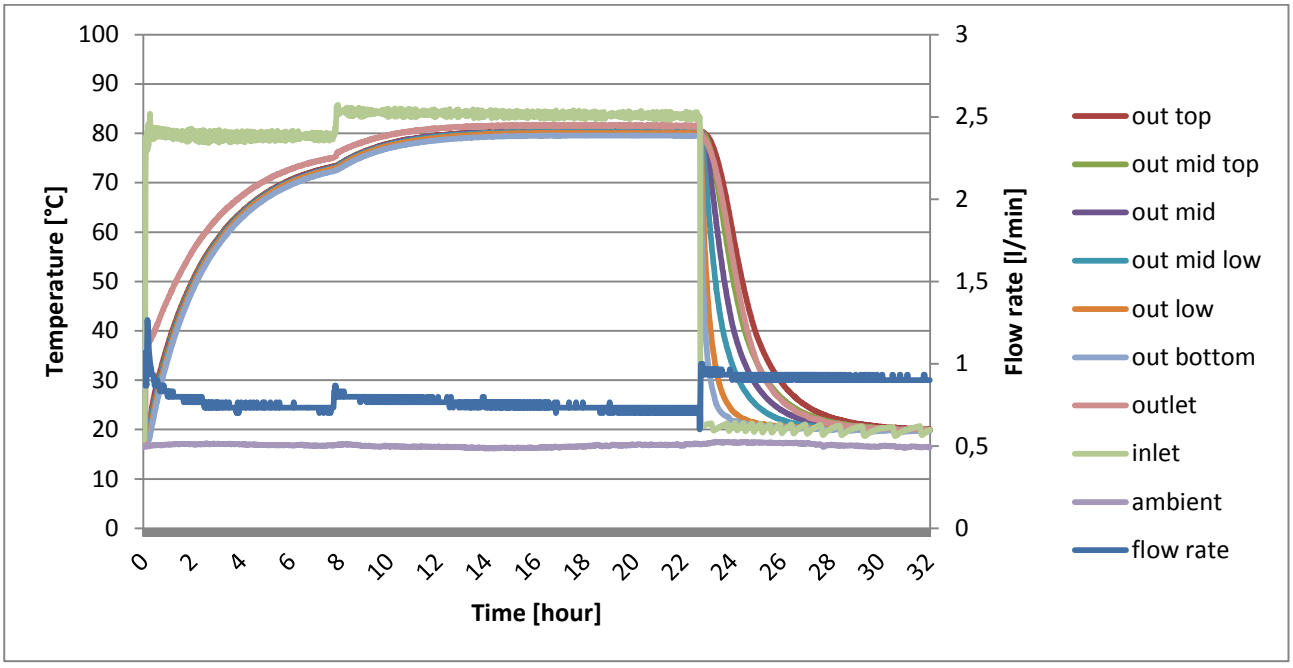

Figure 1. Temperature development and flow rate.

Fig. 2 shows the charge period in more details.

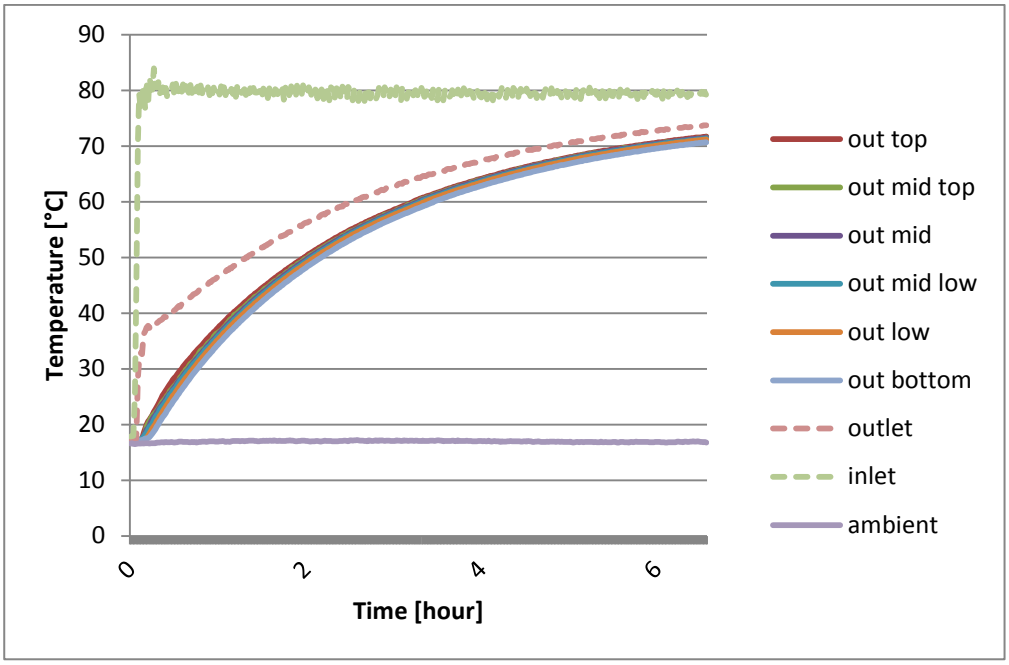

Figure 2. Temperature development for charge period.

Fig. 3 displays the discharge period in details.

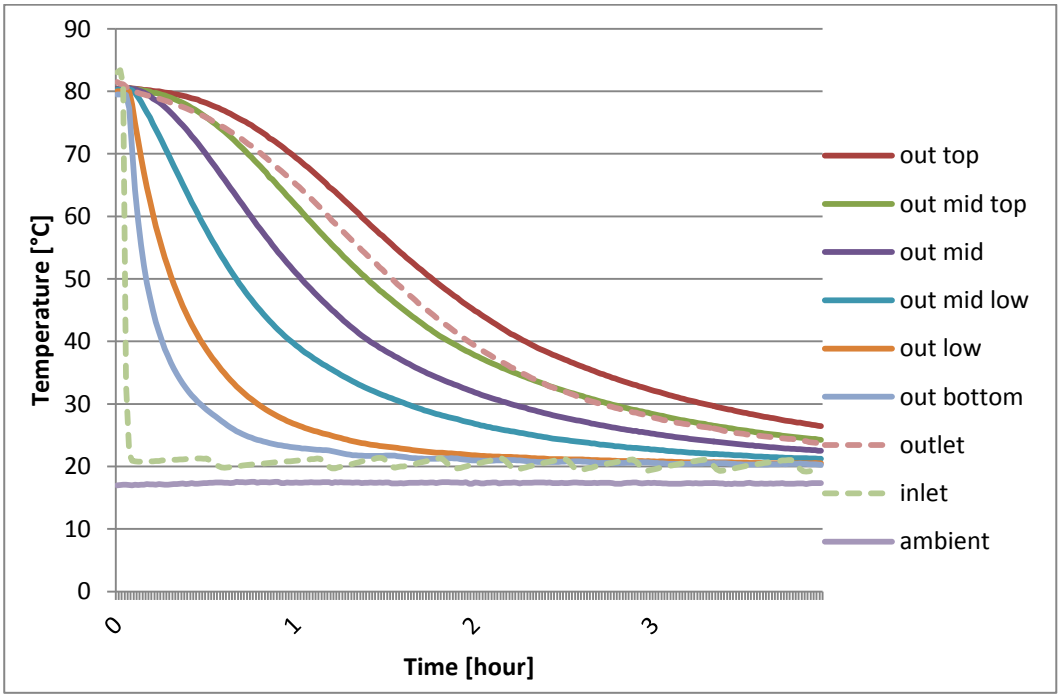

Figure 3. Temperature development for charge period.

Tab. 2 summarizes the start, maximum and end temperature of the storage with water.

Table 2. Start temperature, maximum temperature and end temperature of storage.

T_{start}	T_{max}	T_{end}
17.1 °C	80.3°C	19.9 °C

Figure 4. Energy content and mean storage temperature.Figure 4 displays the measured heat content of the storage above start condition and the mean temperature of the storage over time.

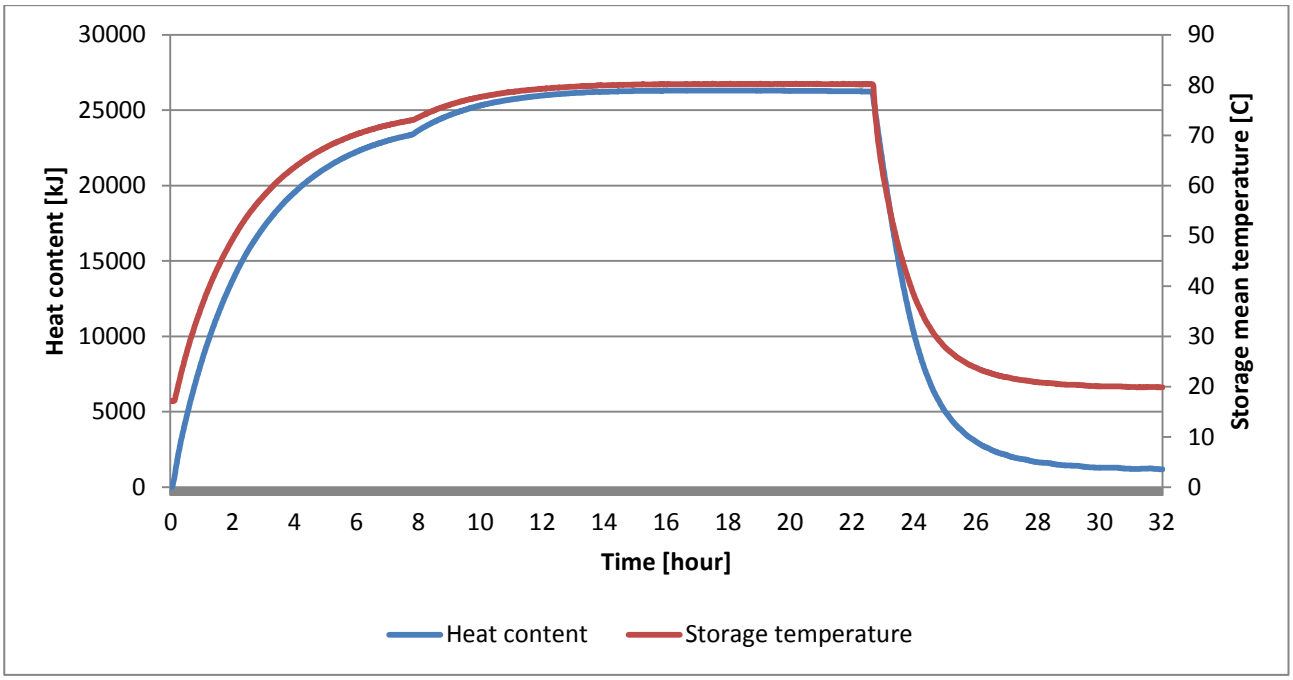

Figure 4. Energy content and mean storage temperature.

The maximum measured heat content of the storage is listed in the Tab. 3 along with the theoretical value.

Table 3. Measured and calculated heat contents during the test.

Max measured energy content $E_{max,exp}$	Theoretical max energy content $E_{max,theo}$
26500 kJ	26607 kJ

The deviation between the measured and the theoretical energy content at hot state is just 0.4%.

The heat exchange capacity rates for the charge and discharge periods are displayed in Fig. 5 and Fig. 6 along with the charge and discharge power.

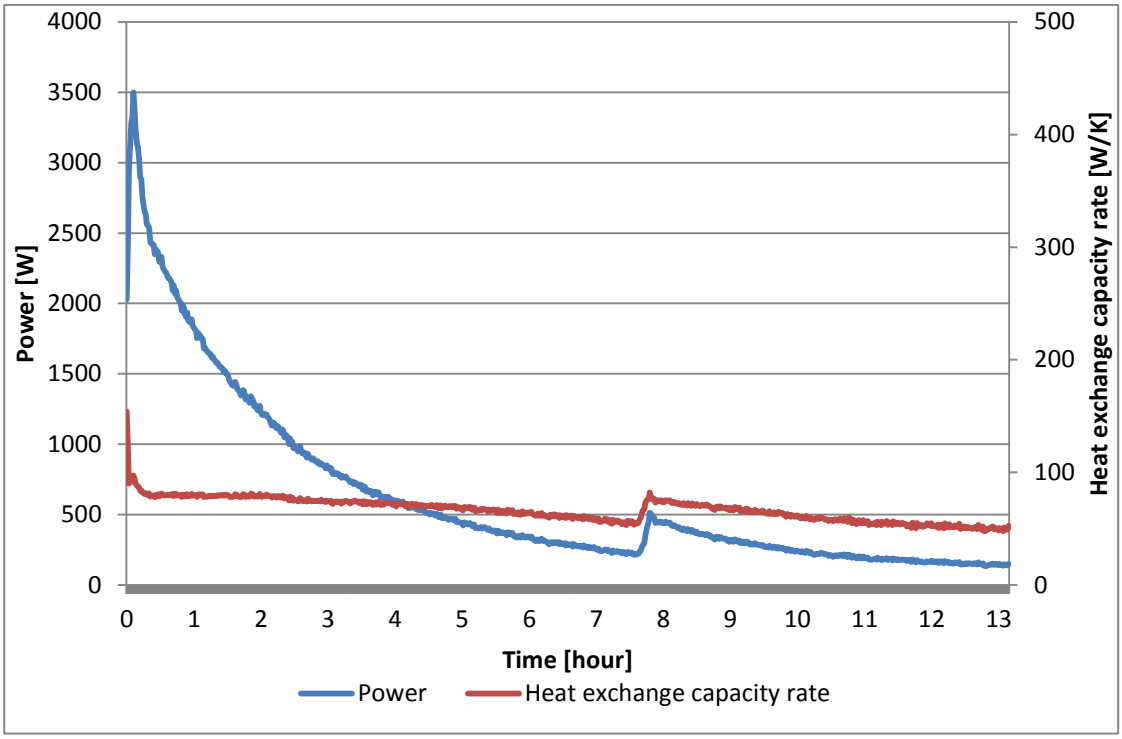

Figure 5. Power and heat exchange capacity rate over time for charge.

It was not possible to calculate the heat exchange capacity rate due to a high thermal stratification in the tank caused by the low flow rate. The outlet temperature was higher than the mean storage temperature and the formula for calculation heat exchange capacity rate is invalid.

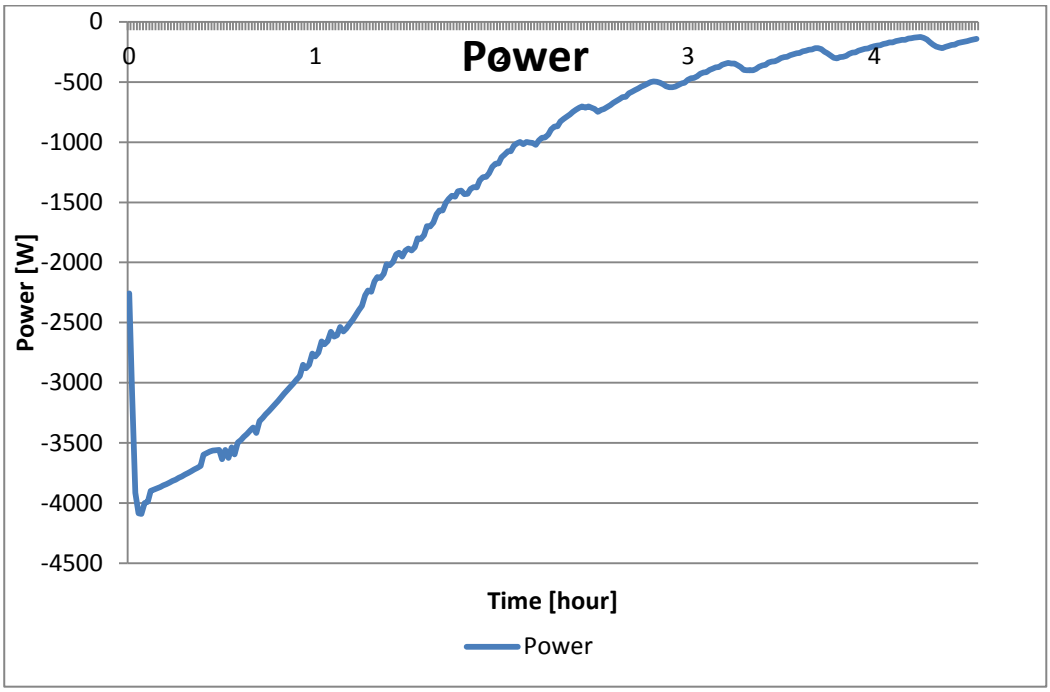

Figure 6. Power over time for discharge.

Heat exchange capacity rate is displayed as a function of the mean storage temperature for charge in Fig. 7.

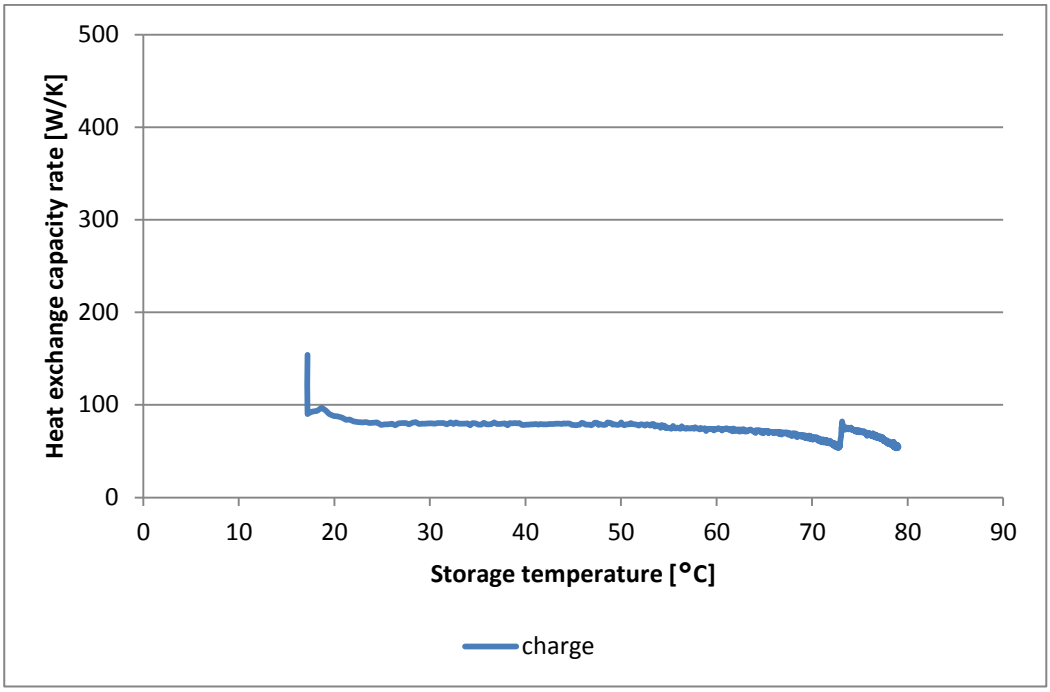

Figure 7. Heat exchange capacity rate as a function of storage temperature.

Heat exchange capacity rate is displayed as a function of the charge power in Fig. 8.

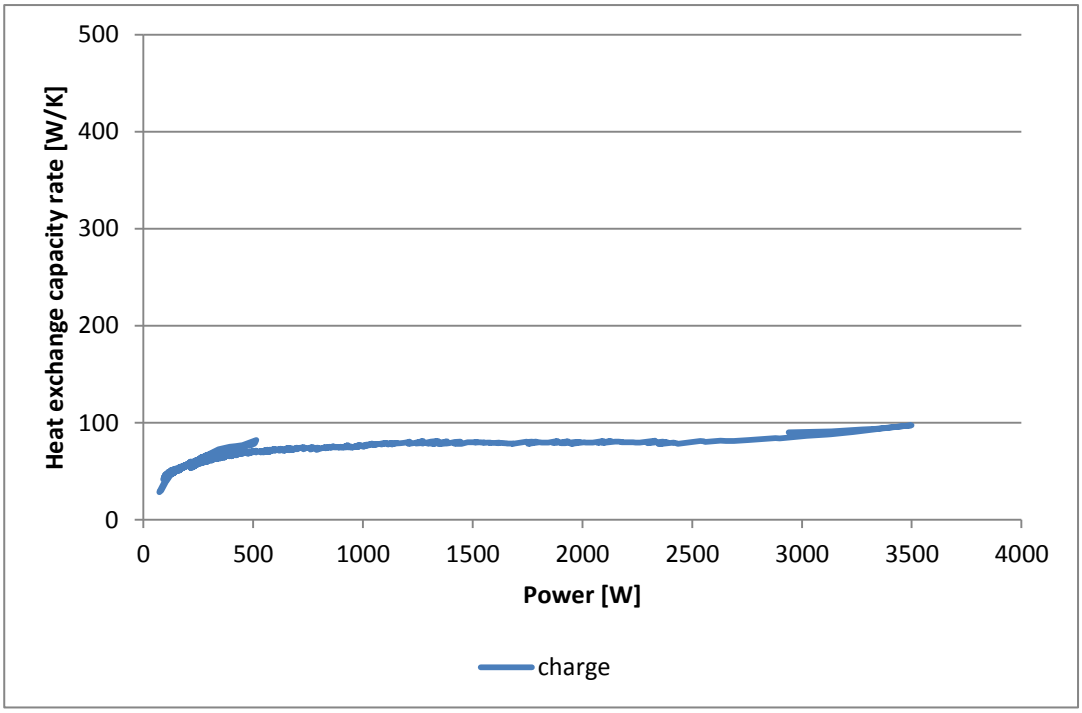

Figure 8. Heat exchange capacity rate as a function of charge and discharge power.

Test cycle 3 with water:

Measurement data and calculations below.

Table 4. Power and flow rate.

	Heating element Power	Flow rate	Set temperature
Charge	**3 kW**	**2 l/min -> 1.3 l/min**	**90°C**
Discharge	**-**	**1.6 l/min**	**18-20°C**

Fig. 9 shows the measured surface temperatures, inlet temperature, outlet temperature, ambient temperature and the flow rate for the heating and cooling cycle.

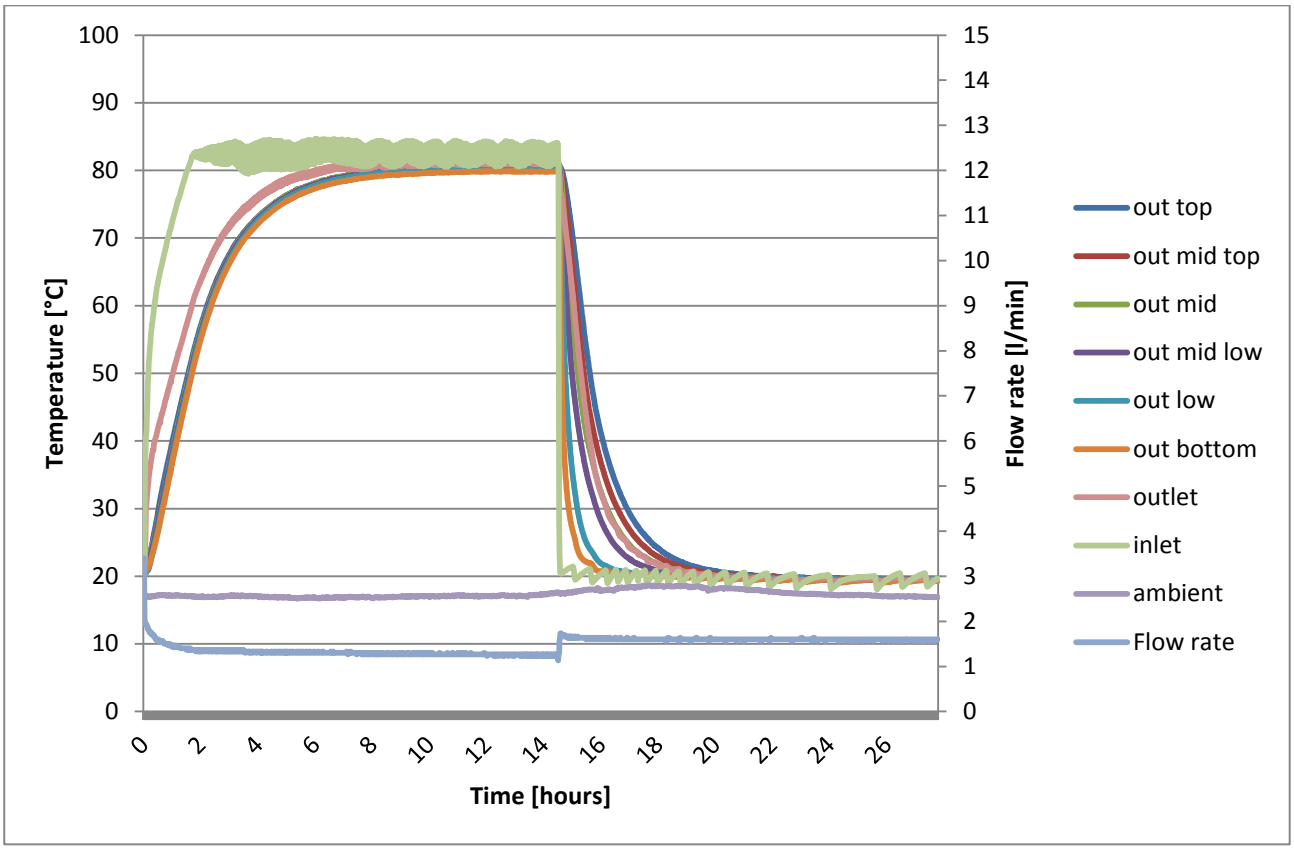

Figure 9. Temperature development and flow rate.

Fig. 10 shows the charge period in more details.

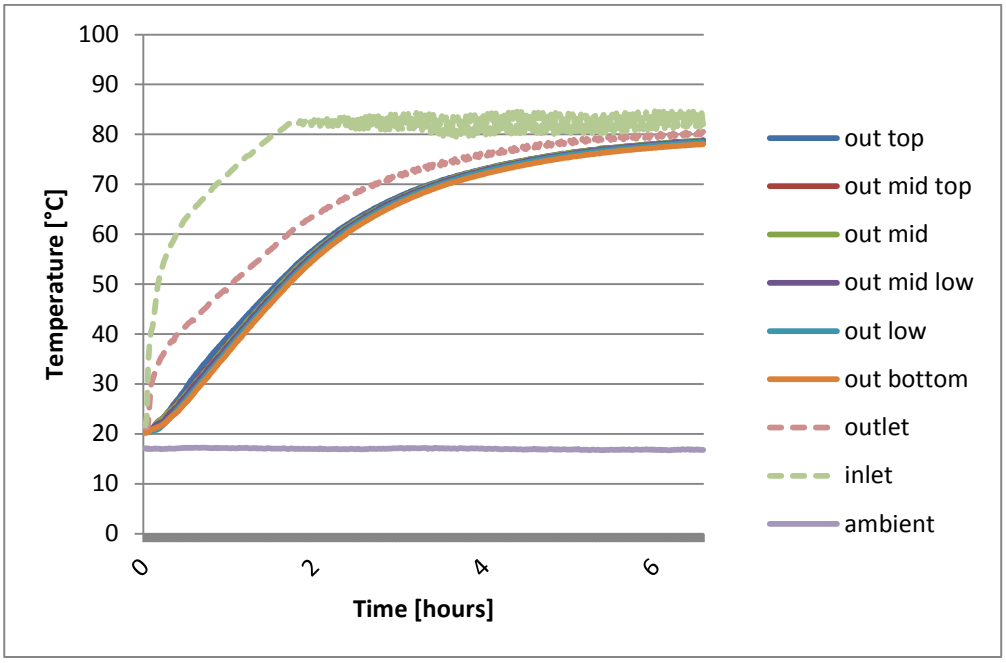

Figure 10. Temperature development for charge period.

Fig. 11 displays the discharge period in details.

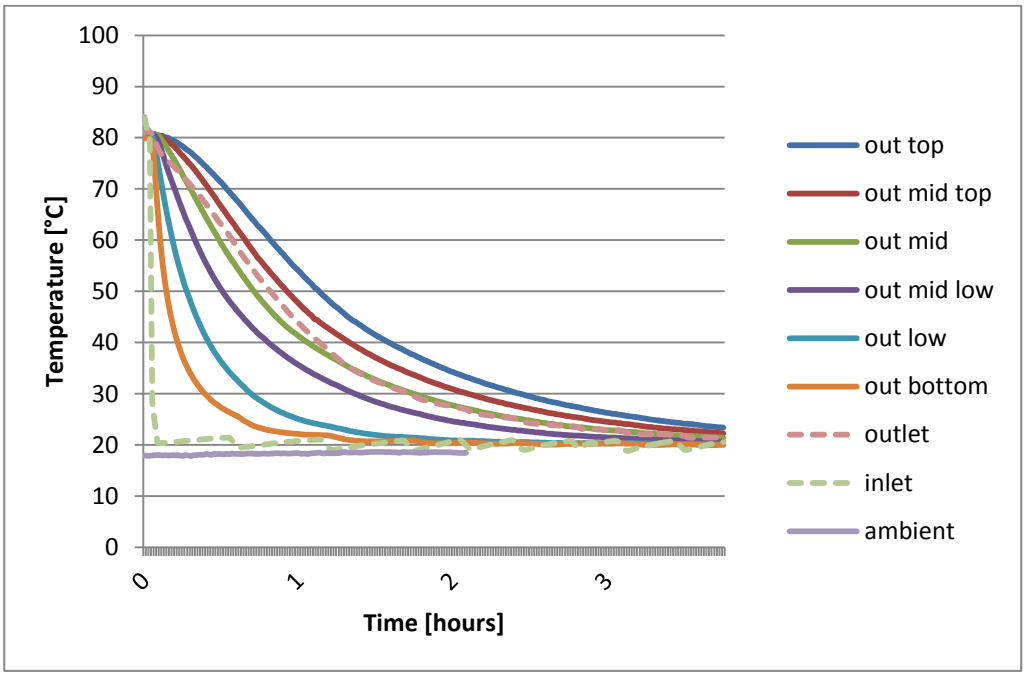

Figure 11. Temperature development for discharge period.

Tab. 5 summarizes the start, maximum and end temperature of the storage for this test cycle.

Table 5. Start temperature, maximum temperature and end temperature of storage.

T_{start}	T_{max}	T_{end}
20.5 °C	80.5°C	19.5 °C

Fig. 12 displays the heat content of the storage above start condition and the mean temperature of the storage over time.

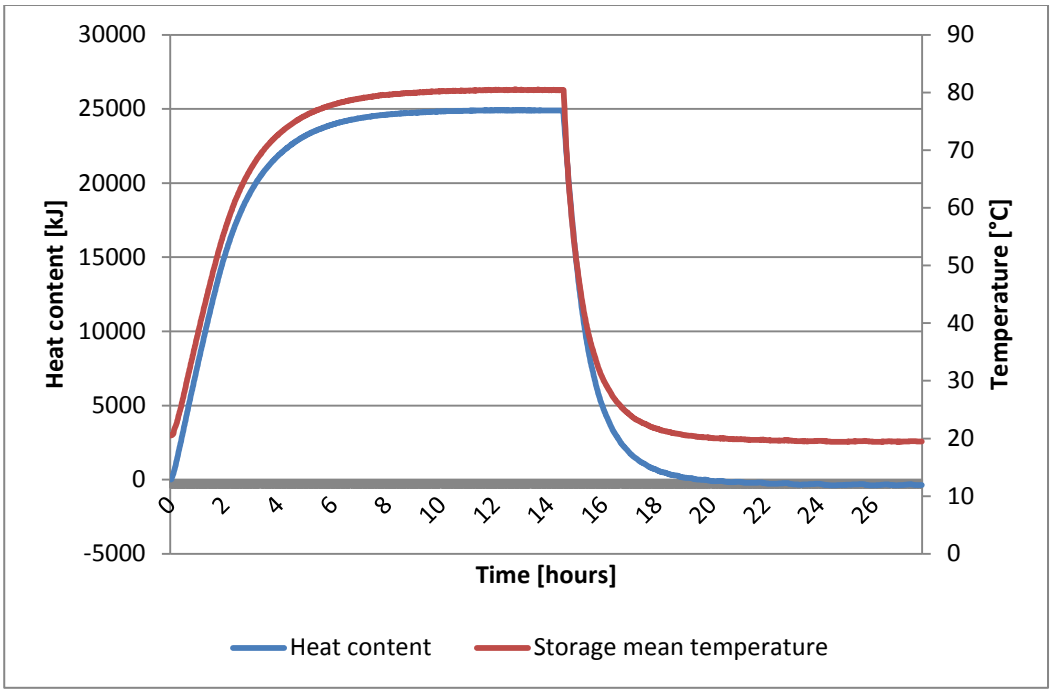

Figure 12. Energy content and mean storage temperature.

The maximum measured heat content of the storage is listed in the table below along with the theoretical value.

Table 6. Measured and calculated heat contents during the test.

Max measured energy content E_{max_exp}	Theoretical max energy content E_{max_theo}
25000 kJ	25260 kJ

The deviation between the measured and the theoretical energy content at hot state was just 0.9%.

The heat exchange capacity rates for the charge and discharge periods are displayed in the diagrams below along with the charge and discharge power.

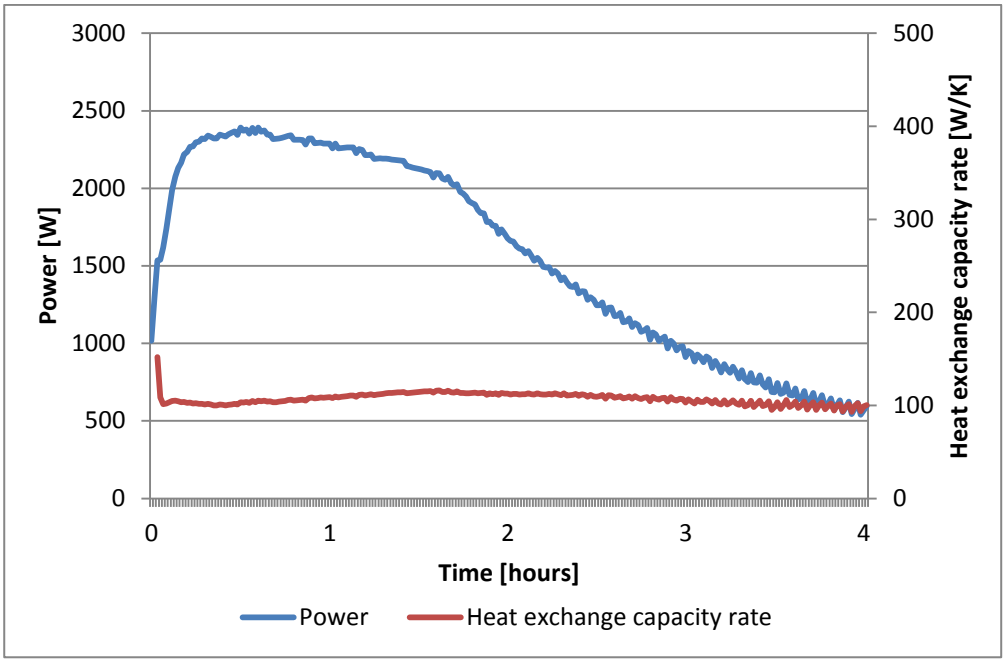

Figure 13. Power and heat exchange capacity rate over time for charge.

The discharge power is displayed in the diagram below. It was not possible to calculate the heat exchange capacity rate due to a high thermal stratification in the tank caused by the low flow rate. The outlet temperature was higher than the mean storage temperature and the formula for calculation heat exchange capacity rate is invalid.

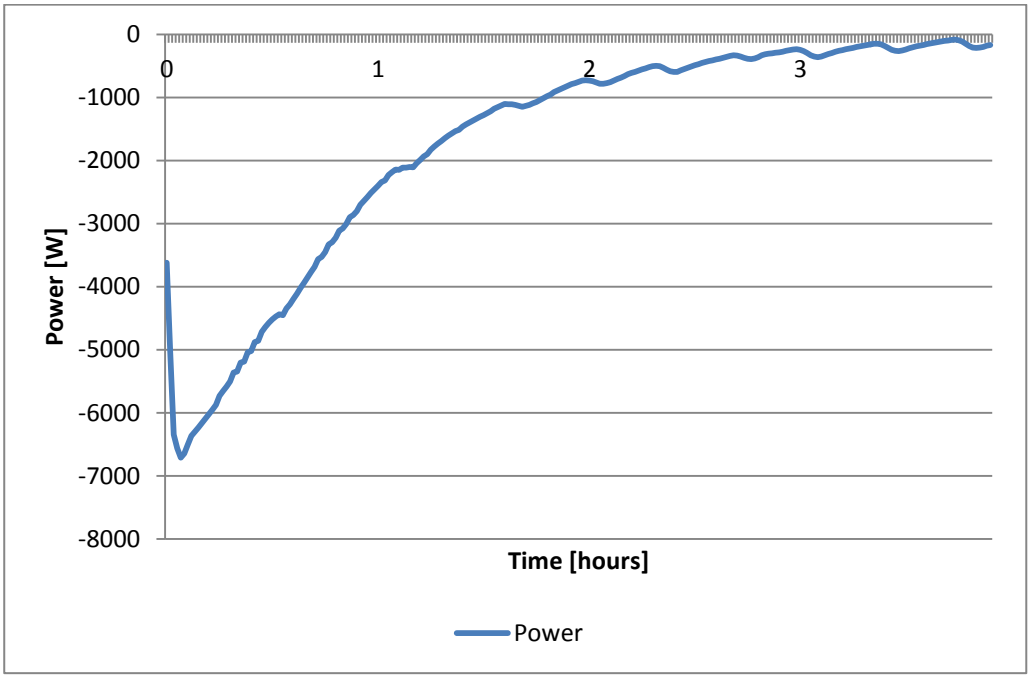

Figure 14. Power over time for discharge.

Heat exchange capacity rate is displayed as a function of the mean storage temperature for charge in Fig. 15.

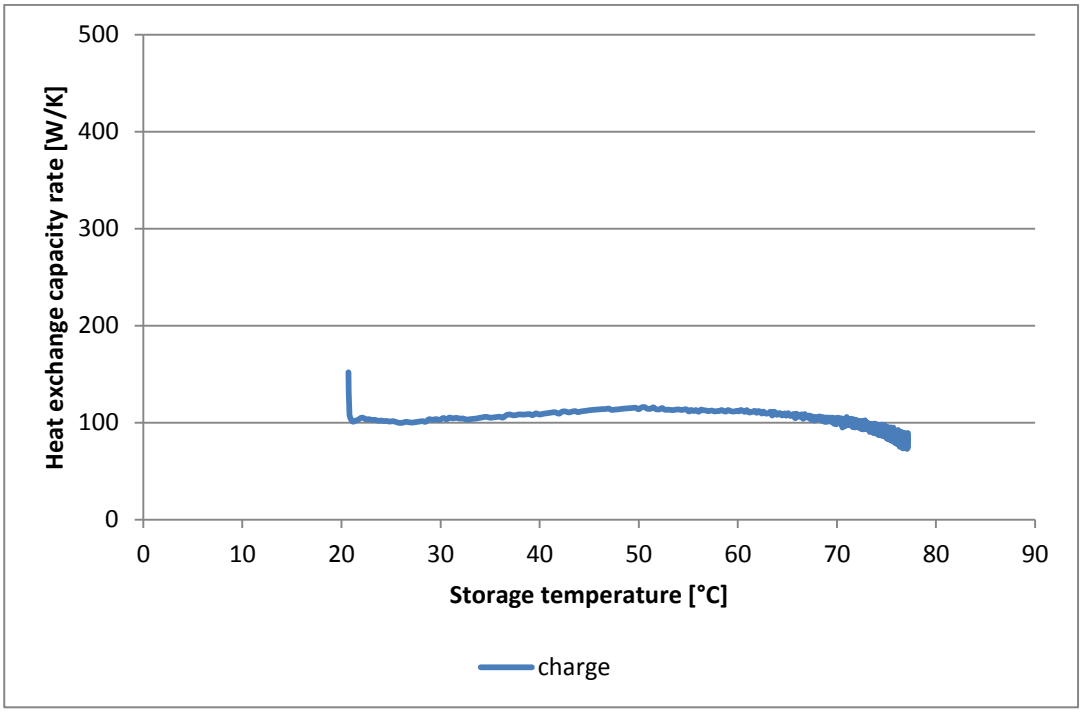

Figure 15. Heat exchange capacity rate as a function of storage temperature.

Heat exchange capacity rate is displayed as a function of the charge power in Fig. 16.

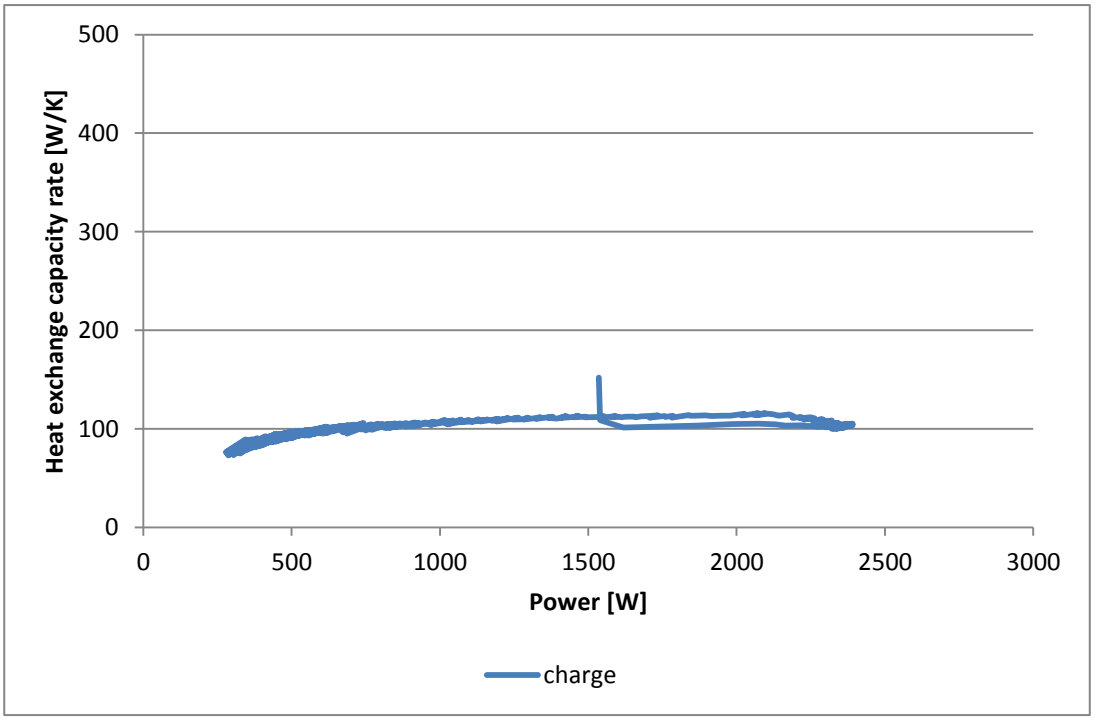

Figure 16. Heat exchange capacity rate as a function of charge power.

Test cycle 4 with water:

Measurement data are listed in Tab. 7.

Table 7. Power and flow rate.

	Heating element Power	Flow rate	Set temperature
Charge	**9 kW**	**6 l/min -> 4.7 l/min**	**90°C**
Discharge	**-**	**5.7 l/min**	**18-20°C**

Fig. 17 shows the measured surface temperatures, inlet temperature, outlet temperature, ambient temperature and the flow rate for the heating and cooling cycle.

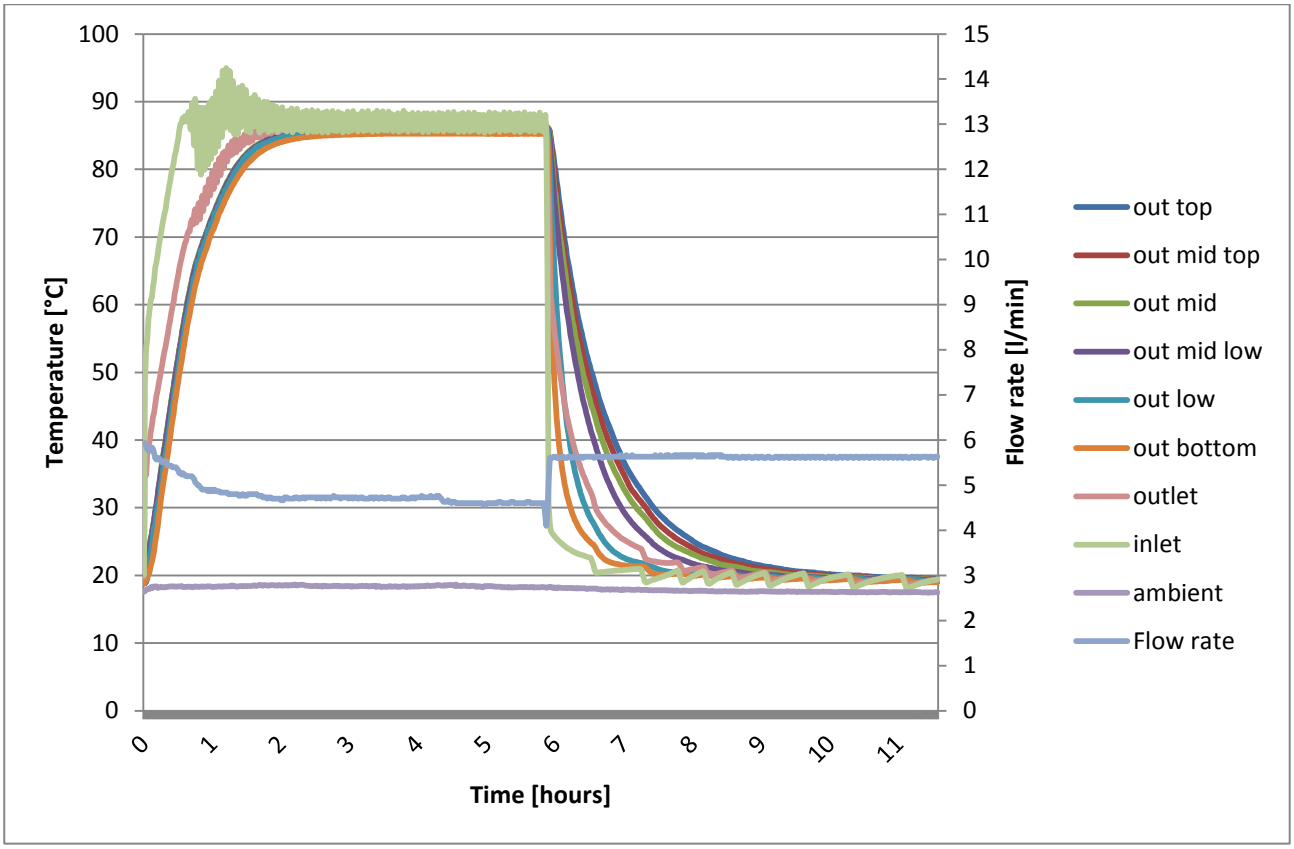

Figure 17. Temperature development and flow rate.

Fig. 18 shows the charge period in more details.

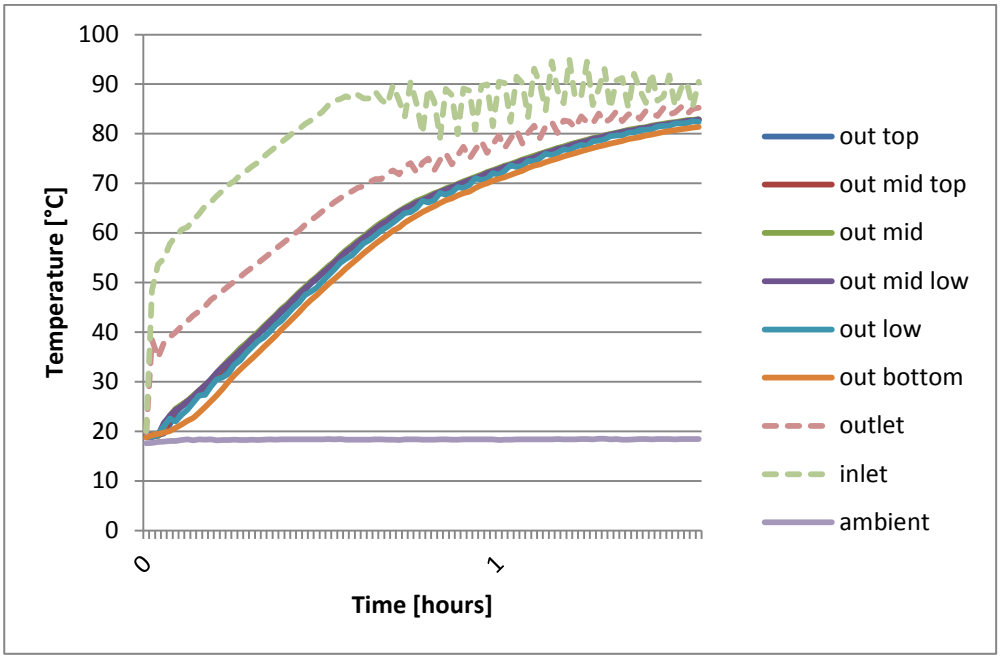

Figure 18. Temperature development for charge period.

Fig. 19 displays the discharge period in details.

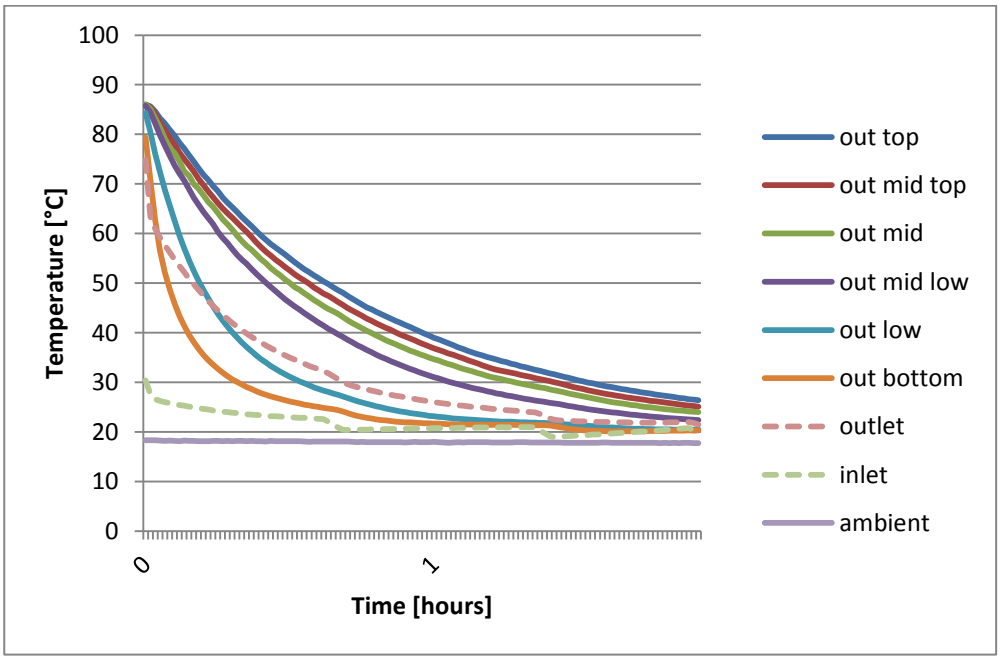

Figure 19. Temperature development for discharge period.

Tab. 8 summarizes the start, maximum and end temperature of the storage with water for this test cycle.

Table 8. Start temperature, maximum temperature and end temperature of storage.

T_{start}	T_{max}	T_{end}
18.9 °C	86.0°C	19.4 °C

Fig. 20 displays the measured heat content of the storage above start condition and the mean temperature of the storage over time.

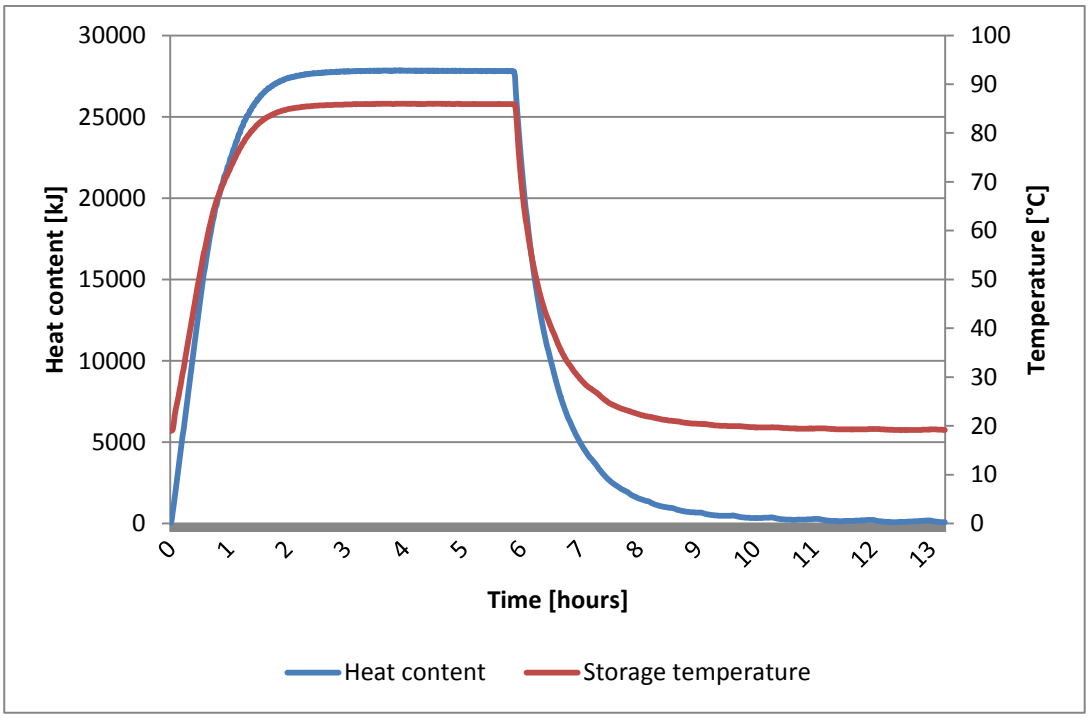

Figure 20. Energy content and mean storage temperature.

The maximum measured heat content of the storage is listed in the table below along with the theoretical value.

Table 9. Measured and calculated heat contents during the test.

Max measured energy content $E_{max,exp}$	Theoretical max energy content $E_{max,theo}$
27900 kJ	28249 kJ

The deviation between the measured and the theoretical energy content at hot state was 2.1%.

The heat exchange capacity rates for the charge and discharge periods are displayed in Fig. 21 and Fig. 22 along with the charge and discharge power.

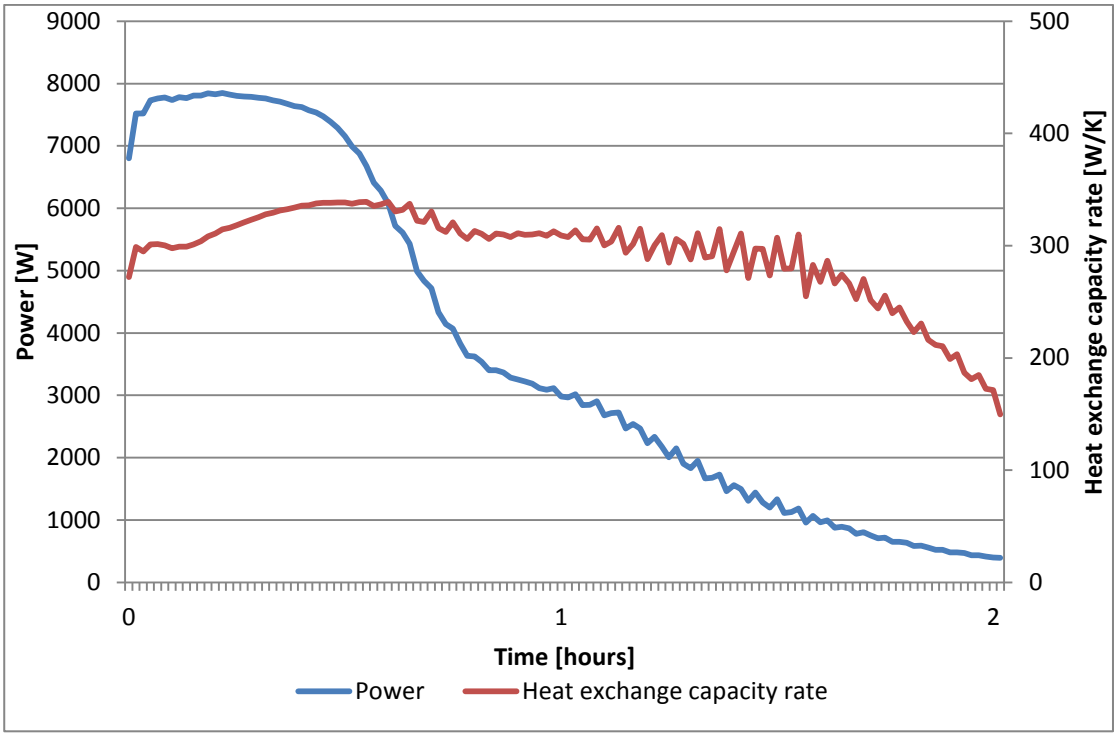

Figure 21. Power and heat exchange capacity rate over time for charge.

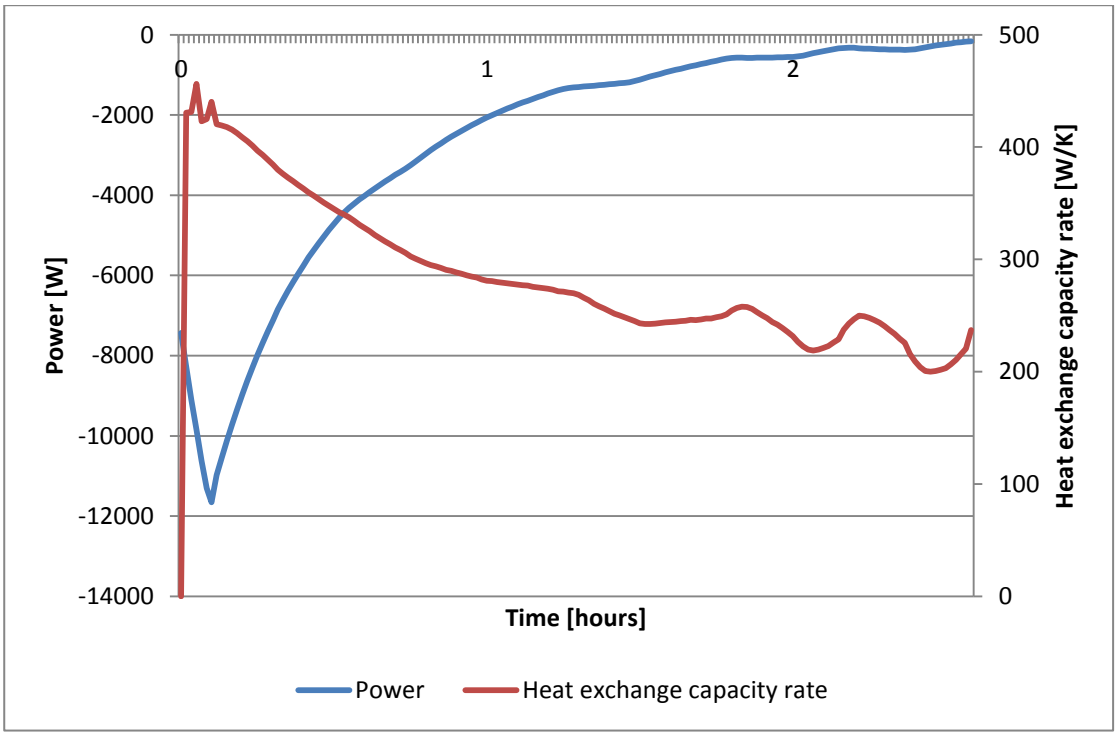

Figure 22. Power and heat exchange capacity rate over time for discharge.

Heat exchange capacity rate is displayed as a function of the mean storage temperature for charge and discharge in Fig 23.

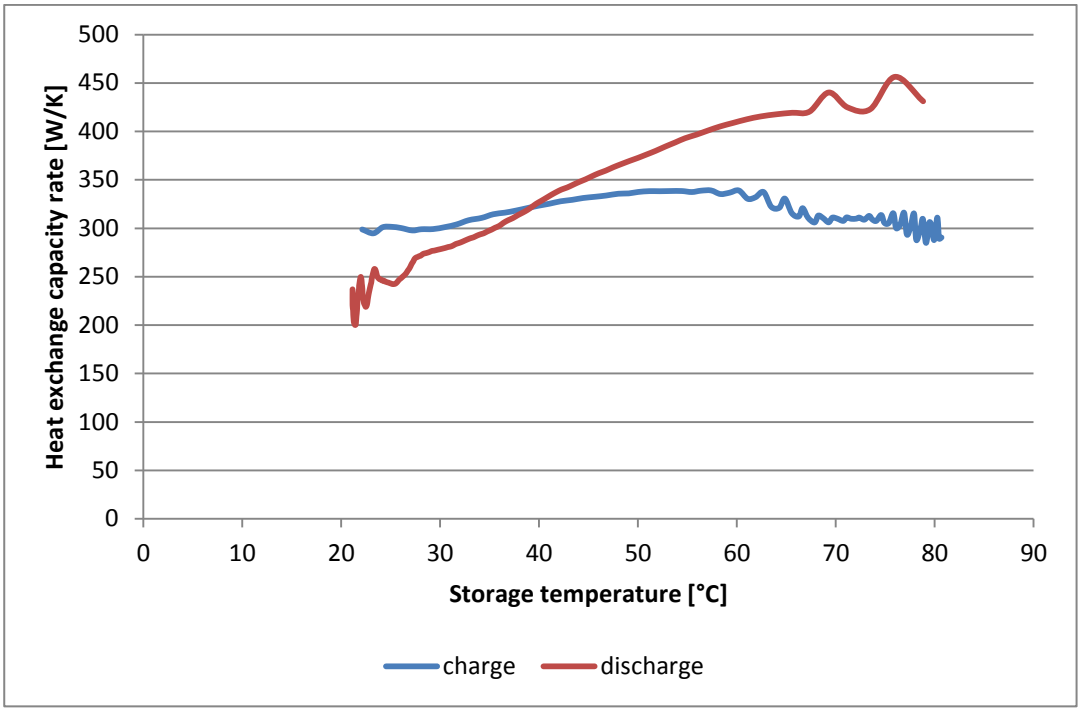

Figure 23. Heat exchange capacity rate as a function of storage temperature.

Heat exchange capacity rate is displayed as a function of the charge and discharge power in Fig. 24.

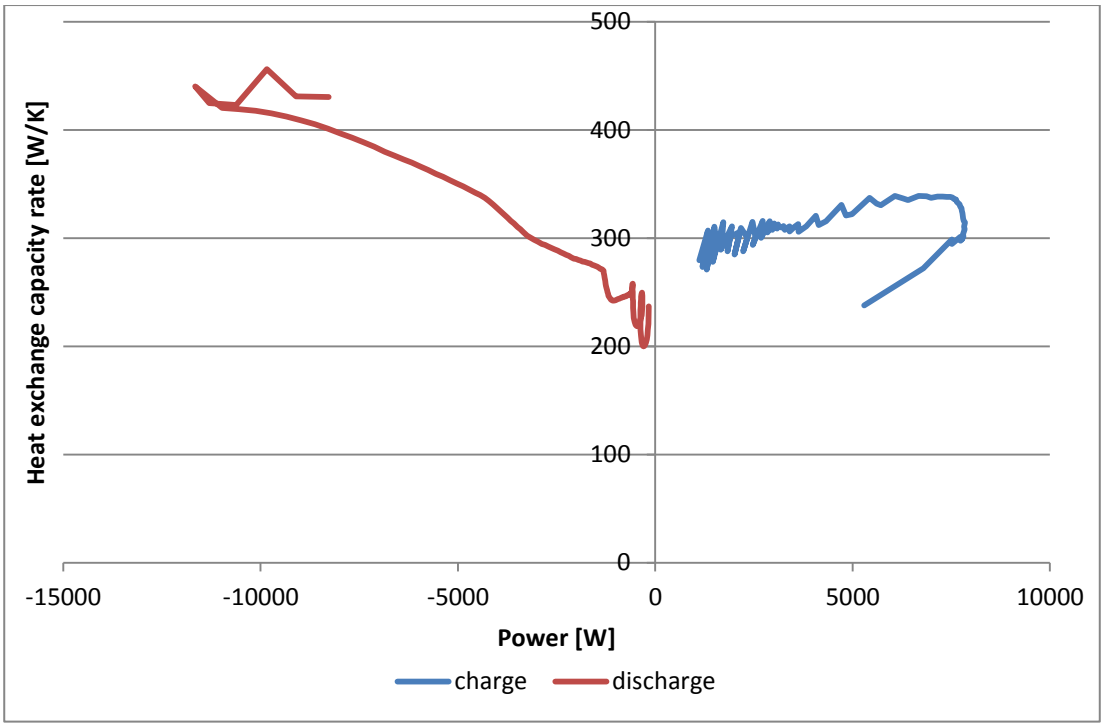

Figure 24. Heat exchange capacity rate as a function of charge and discharge power.

Test cycle 5 with water:

Measurement data and calculations for this test cycle are listed in Tab. 10.

Table 10. Power and flow rate.

	Heating element Power	Flow rate	Set temperature
Charge	**6 kW**	**5.5 l/min**	**90°C**
Discharge	**-**	**5.7 l/min**	**18-20°C**

Fig. 25 shows the measured surface temperatures, inlet temperature, outlet temperature, ambient temperature and the flow rate for the heating and cooling cycle.

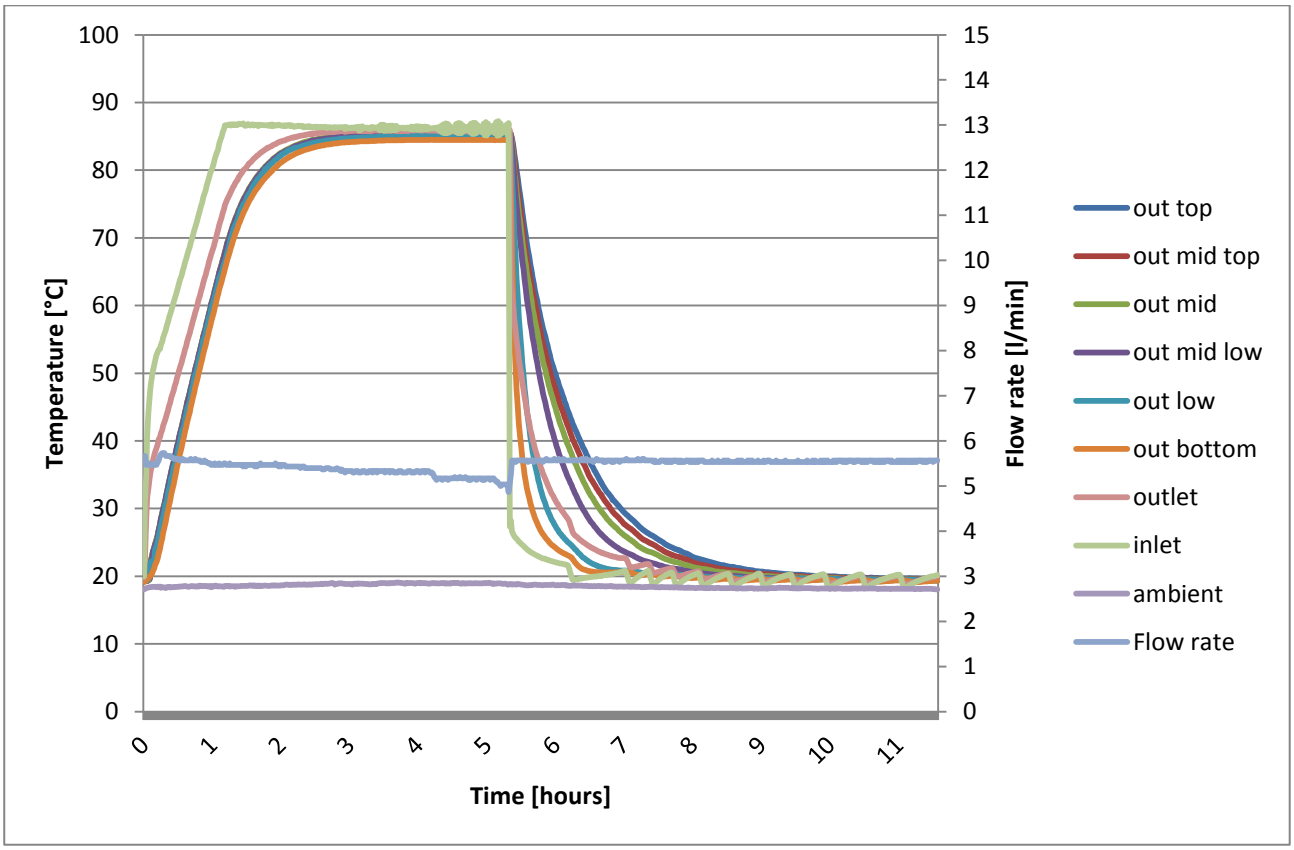

Figure 25. Temperature development and flow rate.

Fig. 26 shows the charge period in more details.

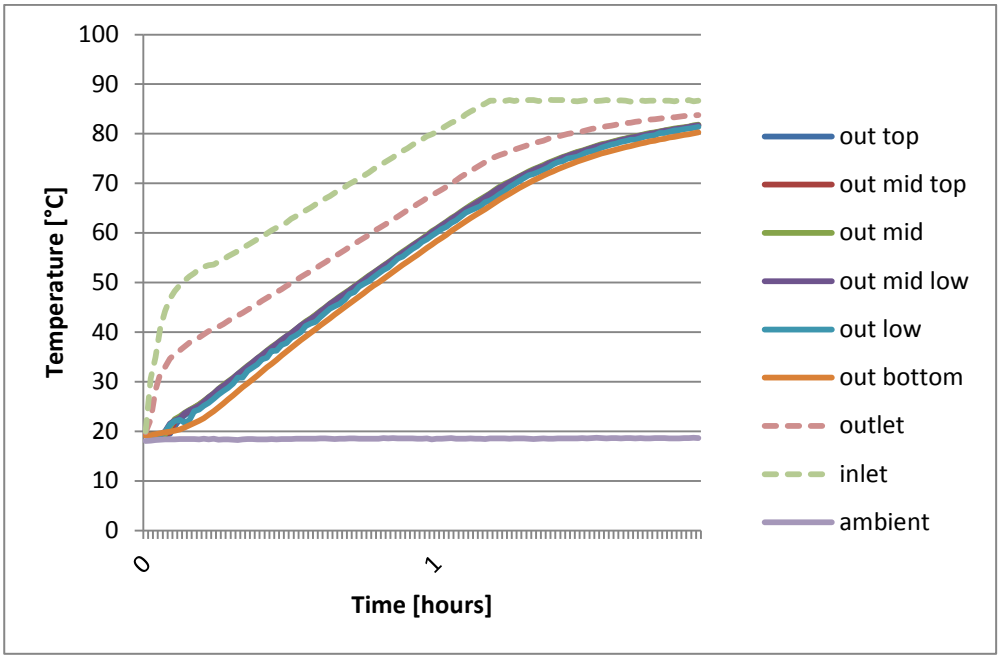

Figure 26. Temperature development for charge period.

Fig. 27 displays the discharge period in details.

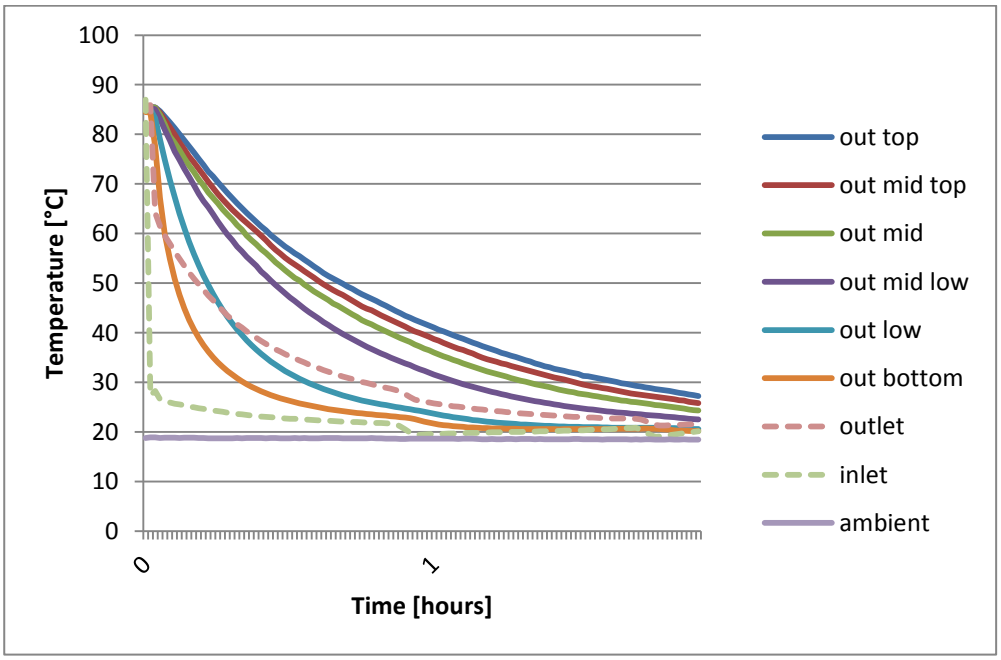

Figure 27. Temperature development for discharge period.

Tab. 11 summarizes the start, maximum and end temperature of the storage with water.

Table 11. Start temperature, maximum temperature and end temperature of storage.

T_{start}	T_{max}	T_{end}
19.3 °C	85.2°C	19.2 °C

Fig. 28 displays the measured heat content of the storage above start condition and the mean temperature of the storage over time.

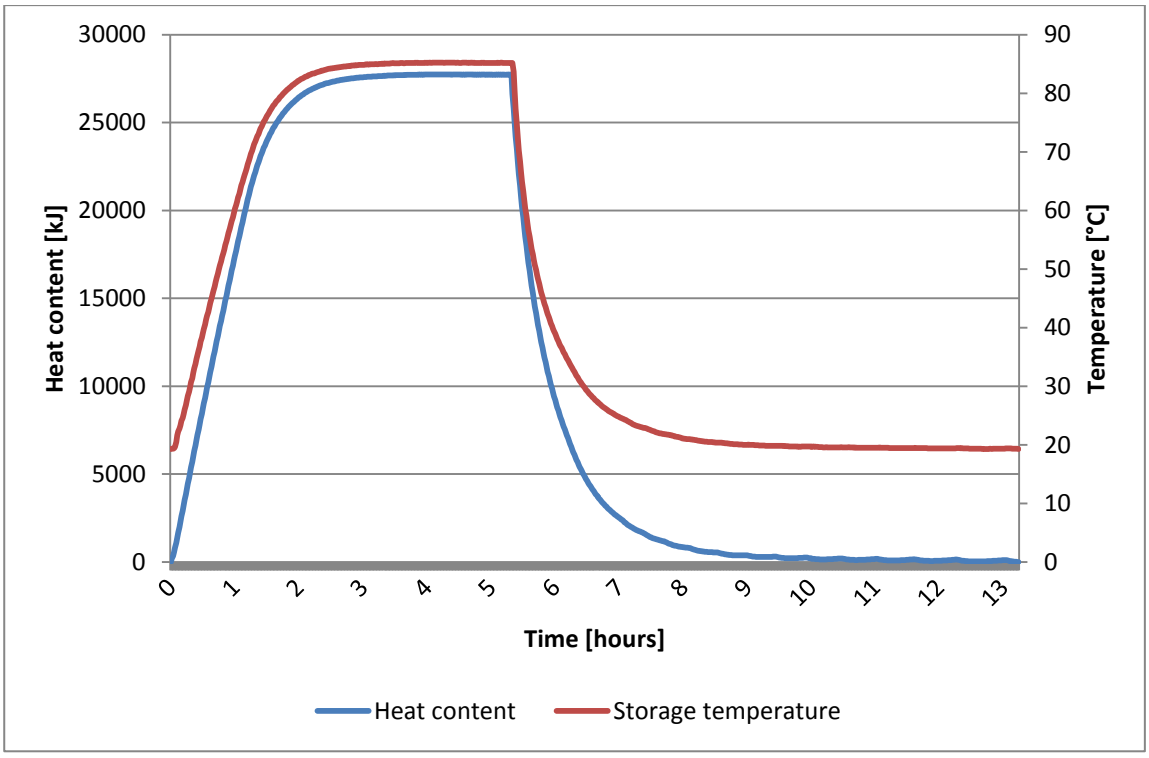

Figure 28. Energy content and mean storage temperature.

The maximum measured heat content of the storage is listed in Tab. 12 along with the theoretical value.

Table 12. Measured and calculated heat contents during the test.

Max measured energy content $E_{max,exp}$	Theoretical max energy content $E_{max,theo}$
27740 kJ	27743

The heat exchange capacity rates for the charge and discharge periods are displayed in the Fig. 29 and Fig. 30 along with the charge and discharge power.

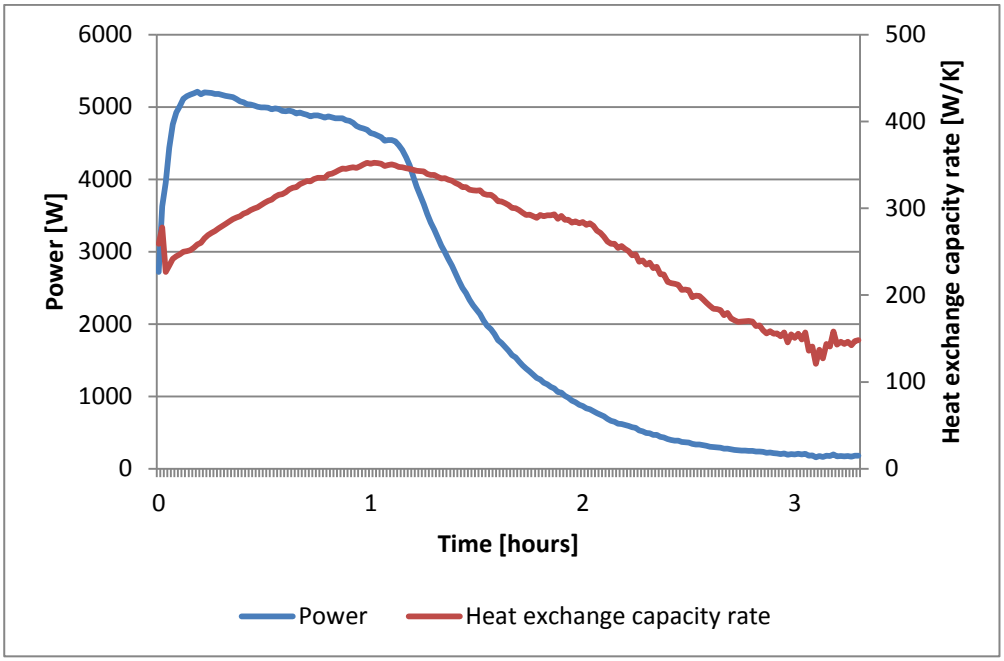

Figure 29. Power and heat exchange capacity rate over time for charge.

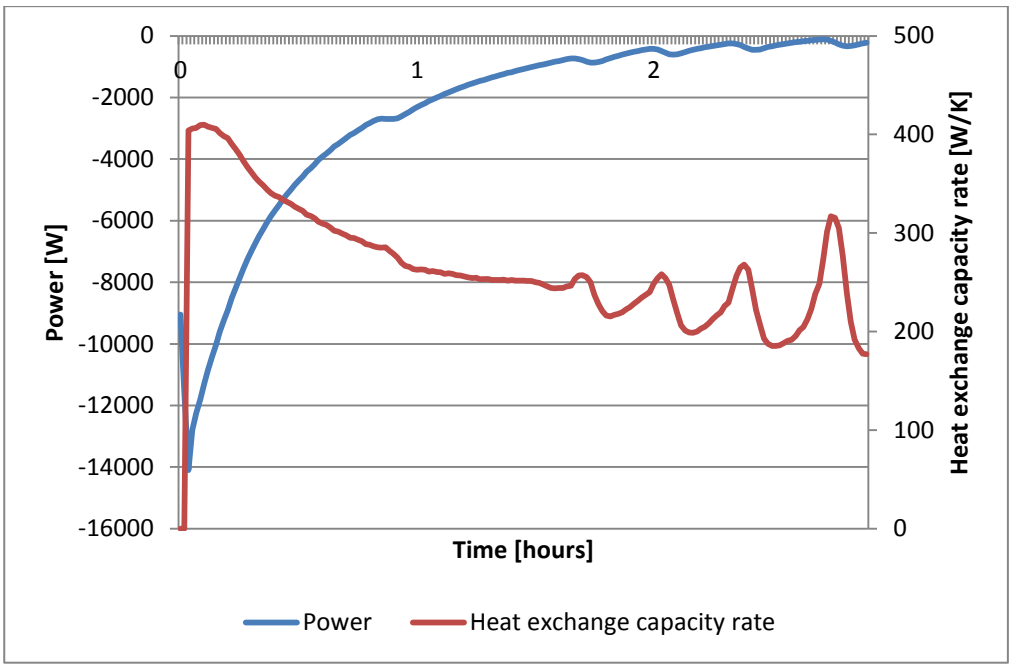

Figure 30. Power and heat exchange capacity rate over time for discharge.

Heat exchange capacity rate is displayed as a function of the mean storage temperature for charge and discharge in Fig 31 and Fig 32.

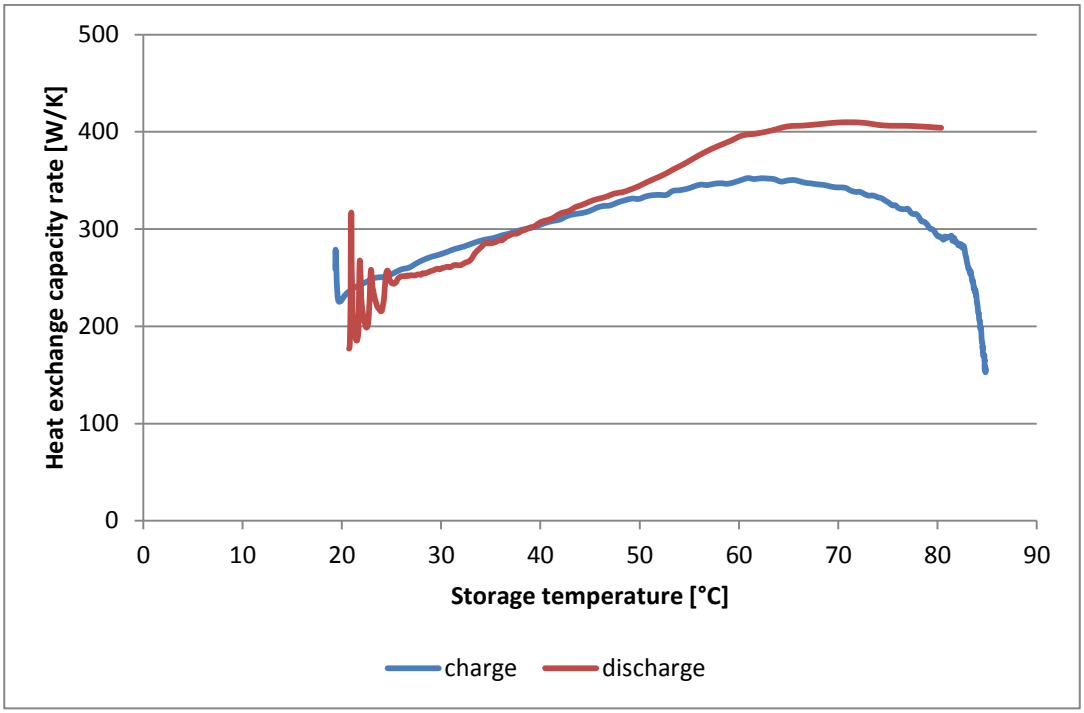

Figure 31. Heat exchange capacity rate as a function of storage temperature.

Heat exchange capacity rate is displayed as a function of the charge and discharge power.

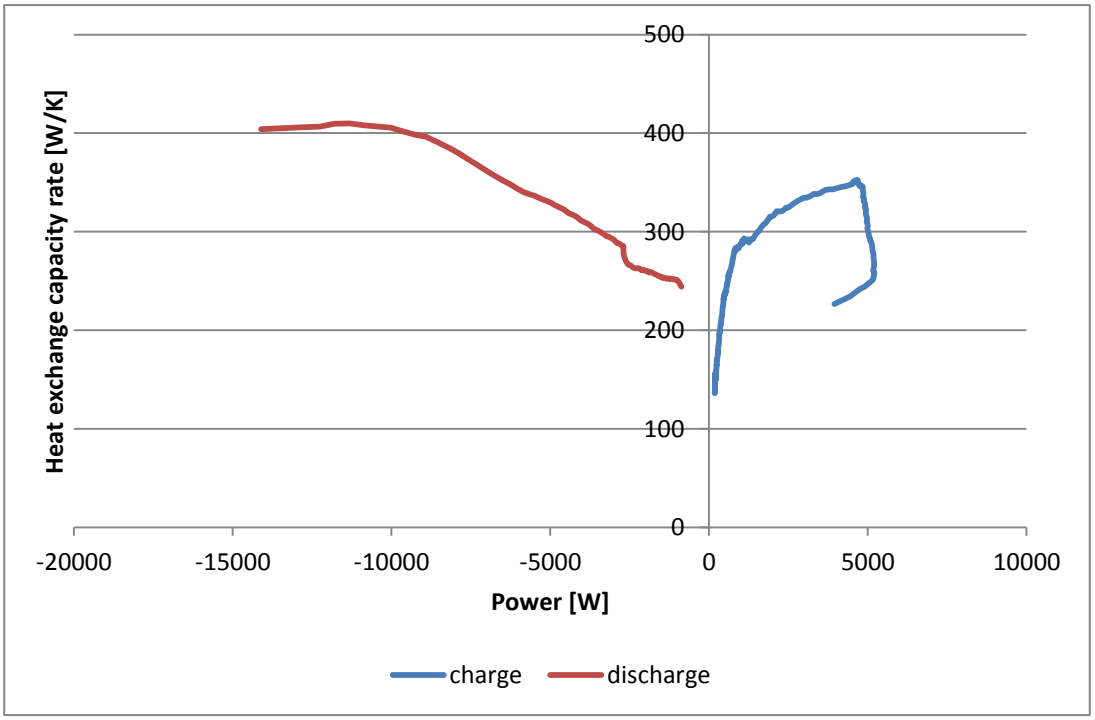

Figure 32. Heat exchange capacity rate as a function of charge and discharge power.

Test cycle 6 with water:

Measurement data and calculations for this test cycle are listed in Tab. 13.

Table 13. Power and flow rate.

	Heating element Power	Flow rate	Set temperature
Charge	**3 kW**	**6.1 l/min**	**90°**
Discharge	**-**	**5.7 l/min**	**18-20°C**

Fig. 33 shows the measured surface temperatures, inlet temperature, outlet temperature, ambient temperature and the flow rate for the heating and cooling cycle.

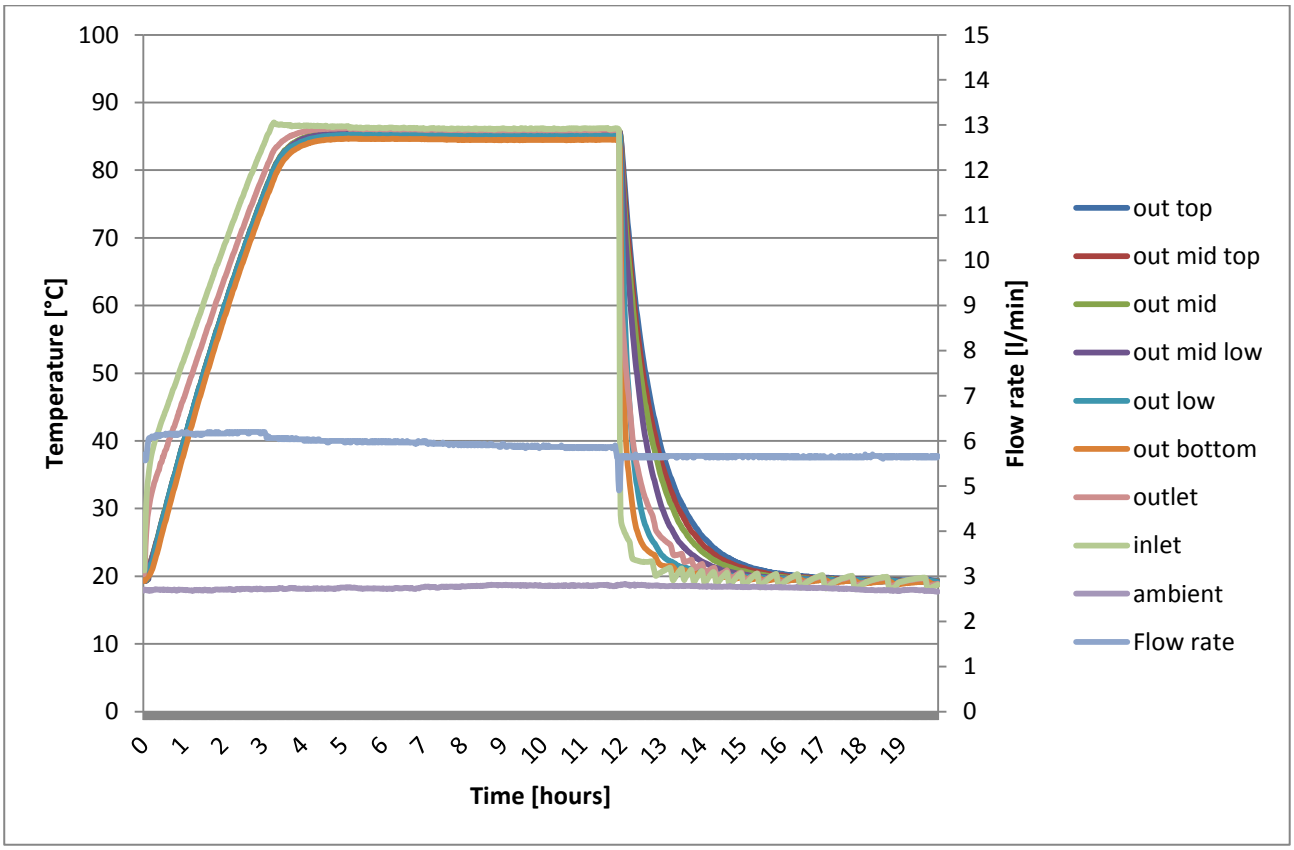

Figure 33. Temperature development and flow rate.

Fig. 34 shows the charge period in more details.

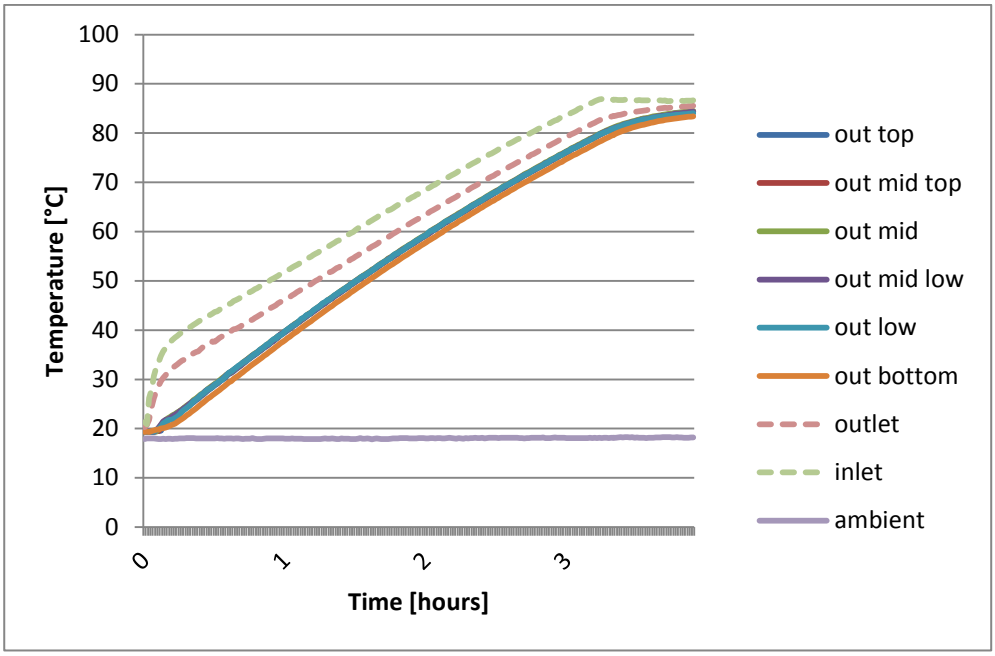

Figure 34. Temperature development for charge period.

Fig. 35 displays the discharge period in details.

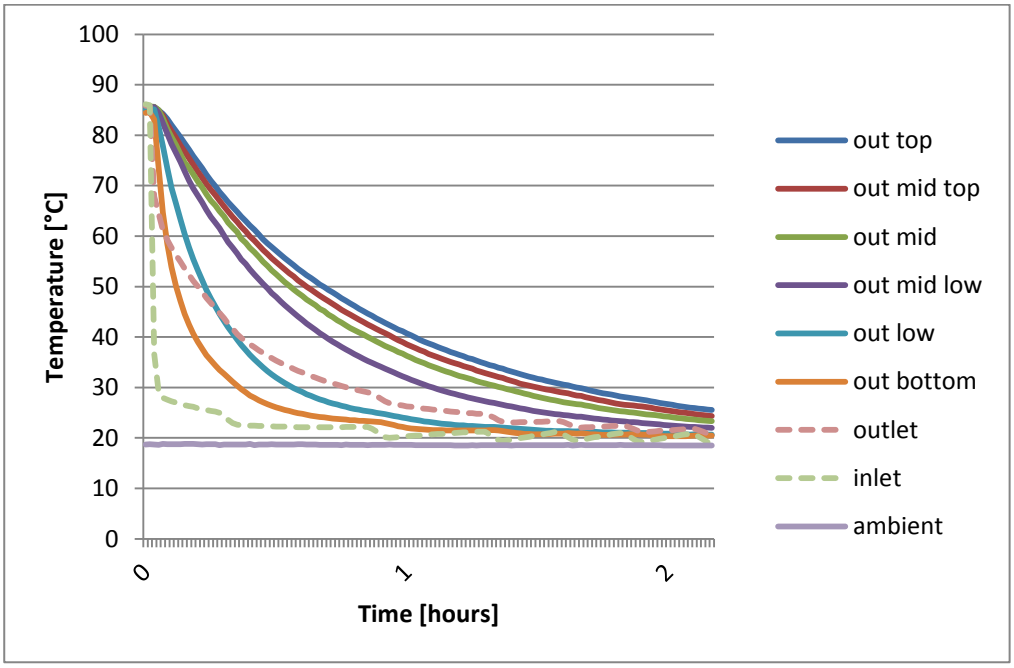

Figure 35. Temperature development for discharge period.

Tab. 14 summarizes the start, maximum and end temperature of the storage with water.

Table 14. Start temperature, maximum temperature and end temperature of storage.

T_{start}	T_{max}	T_{end}
19.3 °C	85.5°C	19.2 °C

Fig. 36 displays the heat content of the storage above start condition and the mean temperature of the storage over time.

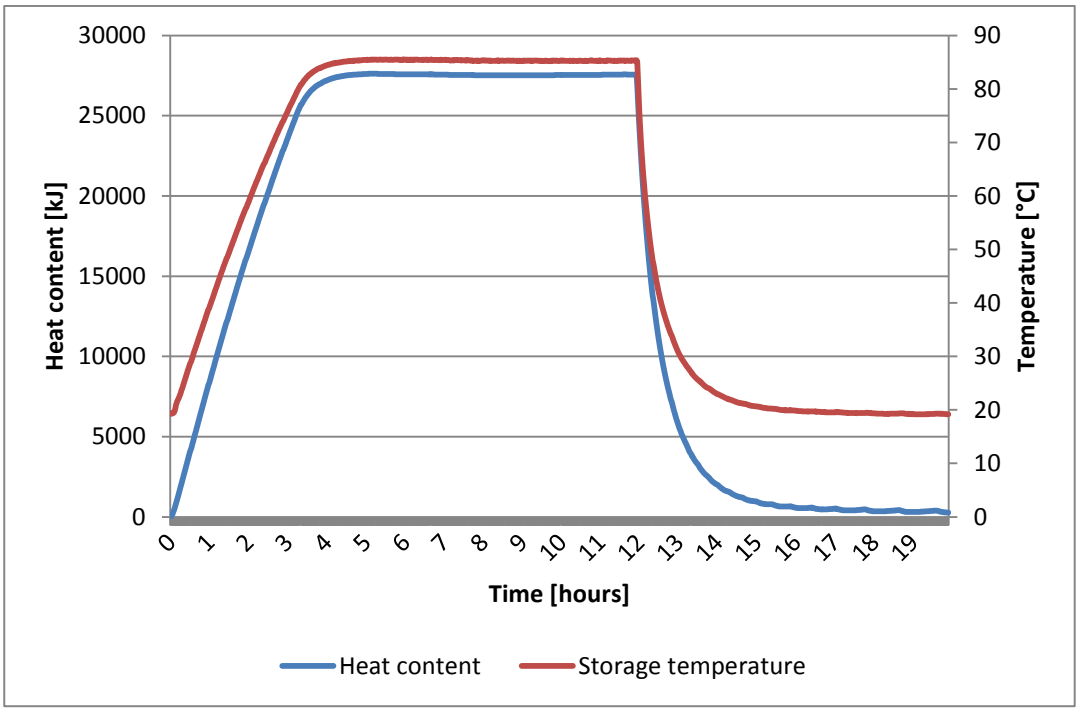

Figure 36. Energy content and mean storage temperature.

The maximum measured heat content of the storage is listed in Tab. 15 along with the theoretical value.

Table 15. Measured and calculated heat contents during the test.

Max measured energy content $E_{max,exp}$	Theoretical max energy content $E_{max,theo}$
27700 kJ	27870

The deviation between the measured and the theoretical energy content at hot state is just 0.8%.

The heat exchange capacity rates for the charge and discharge periods are displayed in Fig. 37 and Fig. 38 along with the charge and discharge power.

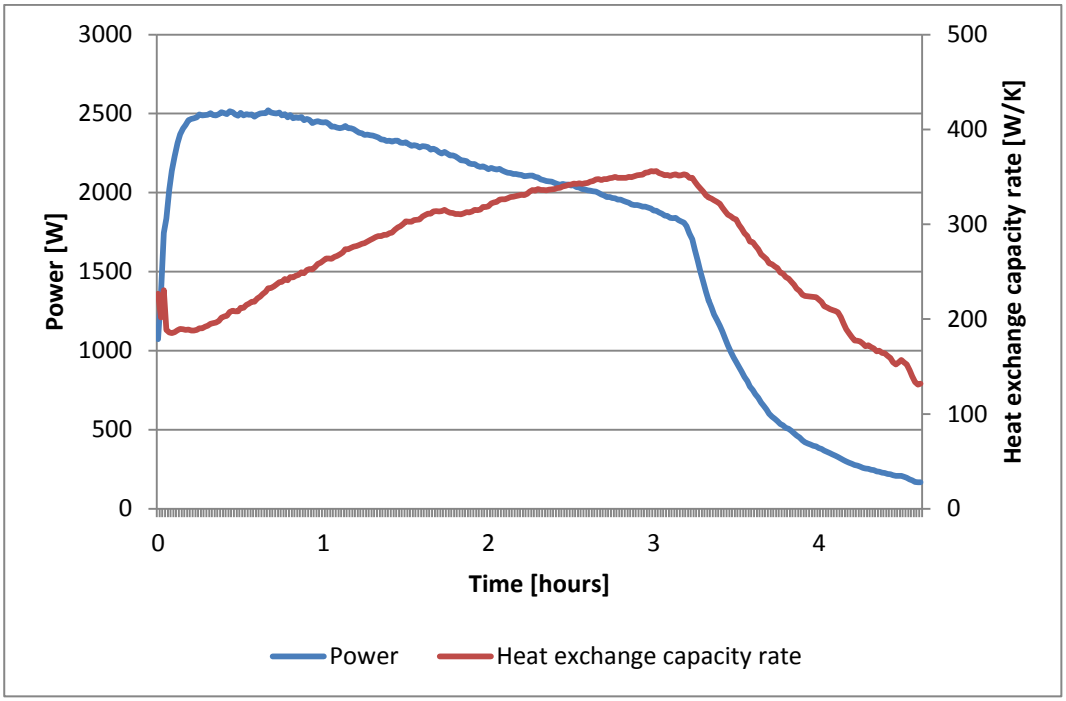

Figure 37. Power and heat exchange capacity rate over time for charge.

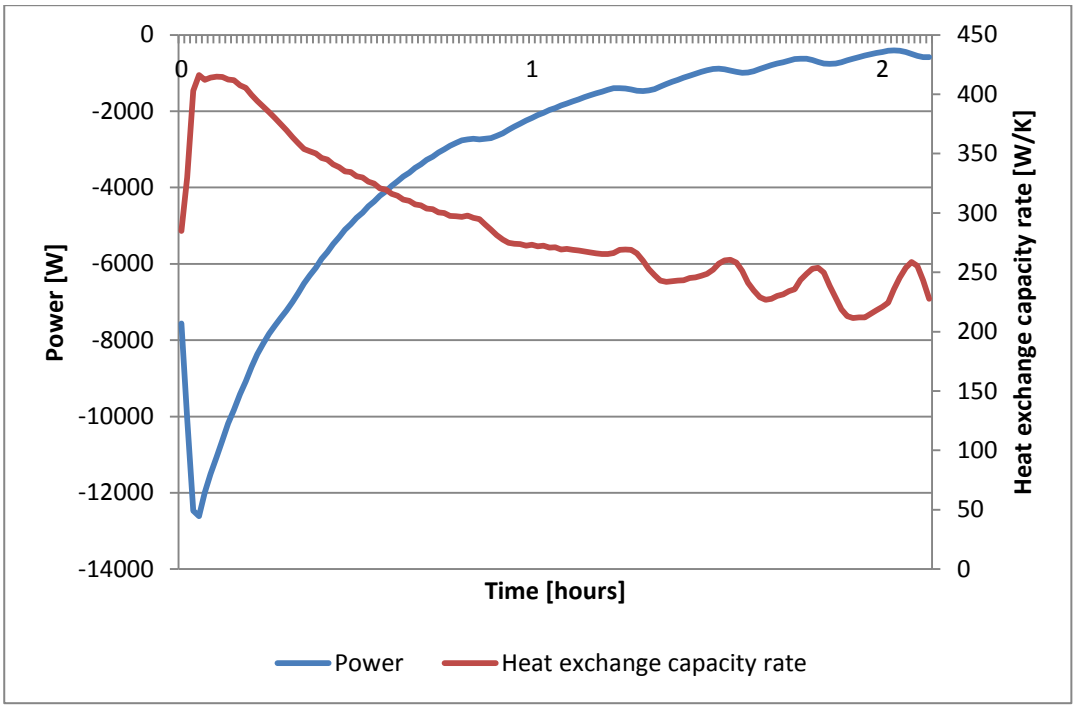

Figure 38. Power and heat exchange capacity rate over time for discharge.

Heat exchange capacity rate is displayed as a function of the mean storage temperature for charge and discharge in Fig. 39.

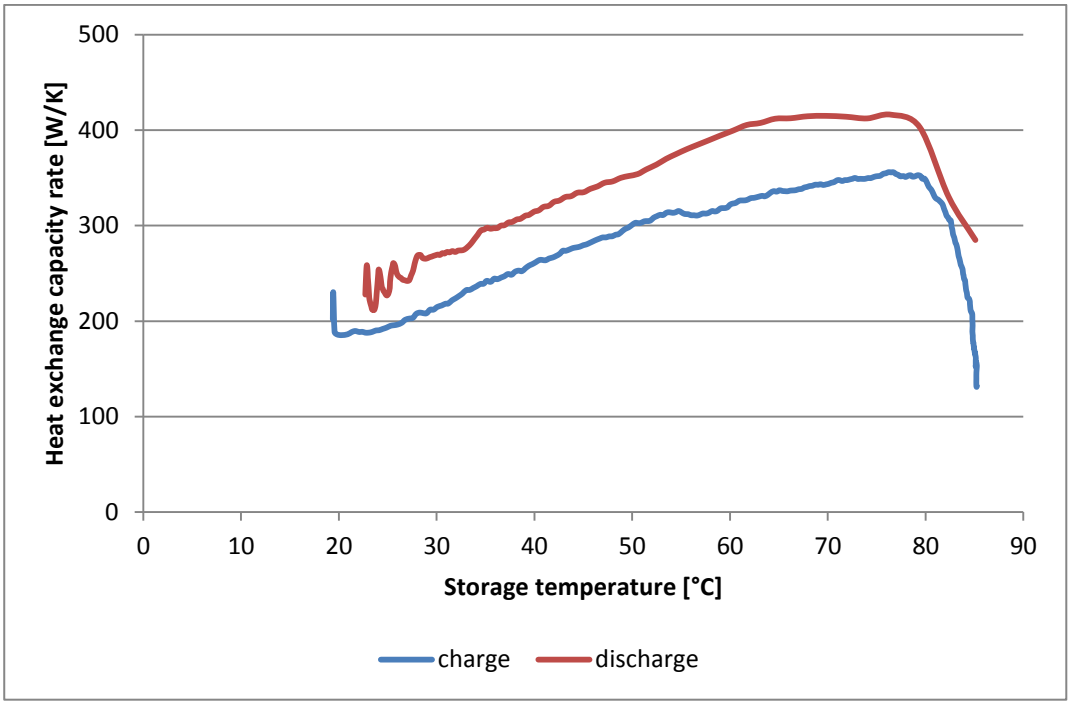

Figure 39. Heat exchange capacity rate as a function of storage temperature.

Heat exchange capacity rate is displayed as a function of the charge and discharge power.

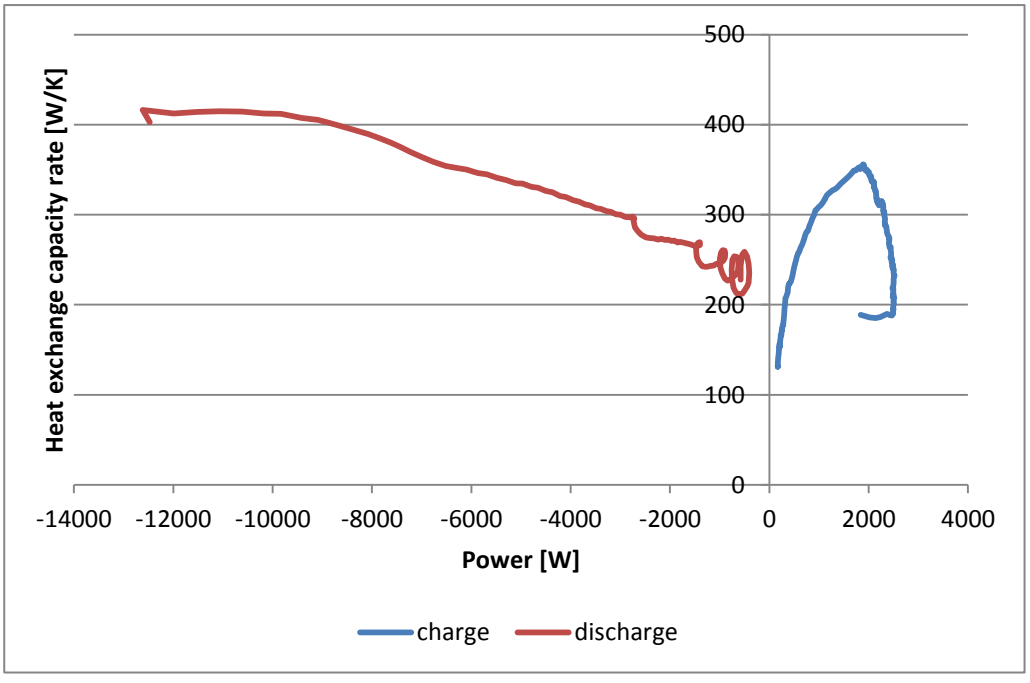

Figure 40. Heat exchange capacity rate as a function of charge and discharge power.

7. Appendix B

Test cycle 1:

The first test cycle was initiated with an average storage temperature of 28°C. Fig. 1 shows the temperature development for the inlet, outlet, ambient, surface and internal temperatures as well as the flow rate for the test cycle. Flow rate was less than 1 l/min.

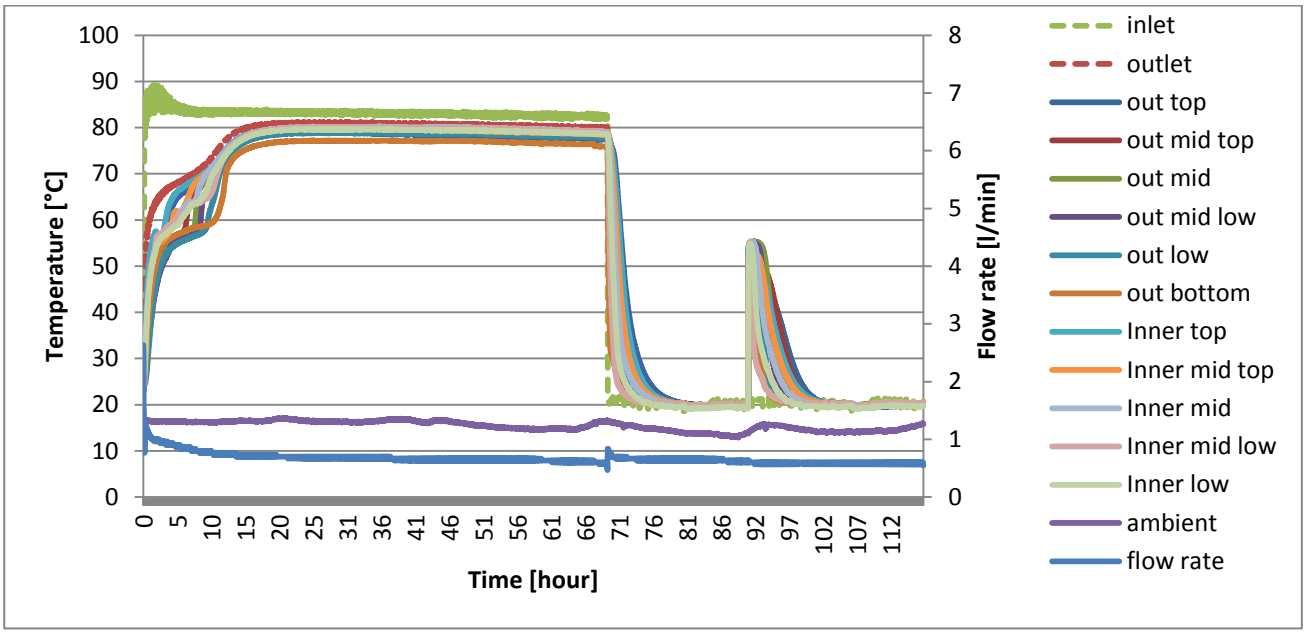

Figure 1. Temperature development and flow rate.

Fig. 2 shows the temperature development for the charging period in detail.

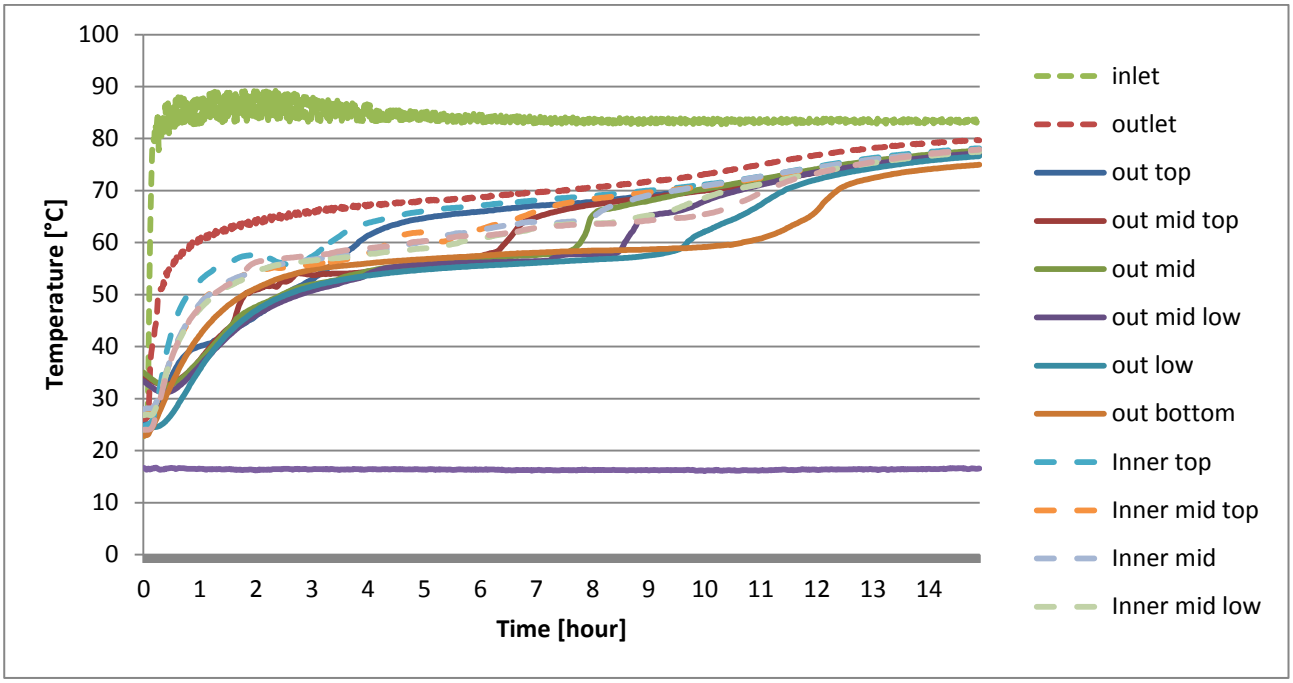

Figure 2. Temperature development during charge.

From Fig. 2 can be seen that the lower part of the storage heats up the slowest even though the module was charged from the bottom.

Fig. 3 shows the active discharge to supercooled state in detail.

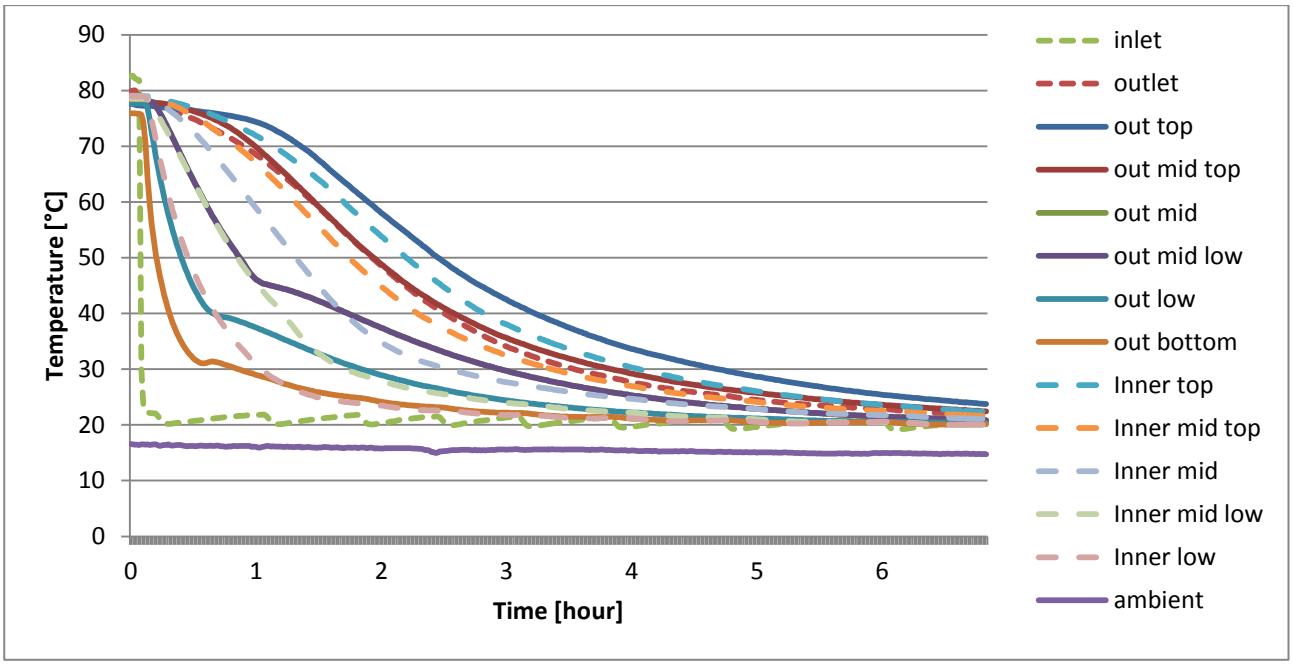

Figure 3. Temperature development for discharge to supercooled state.

Fig. 3 shows there was a high thermal stratification in the storage module during discharge.

Fig. 4 shows the temperature development for the activation and the following discharge. It may be seen that with an inlet temperature of 20°C and a flow rate of 0.6 l/min the outlet temperature was above 40°C for 3 hours.

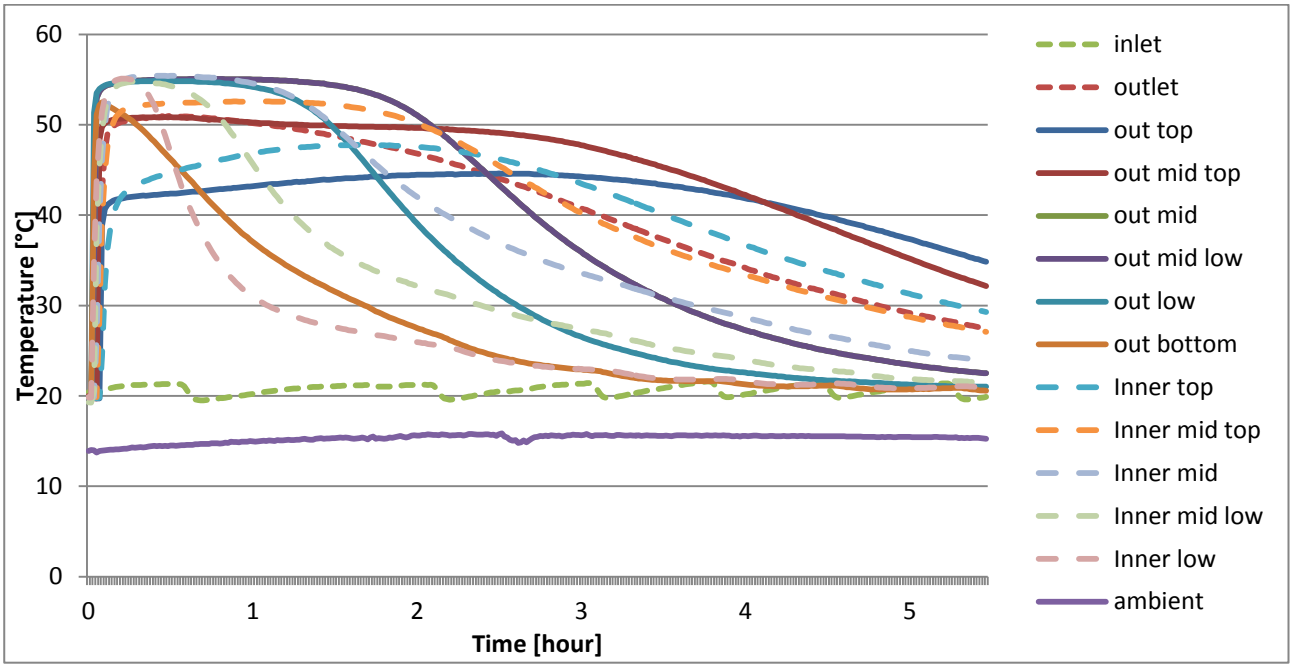

Figure 4. Temperature development for activation and discharge.

Activation started from the bottom initiated by little shaking of the module. The sensor "out low" was the first to react. The sensors in the top of the module did not reach the same temperature of approximately 55°C after activation as the others did.

Fig. 5 shows the mean storage temperature and the thermal energy content of the storage based on the measurements for the test cycle.

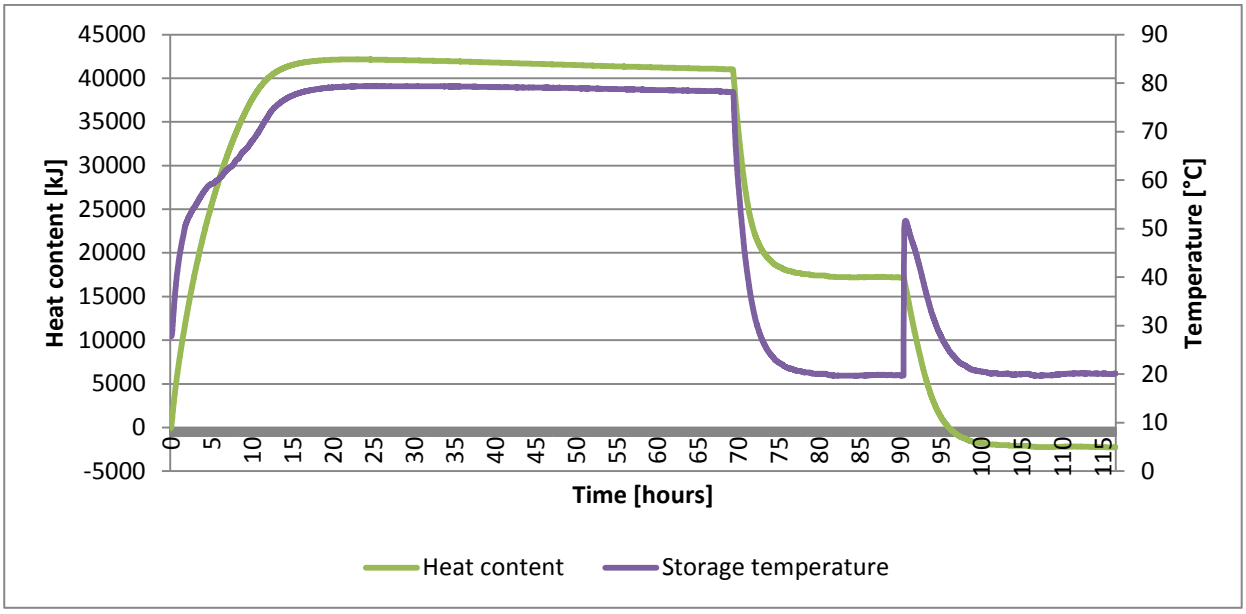

Figure 5. Heat content and storage temperature.

Fig. 5 shows that the energy content of the heat storage was negative at the end condition. This is because the start temperature on the storage was 28 °C, hence the reference temperature of the thermal energy calculation was higher than the end temperature of 20 °C.

Tab. 1 summarizes the start, maximum and end temperature of the storage for the test cycle.

Table 1. Storage start temperature, maximum temperature and end temperatrure.

T_{start}	27.8°C
T_{max}	79.4°C
T_{end}	20°C

Measured energy changes:

Table 2 summarizes the thermal energy content determined by the measurements at T_{max}, after discharge to supercooled state $E_{super,exp}$ and after the activation and discharge $E_{end,exp}$. The start temperature was the reference temperature for the calculation of the energy content.

Table 2. Thermal energy content at start, supercooled state and end of test cycle based on measurements.

E_{start}	0 kJ
$E_{max,exp}$	42160 kJ
$E_{super,exp}$	17200 kJ
$E_{end,exp}$	-2200 kJ

Theoretical energy change:

Based on the simple ideal melting theory and the measured temperatures of the heat storage module the theoretical thermal energy change of the storage module is listed in the table below.

Table 3. Thermal energy content based on simple ideal thermal energy content theory.

$E_{start,theo}$	0 kJ
$E_{charge,theo}$	42240 kJ
$E_{super,theo}$	17900 kJ
$E_{end,theo}$	-2220 kJ

Based on the theory of thermal energy content for incongruently melting salt hydrates the theoretical energy content of the storage at the different states are listed in the Tab. 4.

Table 4. Thermal energy content based on incongruently melting salt hydrate's thermal energy content.

$E_{start,theo}$	0 kJ
$E_{charge,theo}$	41700 kJ
$E_{super,theo}$	18000 kJ
$E_{end,theo}$	-2700 kJ

Fig. 6 summarizes the theoretical and the measured thermal energy content of the salt water mixture per mass unit as a function of the storage temperature. The thermal energy content is shown in kJ/kg salt water mixture excluding tank material. The measured thermal energy content was calculated by:

$$C_{test} = \frac{E_{charge} - C_{tank} \cdot (T_s - T_{start})}{m}$$

The mean storage temperature of 27.8°C at the start of the charging was used as the reference temperature. The measured and the theoretical energy contents were therefore 0 kJ at this temperature. As the storage was discharged to below the reference temperatures, the thermal energy content appears to be negative at this point.

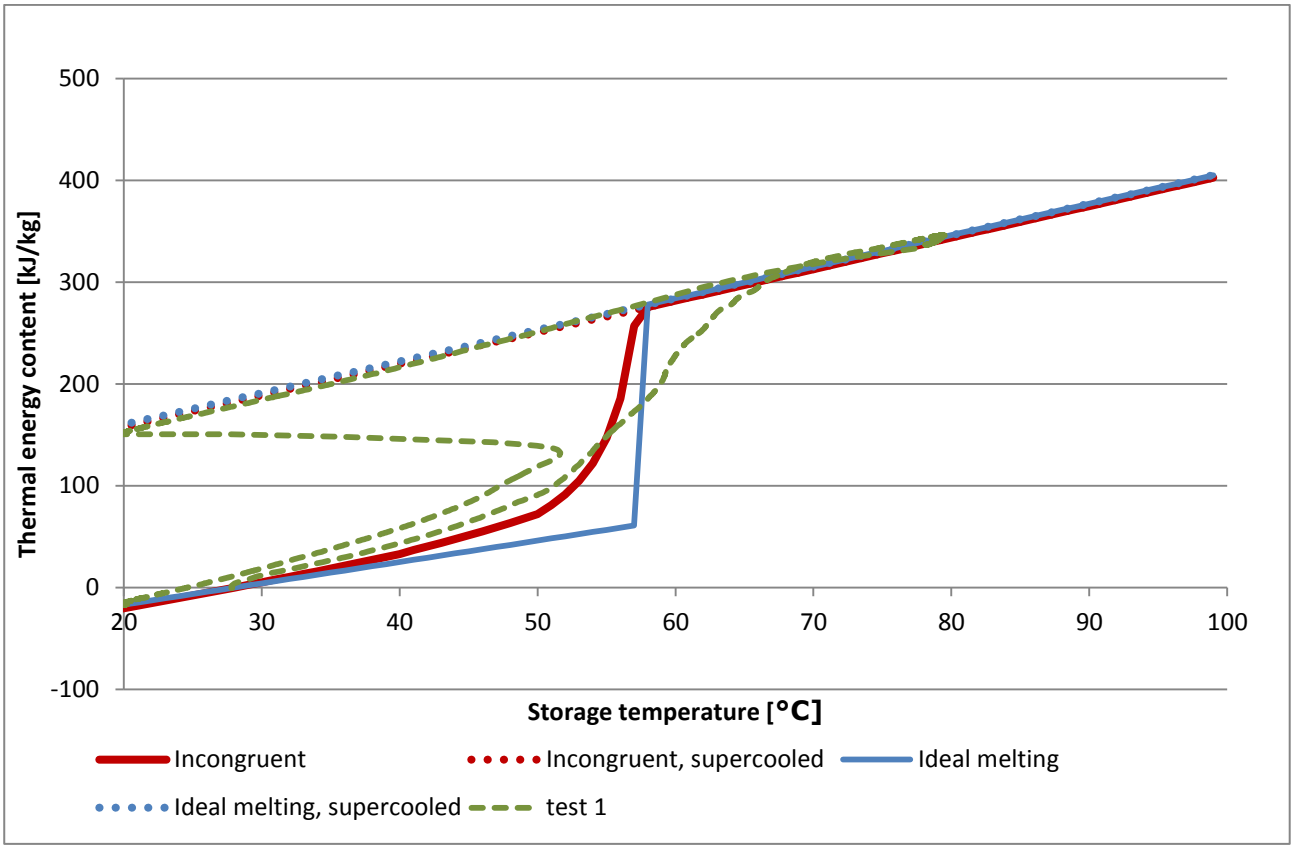

Figure 6. Theoretical and measured thermal energy content of salt water mixture per mass.

Fig. 6 shows that the simple ideal thermal energy content has a good agreement with the measurement when considering the start and end condition of the experiment only. The theory with the incongruently melting salt hydrate does give a better agreement with the measurement in the temperature interval between the start and end condition. The energy content at supercooled state does for both theories agree well with the measurement.

The power of the charge is displayed in Fig. 7 along with the heat exchange capacity rate for the same period.

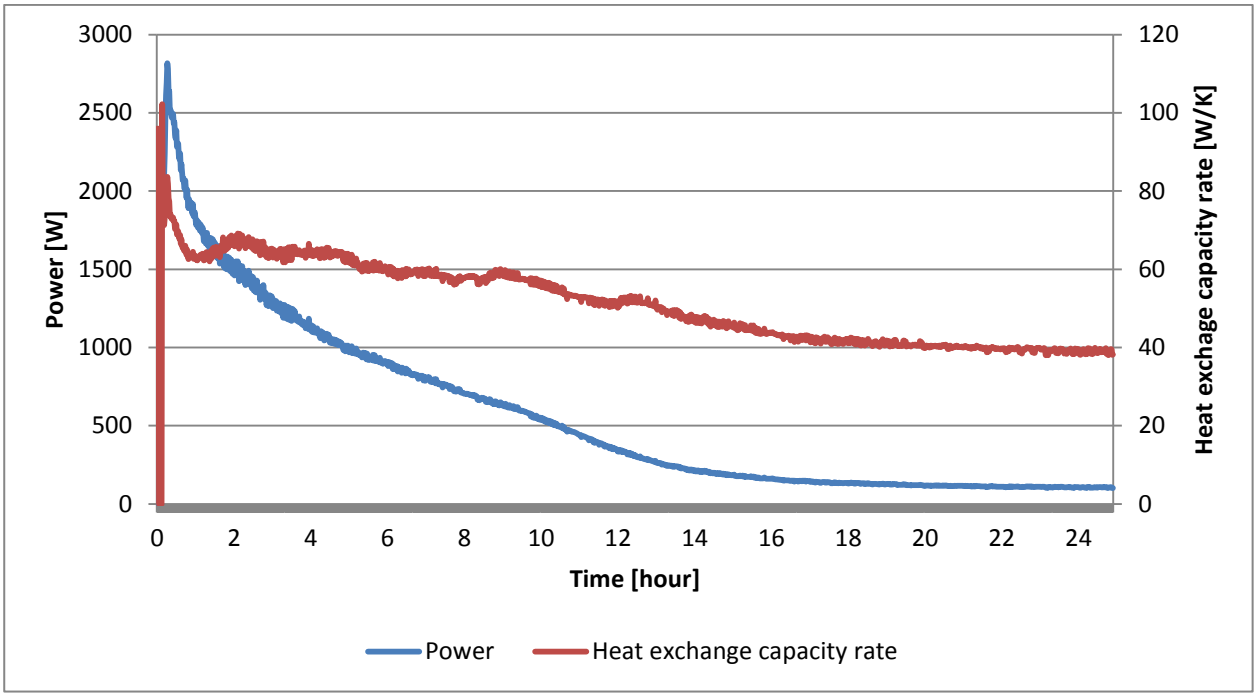

Figure 7. Power and heat exchange capacity rate over time.

The discharge power from T_{max} to supercooled state is displayed in Fig. 8. It was not possible to calculate the heat exchange capacity rate for the discharge due to the fact that the outlet temperature was higher than the average storage temperature due to thermal stratification in the storage and the low flow rate.

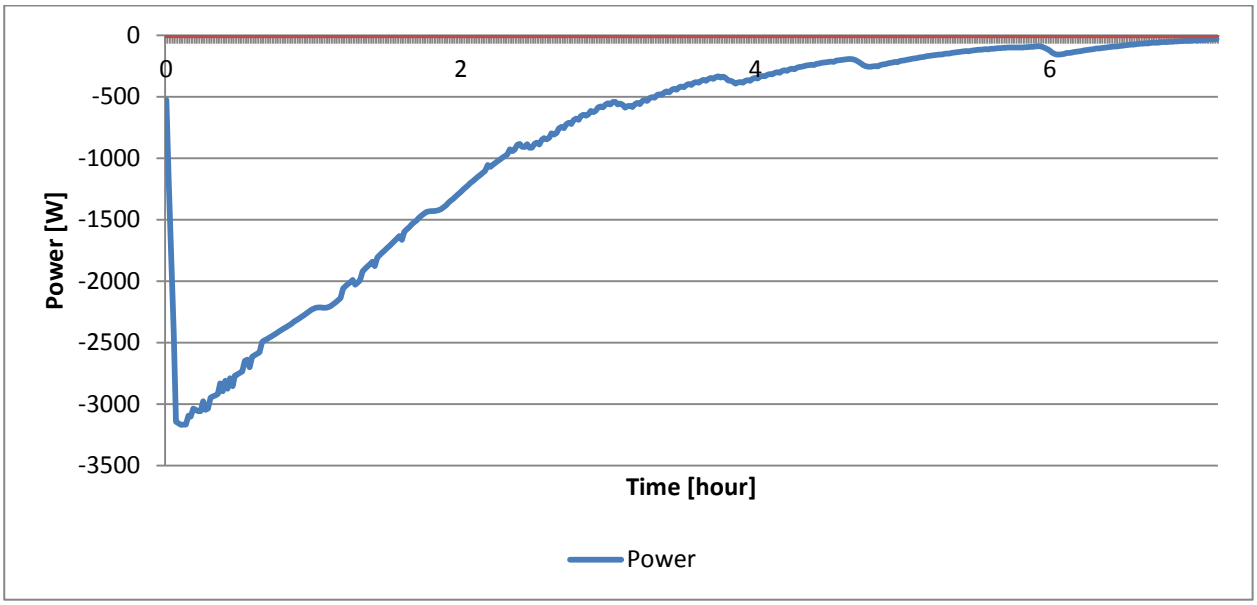

Figure 8. Discharge to supercooled state.

Discharge power after the activation is displayed in the Fig. 9.

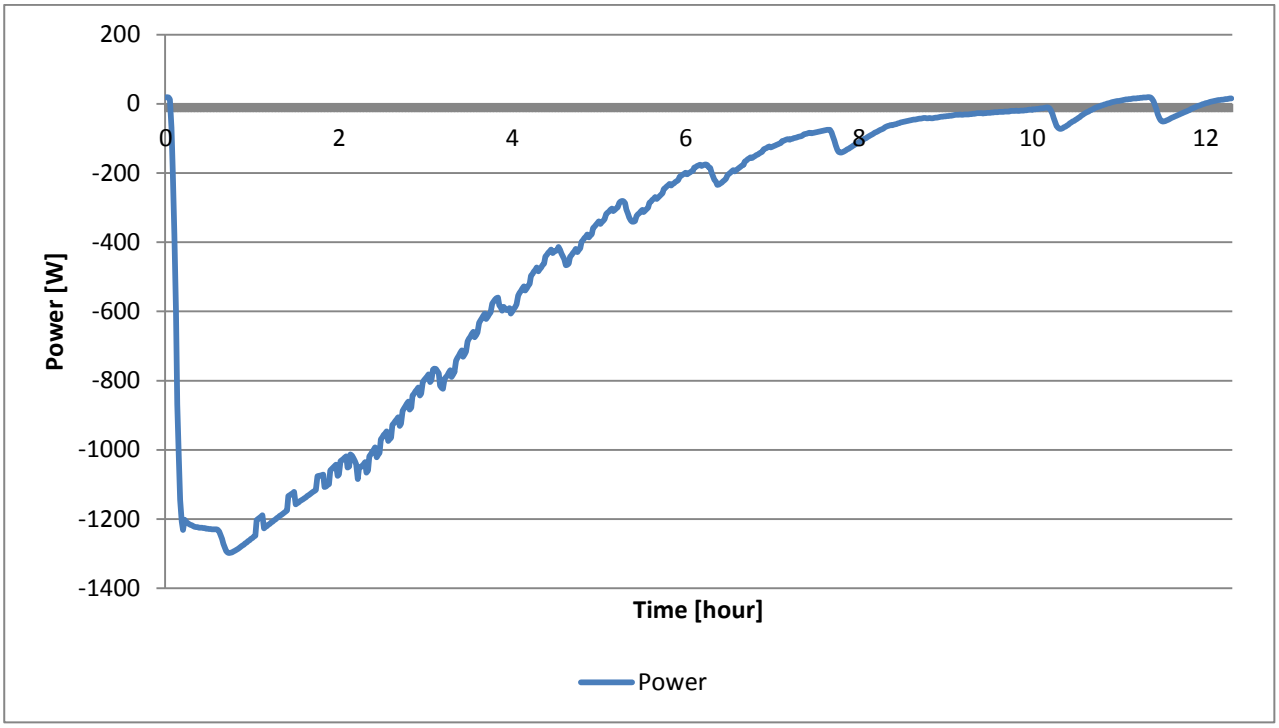

Figure 9. Discharge after activation.

Fig. 10 shows the heat exchange capacity rate as a function of storage temperature for charging.

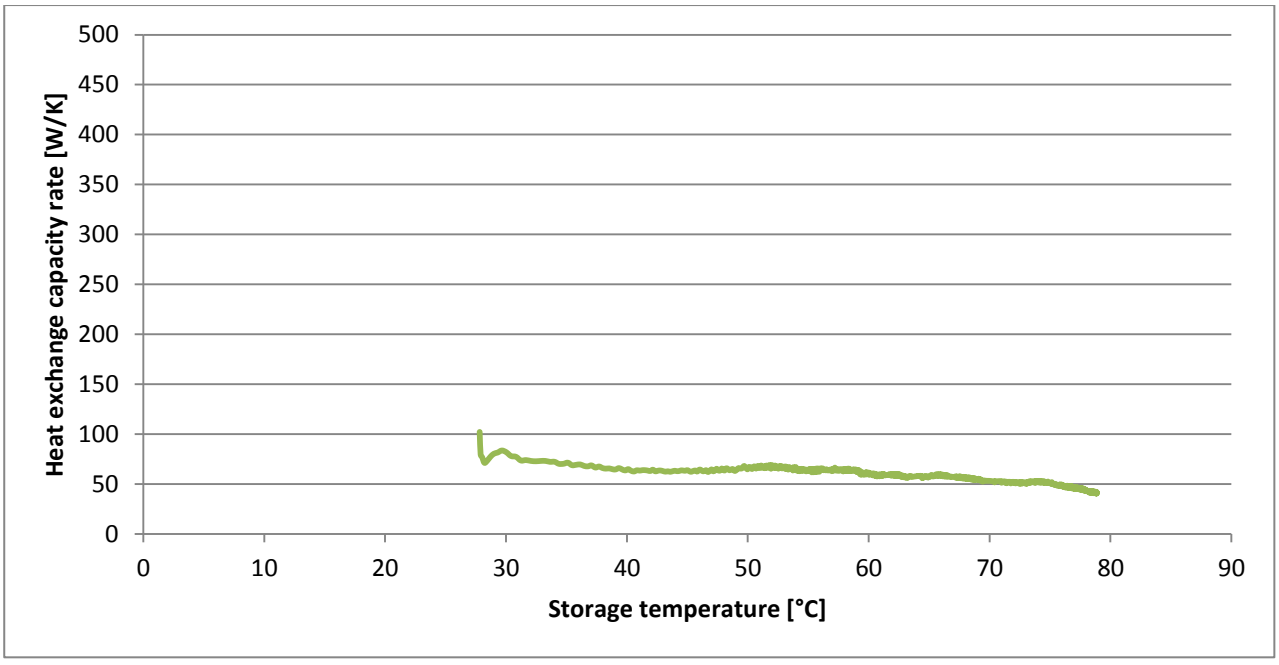

Figure 10. heat exchange capacity rate as a function of storage temperature.

Fig. 11 shows the heat exchange capacity rate as a function of the charge power for charging.

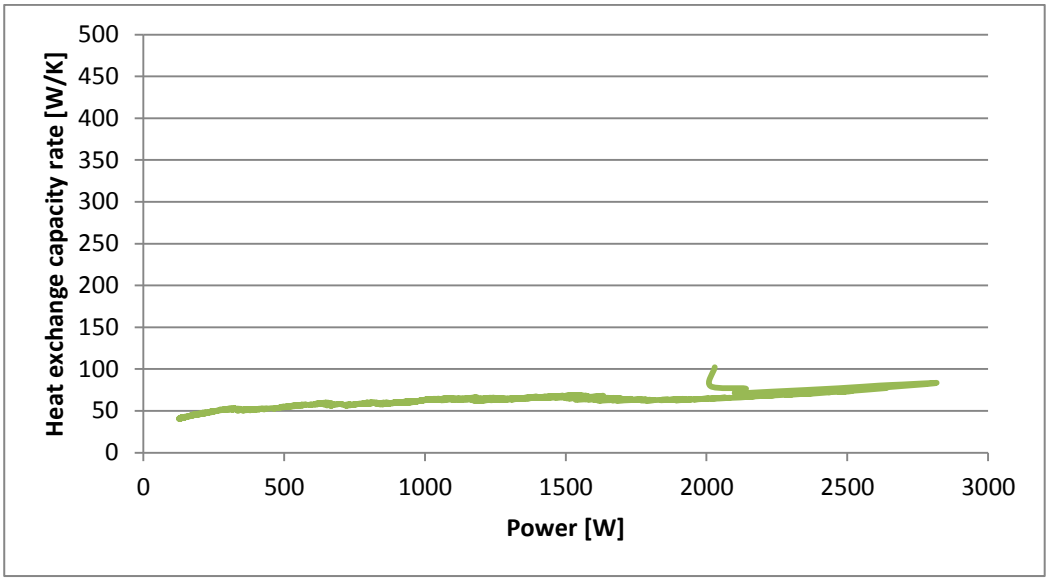

Figure 11. Heat exchange capacity rate as a function of charge power.

With a flow rate of 0.6 l/min the heat exchange capacity rate was in the order of 40 – 60 W/K. The charge period until stable above 80°C was more than 20 hours.

Test cycle 3:

Test cycle 3 was initiated with an average storage temperature of 19°C. Fig. 12 shows the temperature development for the inlet, outlet, ambient, surface and internal temperatures as well as the flow rate for the test cycle. Flow rate was approximately 2 l/min for charge, discharge was passive and for the discharge after activation the flow rate was 2 l/min.

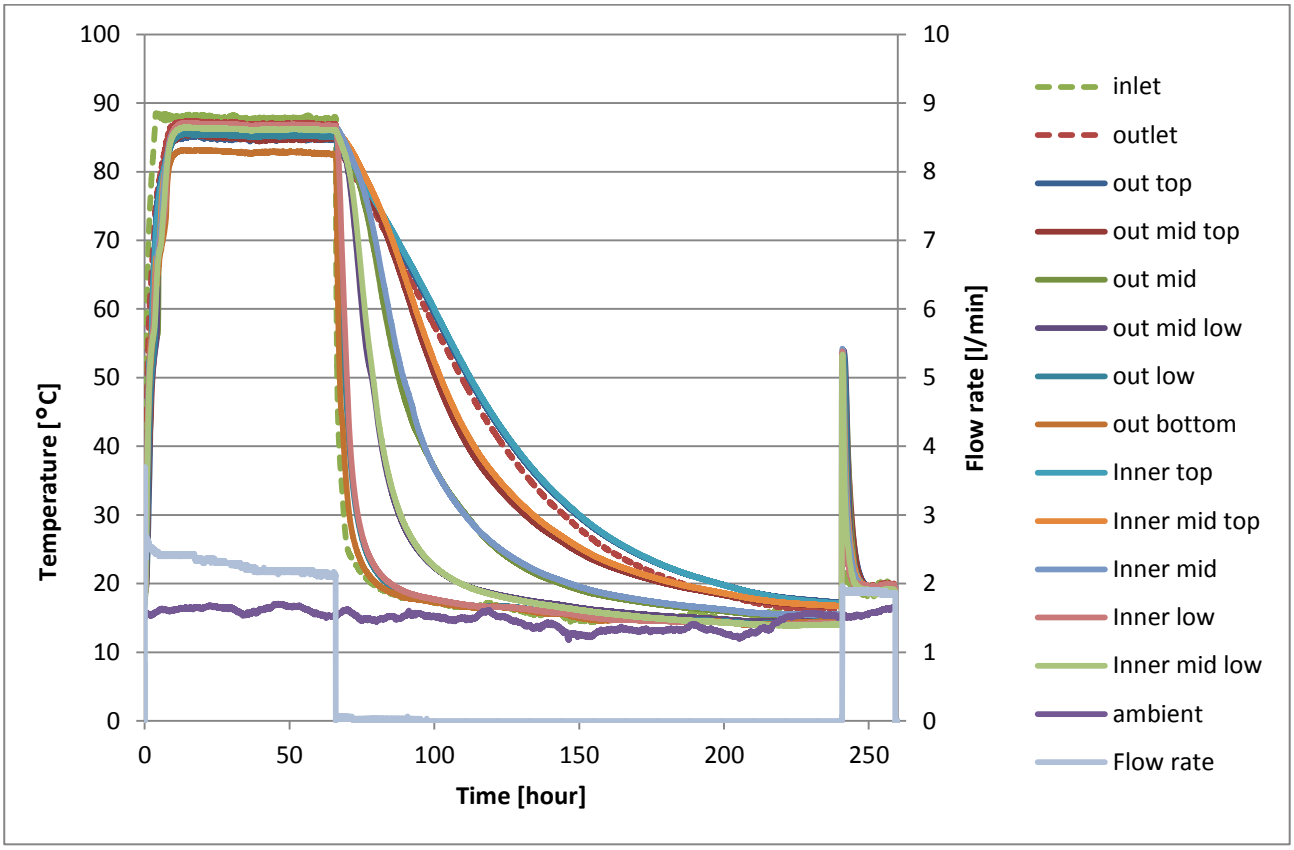

Figure 12. Temperature development and flow rate.

Fig 13 shows the temperature development in the charging period in detail.

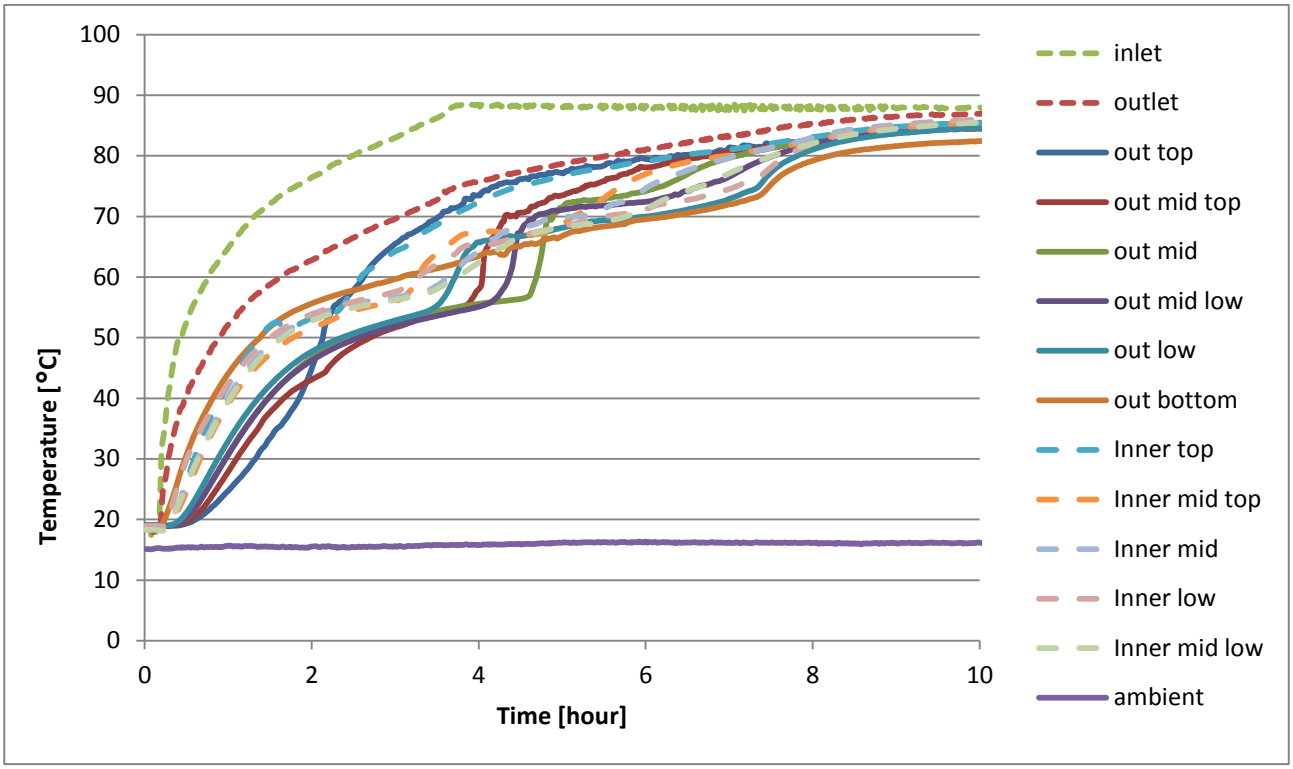

Figure 13. Temperature development during charge.

Fig. 14 shows the passive discharge to supercooled state in detail.

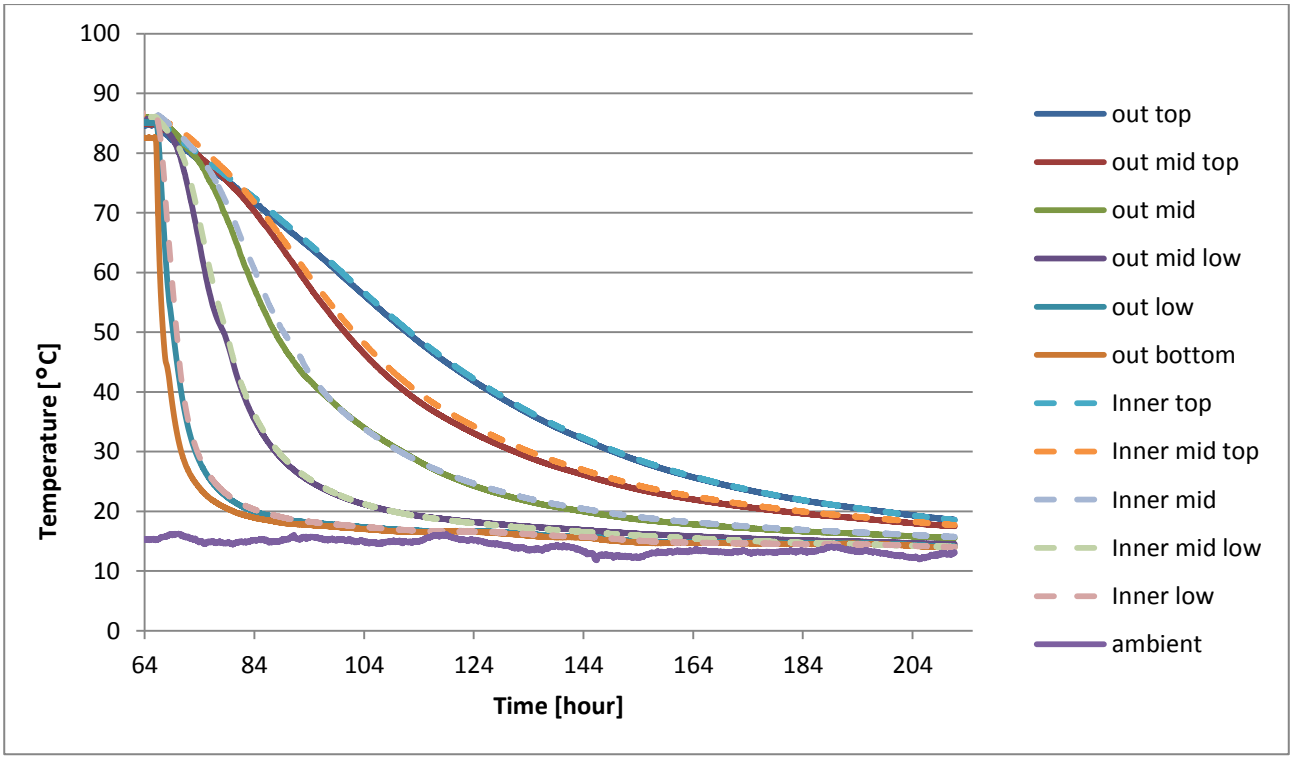

Figure 14. Temperature development for passive discharge to supercooled state.

Fig. 15 shows the temperature development for the activation and the following discharge. Activation was started by a hit with a hammer on the lower window frame. Flow rate was 2 l/min.

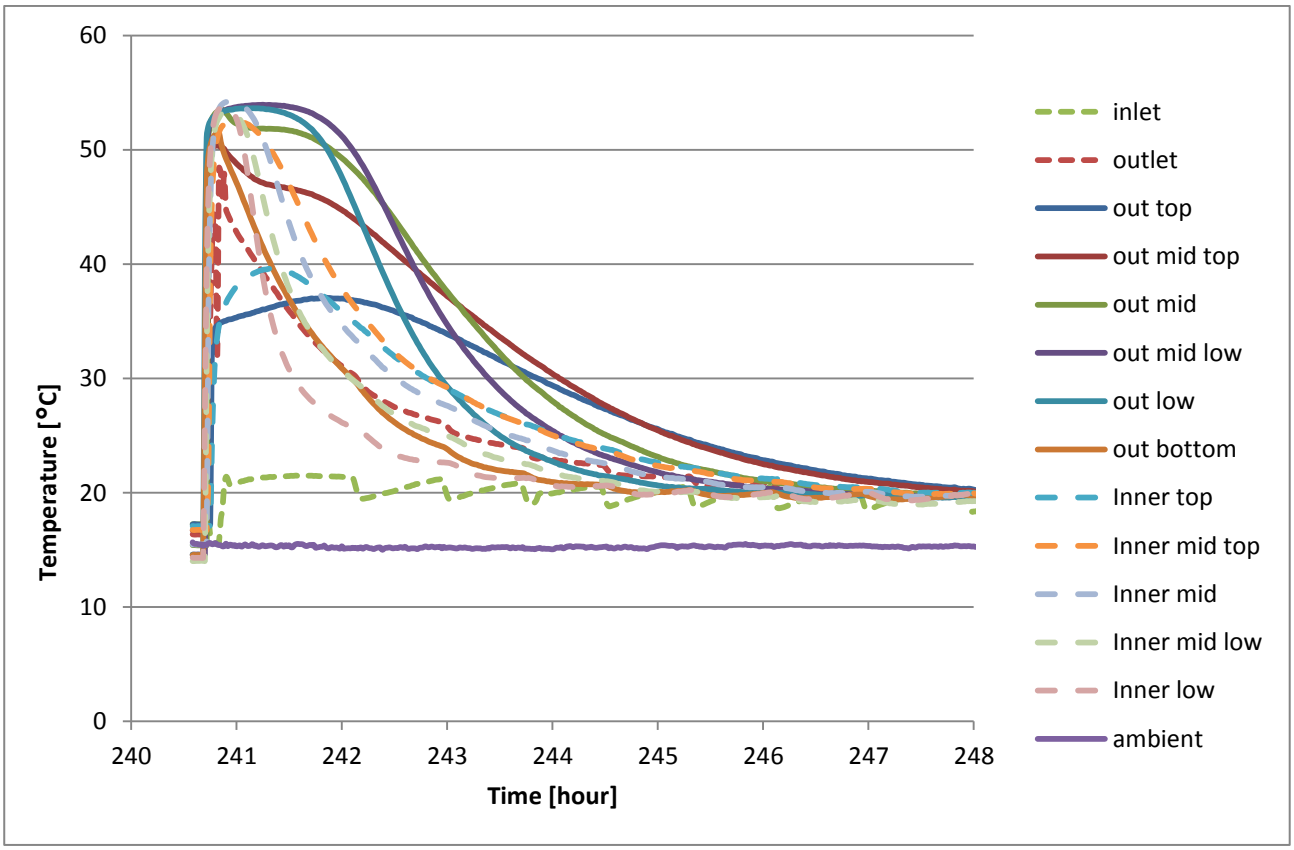

Figure 15. Temperature development for activation and discharge.

With a flow rate of 2 l/min the outlet temperature dropped below 40°C after approximately 0.5 hours.

Tab. 22 below summarizes the start, maximum and end temperature of the storage for the test cycle.

Table 5. Storage start temperature, maximum temperature and end temperatrure.

T_{start}	18.9°C
T_{max}	86.0°C
T_{super}	15.5°C
T_{end}	19.5°C

Measured energy changes:

Tab. 6 summarizes the thermal energy content determined by the measurements at T_{max}, and the energy released after the activation of the supercooled salt water mixture. The start temperature was the reference temperature for the calculation of the energy content.

Table 6. Thermal energy content at start, supercooled state and end of test cycle based on measurements.

E_{start}	0 kJ
$E_{max,exp}$	48000 kJ
$E_{activated,exp}$	16800 kJ

Theoretical energy change:

The salt water mixture was passively cooled to 15.5°C before activated. After activation the module was discharged to 19.5°C. The theoretical discharged energy after activation calculated and listed in the Tab. 7 and Tab. 8 were corrected for this temperature difference so that they can be directly compared to the measured value. Based on the simple ideal melting theory and the measured temperatures of the heat storage module the theoretical thermal energy change of the storage module is listed in the Tab. 7.

Table 7. Thermal energy content based on simple ideal thermal energy content theory.

$E_{start,theo}$	0 kJ
$E_{charge,theo}$	47160 kJ
$E_{activated,theo}$	18370 kJ

Based on the theory of thermal energy content for incongruently melting salt hydrates the theoretical energy content of the storage at different states are listed in the table below.

Table 8. Thermal energy content based on incongruently melting salt hydrate's thermal energy content.

$E_{start,theo}$	0 kJ
$E_{charge,theo}$	47600 kJ
$E_{activated,theo}$	18460 kJ

The energy discharged from the module was 10% lower than the theoretical energy content of the module. One explanation for this loss in energy is the phase separation occurring over the 7 days of passive discharge.

Fig. 16 summarizes the theoretical and the measured thermal energy content of the salt water mixture per mass unit as a function of the storage temperature.

The mean storage temperature of 18.9°C at the start of the charging was used as the reference temperature. The measured and the theoretical energy contents are therefore 0 kJ at this temperature.

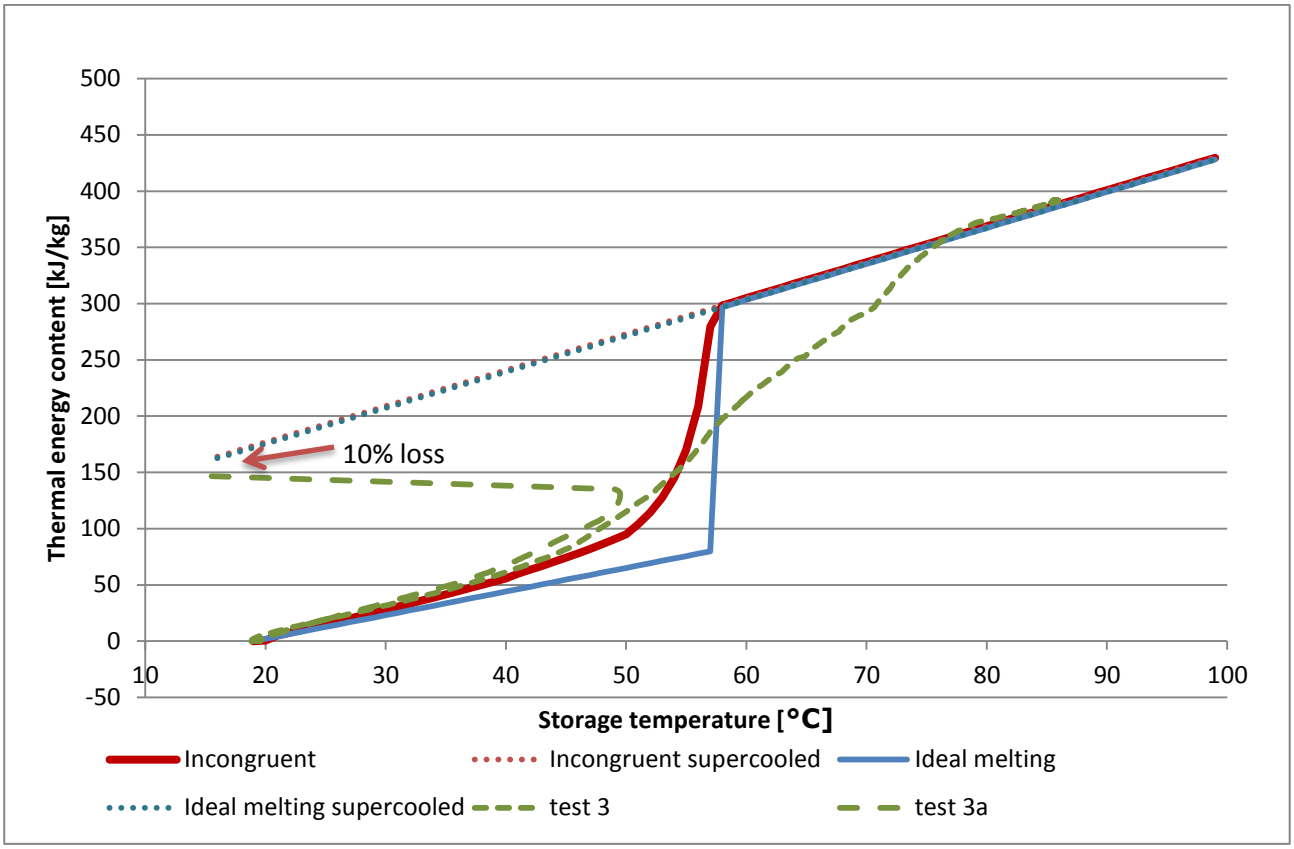

Figure 16. Theoretical and measured thermal energy content of salt water mixture per mass.

Fig. 16 shows that the simple ideal thermal energy content has a good agreement with the measurements when considering the start and end condition of the experiment for the charge. The passive discharge to supercooled stated was not included in this diagram as heat loss for this long period was uncertain and leads to large deviations. The activation and following discharge was fitted to the diagram by assuming the energy content at the end of discharge was 0 kJ/kg. The measured thermal energy released from supercooled state was 10% lower that the theoretical.

The power of the charge is displayed in Fig. 17 along with the heat exchange capacity rate for the same period.

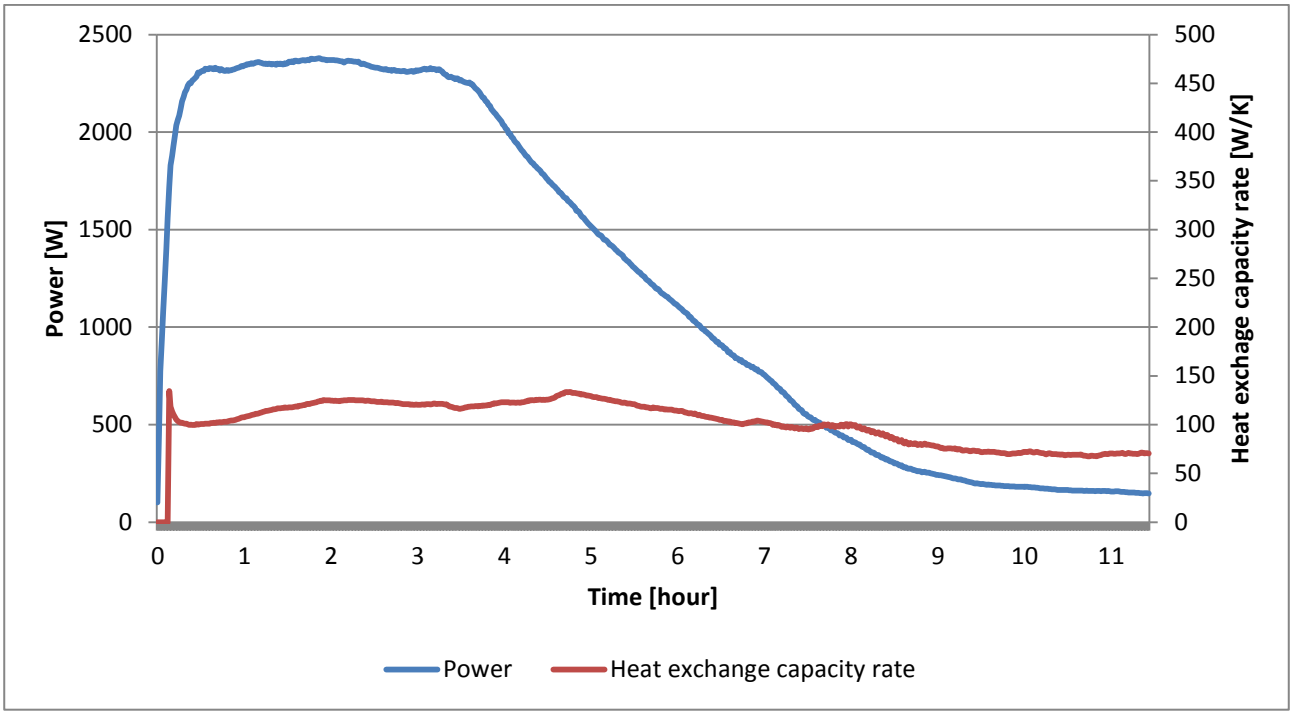

Figure 17. Power and heat exchange capacity rate over time for charge.

Discharge power after the activation and heat exchange capacity rate is displayed in Fig. 18.

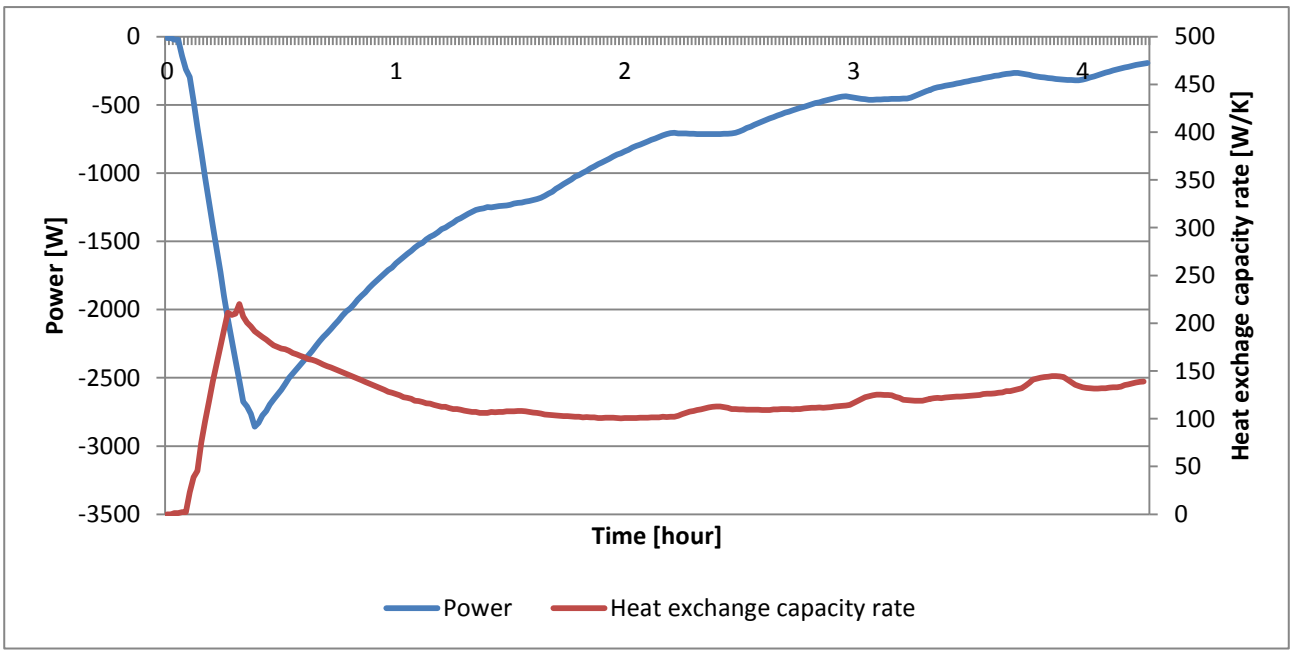

Figure 18. Discharge after activation.

Fig. 19 shows the heat exchange capacity rate as a function of storage temperature for charge and activation.

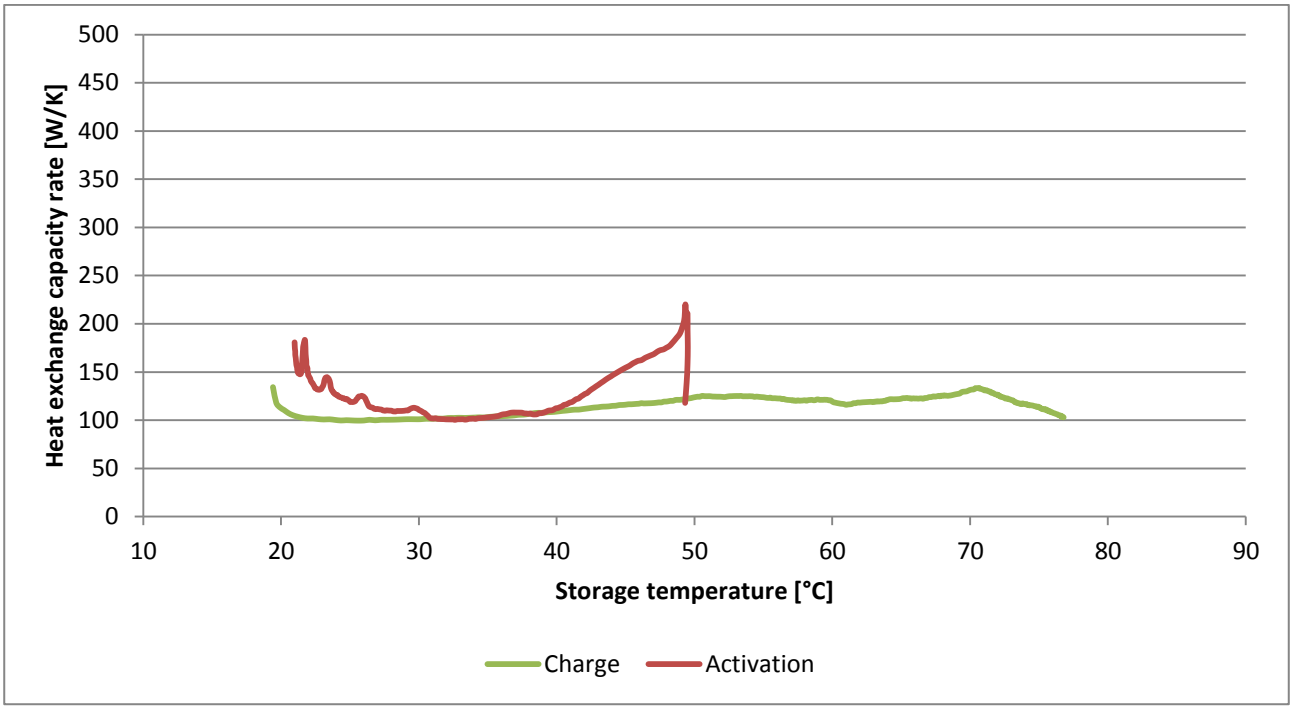

Figure 19. Heat exchange capacity rate as a function of storage temperature.

Fig. 20 shows the heat exchange capacity rate as a function of the charge power.

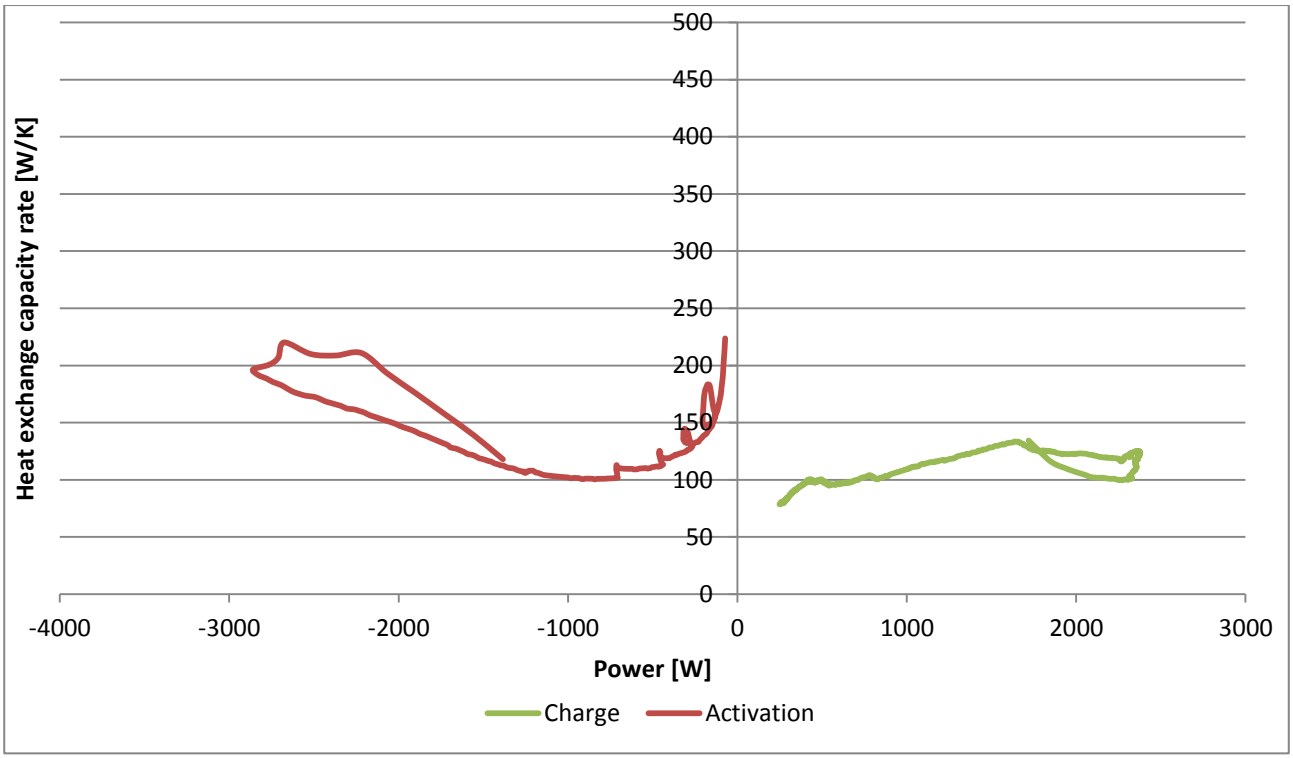

Figure 20. Heat exchange capacity rate as a function of charge power.

With a flow rate of 2 l/min the heat exchange capacity rate is 100 – 130 W/K for charge and 100 – 200 W/K for discharge.

Test cycle 4a:

Module was charged with a flow rate of 7.4 l/min, an inlet temperature topping at 88.5°C, an average charge power of 3 kW, topping at 8 kW in the beginning of the charge period, for 5 hours until a minimum temperature of 82.8°C was reached at the bottom sensor of the storage. The module was set to discharge passively to ambient temperature. The crystallization started spontaneously after 7 days just before ambient temperature was reached. Crystallization started from the bottom. After the passive discharge a 10 cm liquid layer was observed at the top of the cylinder.

Test cycle 4b:

Module was charged with a flow rate of 7.4 l/min, an inlet temperature topping at 88.5°C, an average charge power of 3 kW topping at 8 kW for 25 hours until a minimum temperature of 83.2°C was reached. Temperatures at charged state were kept stable for 20 hours. The module was set to discharge passively. The crystallization started after 19 hours of passive discharge when the temperature in the bottom had reached 19°C. The temperature in the top was 70°C. It is unclear from where the crystallization started. After discharge a 10 cm liquid layer was observed at the top of the cylinder.

Test cycle 5:

Module was charged with a flow rate of 7.4 l/min, an inlet temperature topping at 90.5°C an average charge power of 3 kW, topping at 8 kW in the beginning of the charge period. Stable conditions were reached after 5 hours where the minimum temperature in the bottom of the storage module was 85°C. The storage was kept stable over a period of 12 hours. Module was discharge actively with a flow rate of 5.7 l/min. Crystallization started without subcooling during active discharge.

Test cycle 6:

Charge and discharge was carried out with a low flow rate of approximately 2 l/min. The crystallization started just before the module reached stable supercooled state at 19°C. The energy content at fully charged and supercooled state was slightly higher than the theoretical energy content as may be seen on Fig. 21. The energy content released after activation was 10 % lower than the theoretical energy content, most likely due to phase separation. Fig 21 shows the measured and theoretical thermal energy content of the salt water mixture in the module for the 6th test cycle.

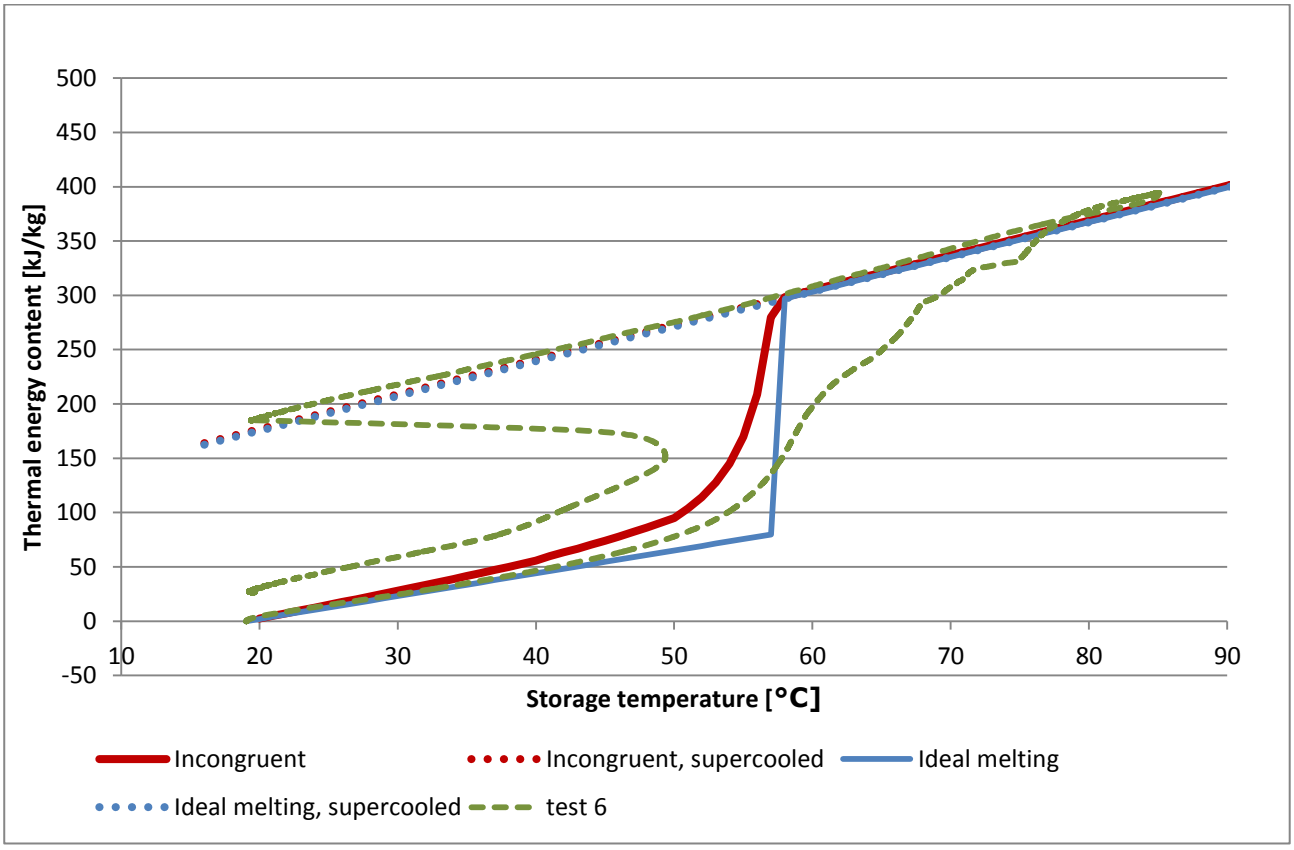

Figure 21. Measured and theoretical energy content.

Test cycle 7:

In test cycle 7 the module was charged with a flow rate of 4 l/min to a temperature of 48°C to investigate the behavior of the salt water mixture below the melting point of sodium acetate trihydrate. The heat loss coefficient with the module at 48°C and an ambient temperature of 15°C was 1.2 W/K.

The temperature of the storage and the energy content is shown in Fig. 22.

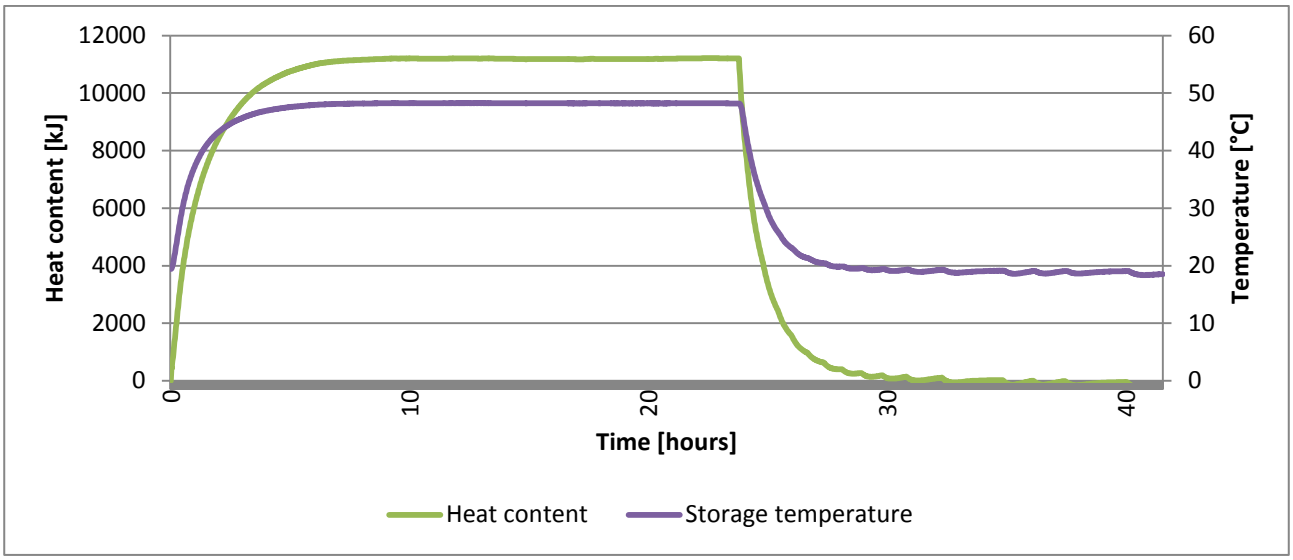

Figure 22. Storage mean temperature and thermal energy content.

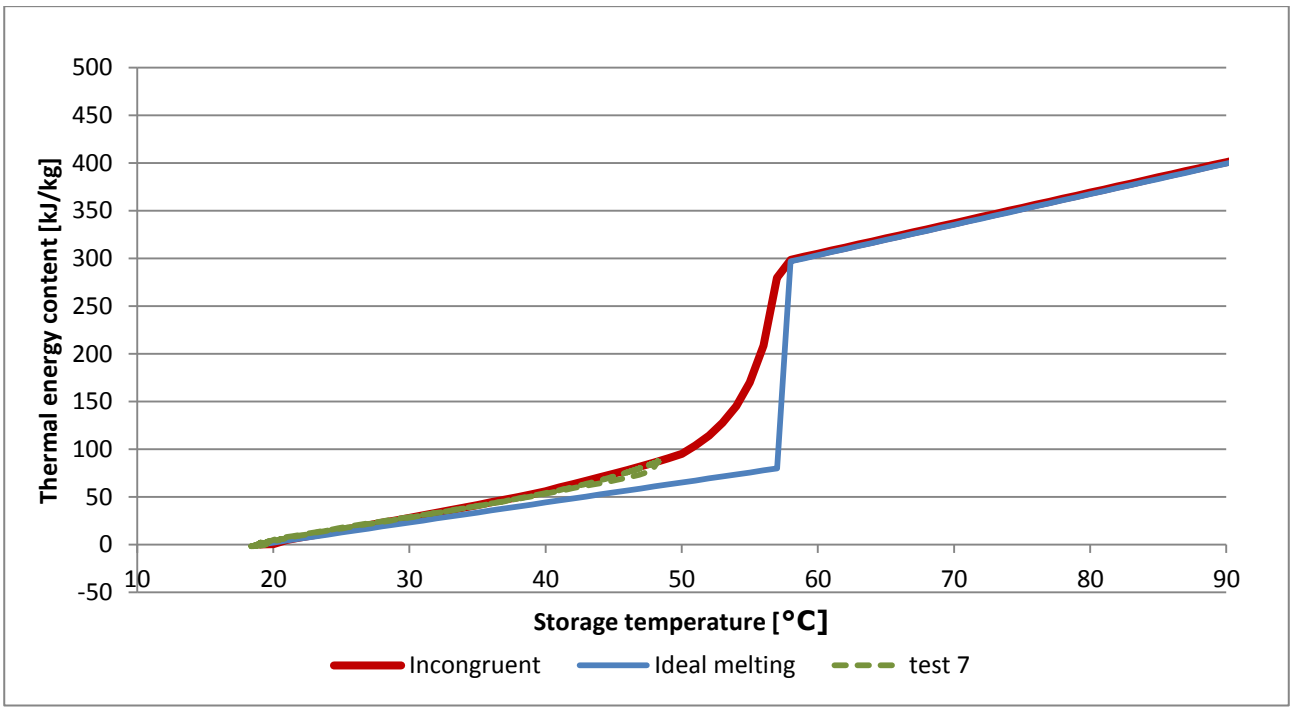

Figure 23. Measured and theoretical energy content.

The measured energy content fits excellent with the theory of the incongruently melting salt water mixture in the temperature interval 19°C to 48°C as may be seen in Fig. 23.

Test cycle 8:

Module was charged and discharged with a flow rate of 3.7 – 4.0 l/min. The charge period was 28 hours. The module was actively discharged to supercooled state and stable for approximately 40 hours. The module was activated by slight shaking.

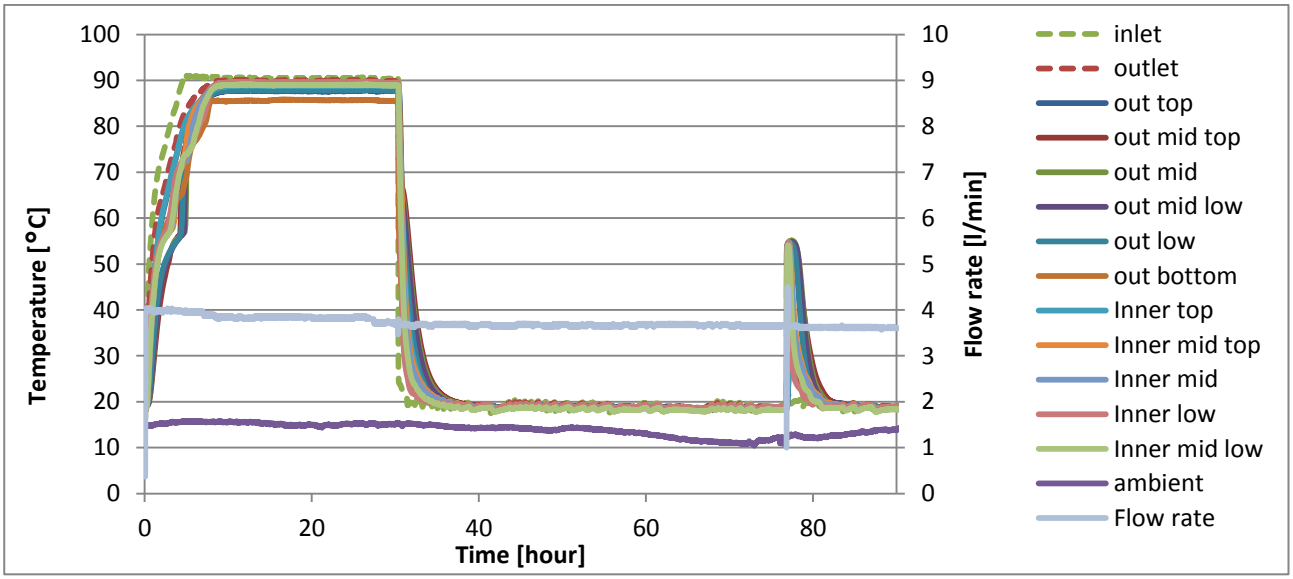

Figure 24. Temperature over time for test cycle.

It may be seen from Fig. 25 that the energy charged to the system is slightly lower than the theoretical capacity. After the activation of the supercooled salt water mixture the measured energy discharged from the storage module was approximately 5% lower than the theoretical energy content.

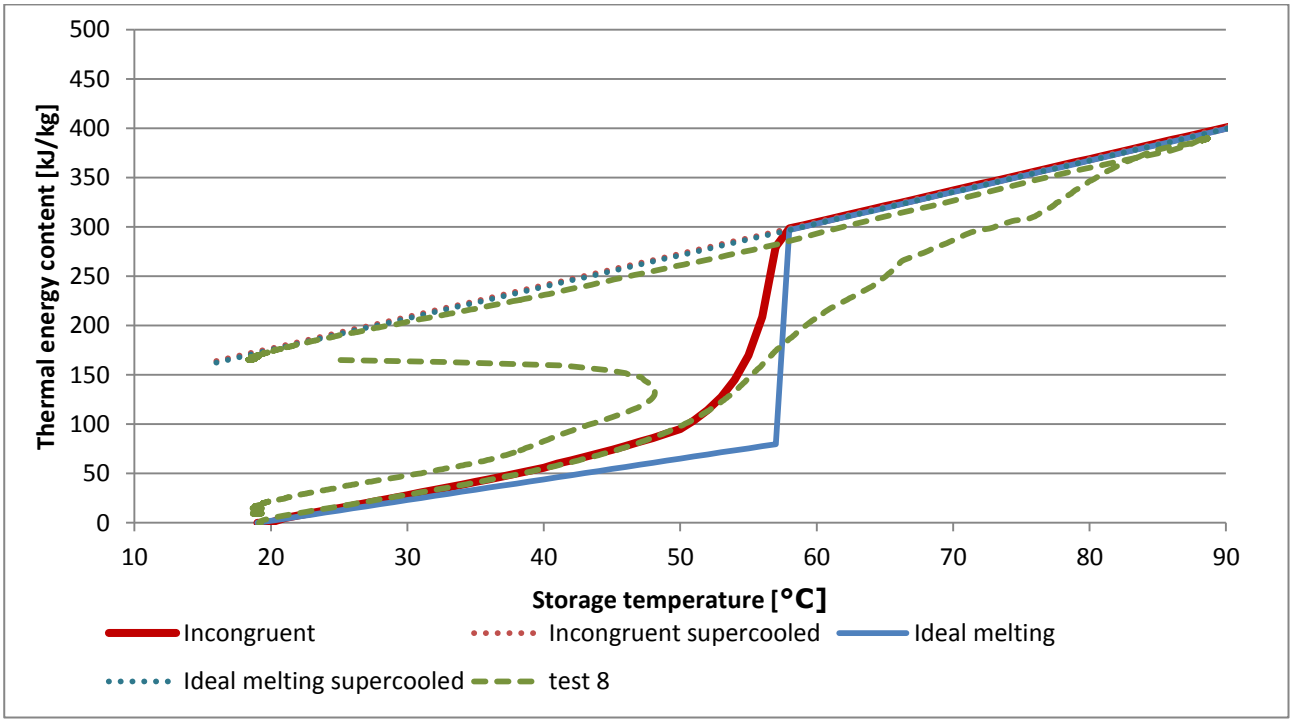

Figure 25. Measured and theoretical energy content of salt water mixture.

Test cycle 10:

In test cycle 10 the module was heated up in steps to determine the heat loss coefficient at different temperature levels and to evaluate the specific heat capacity for the salt water mixture in smaller temperature steps not including the phase change.

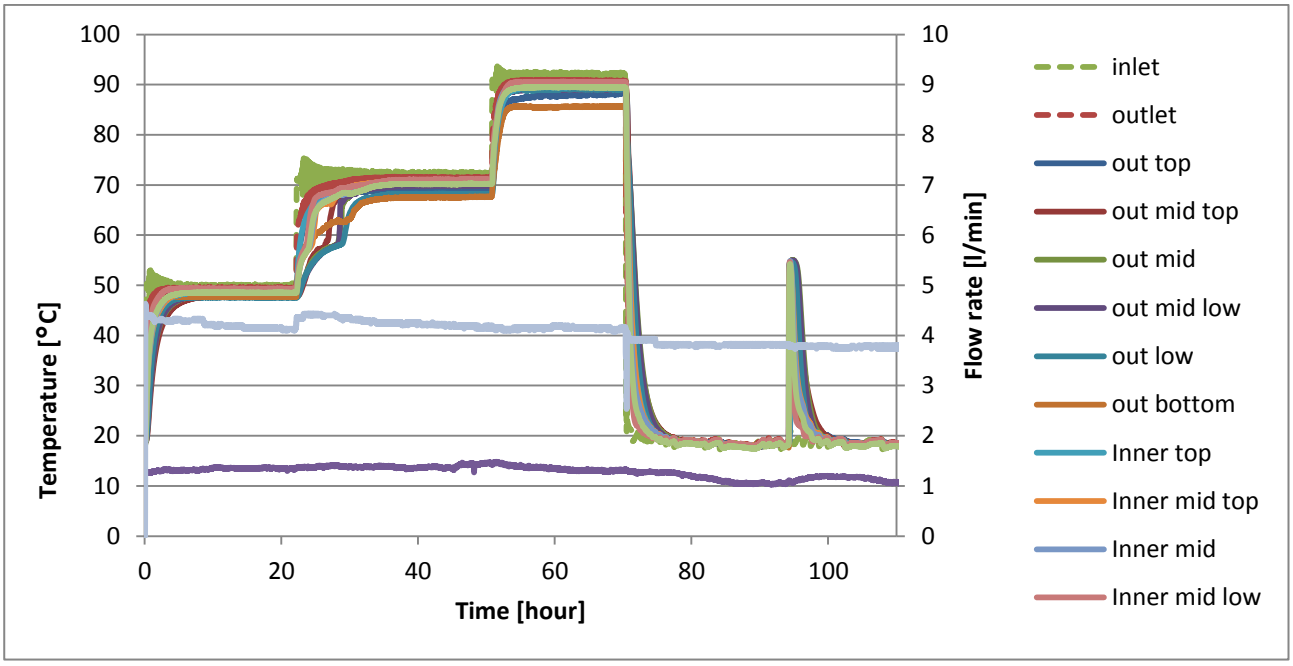

Figure 26. Temperature development over time and flow rate for test cycle 10.

With an ambient temperature of 13-14°C the heat loss coefficient for the stable periods are listed in Tab. 9

Table 9. Heat loss coefficient at different temperatures.

Storage mean temperature	Heat loss coefficient
48.4°C	1.3 W/K
69.8°C	1.7 W/K
89.1°C	1.8 W/K

Fig. 27 shows mean storage temperature and the energy content of the storage for the test cycle.

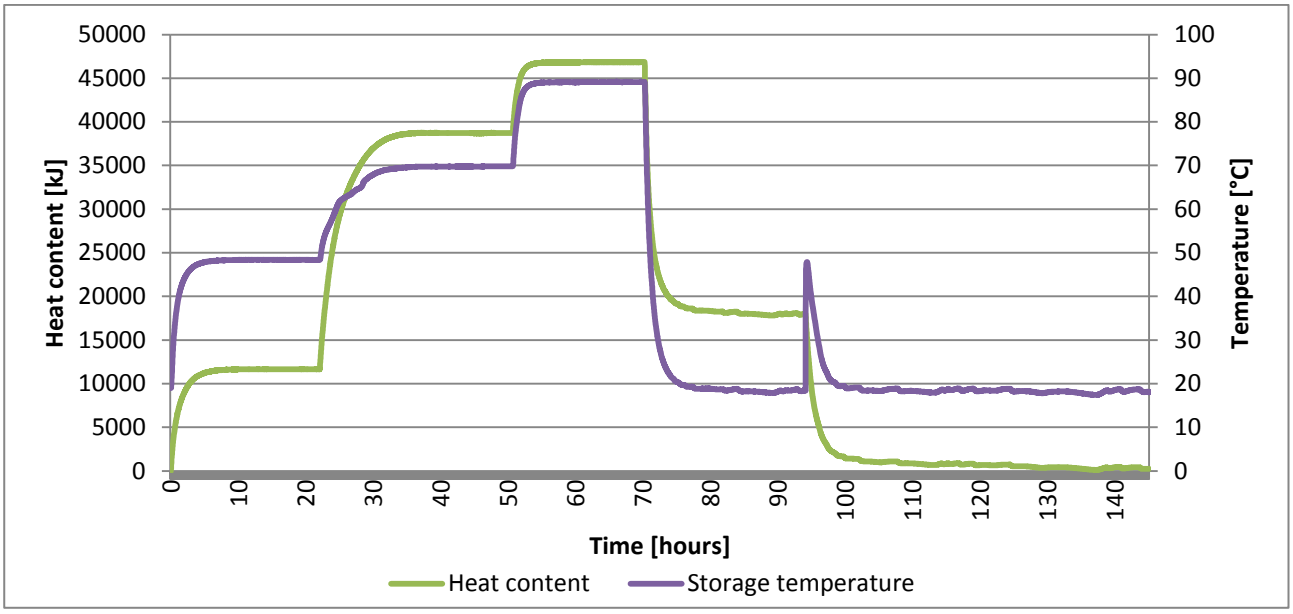

Figure 27. Mean temperature of storage and measured energy content over the test cycle.

The fit between the measured and theoretical energy content was good for temperature below 48°C. For the charge over the phase change from 48°C to 69°C the measurement was approximately 20 kJ/kg lower than the theoretical energy content for the salt water mixture which corresponds to approximately 10% of the heat of fusion. For the charging from 69°C to 89°C the measured energy content fits excellent with the theory except being at a level 20 kJ/kg below the theoretical values.

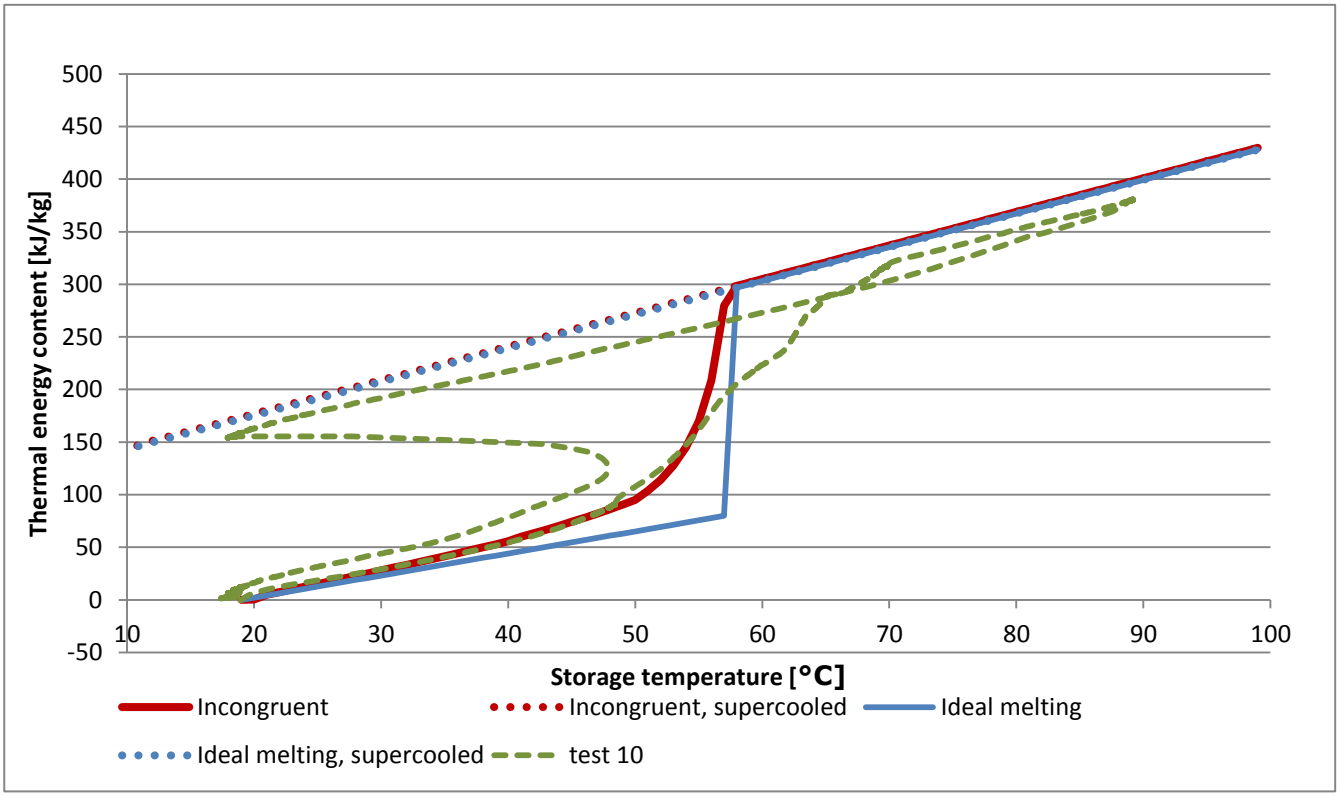

Figure 28. Measured and theoretical energy content of salt water mixture in storage module.

The energy discharged after activation was approximately 9% under the theoretical dischargeable energy.

This test cycles showed that the theoretical specific heat capacities for solid and liquid state agree well with the measured values.

Test cycle 11:

The test conditions and progress for test cycle 11 is displayed in the Fig. 29.

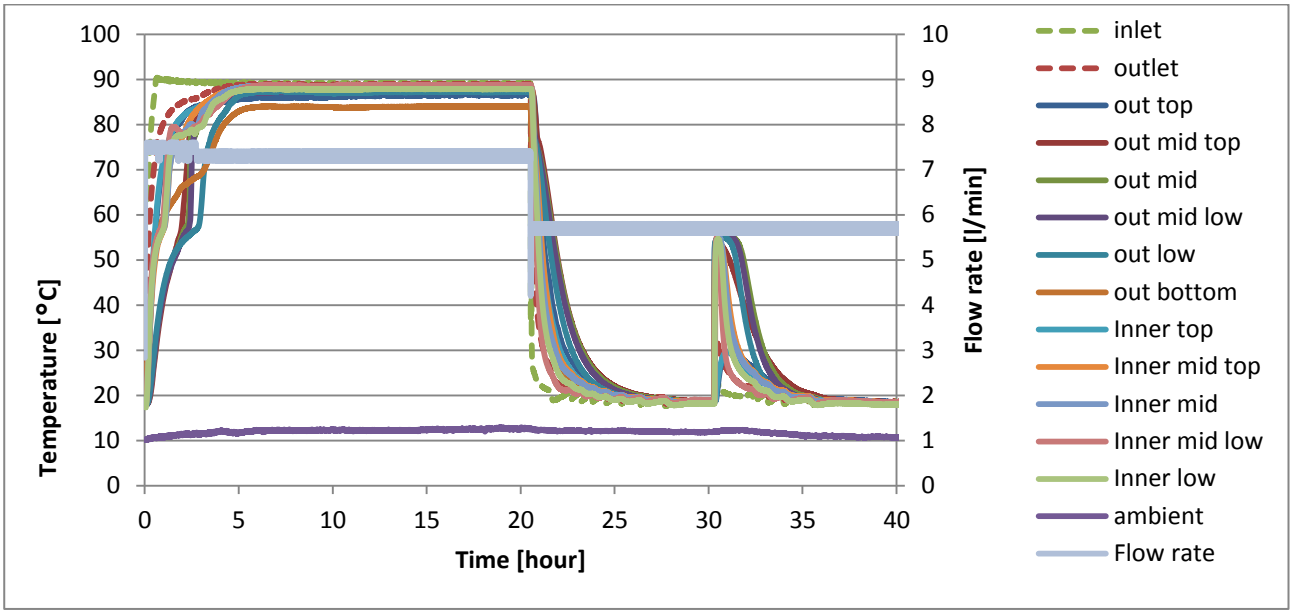

Figure 29. Temperature development over time and flow rate for test cycle 11.

The module reached supercooled state after active discharge. It was activated manually by shaking the module slightly. The measured energy content of the salt water mixture in both hot and supercooled state was 3 – 6 % lower than the theoretical energy content as may be seen in Fig. 30.

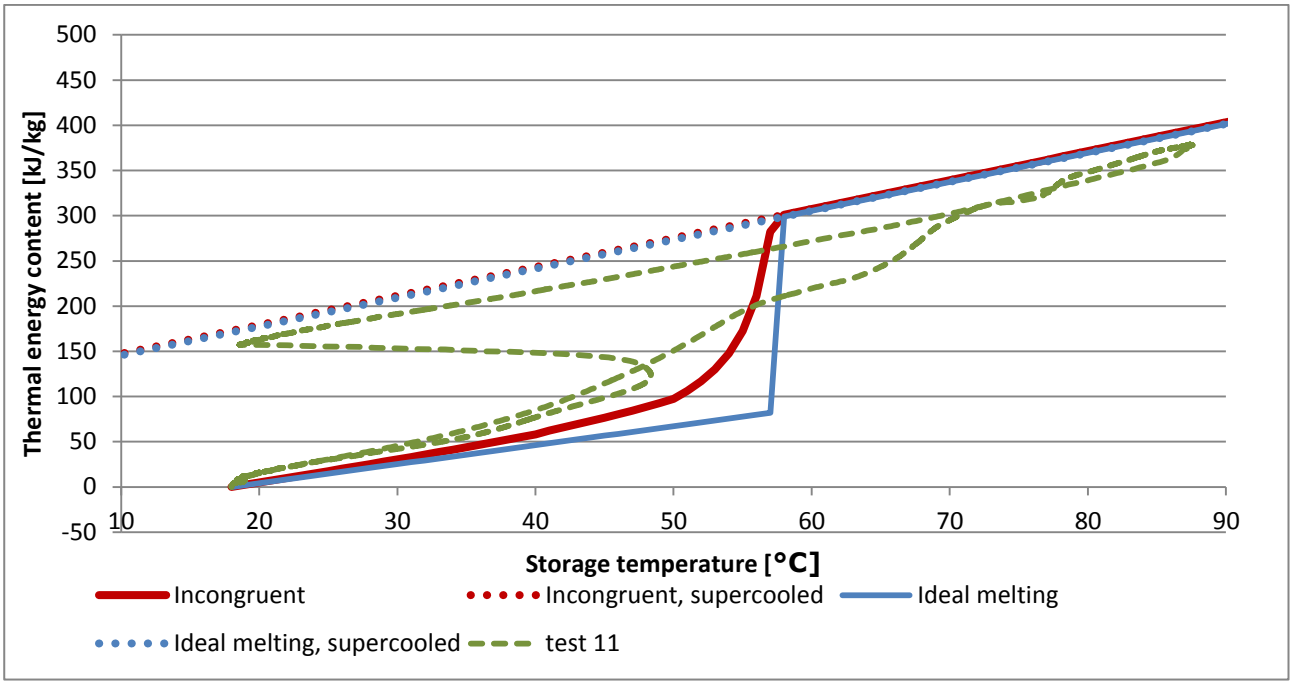

Figure 30. Measured and theoretical energy content of salt water mixture in storage module.

Test cycle 12:

The module was charged and discharged with a flow rate of 2 – 2.4 l/min. It activated spontaneously during discharge before stable supercooled state was reached. Test development may be seen in Fig. 31.

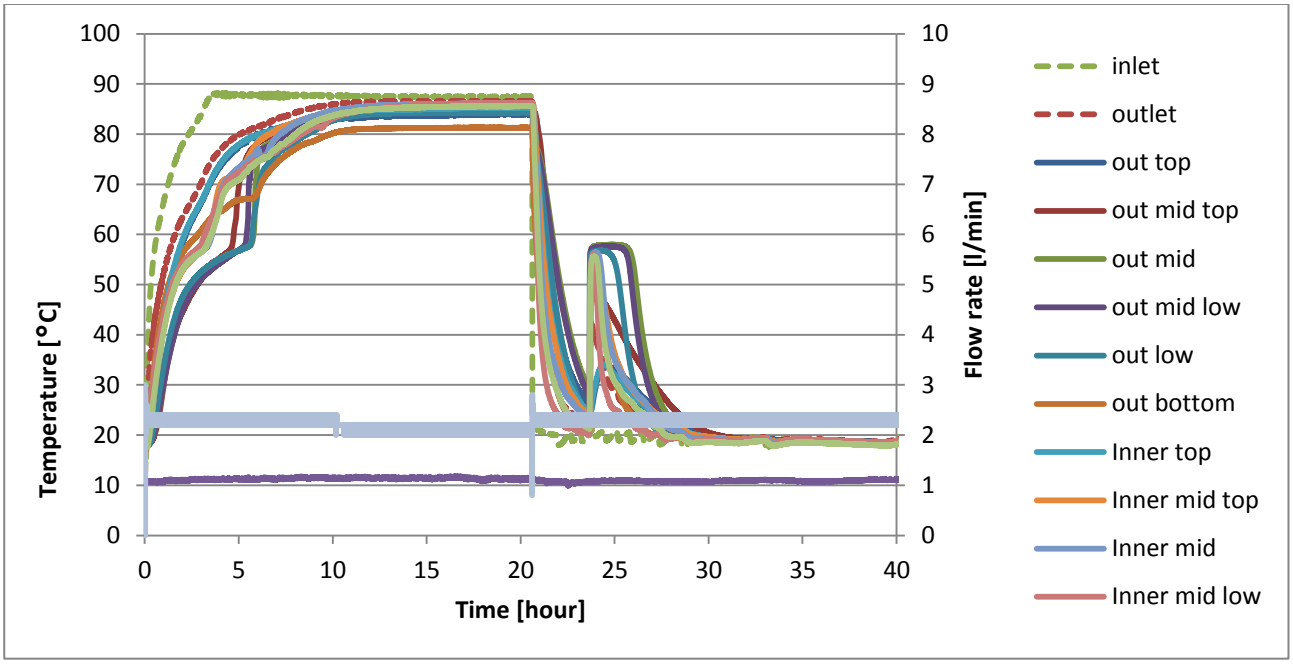

Figure 31. Temperature development over time and flow rate for test cycle 12.

The measured energy content of the salt water mixture was approximately 5% lower than the theoretical energy content in the fully charged state as may be seen in Fig. 32.

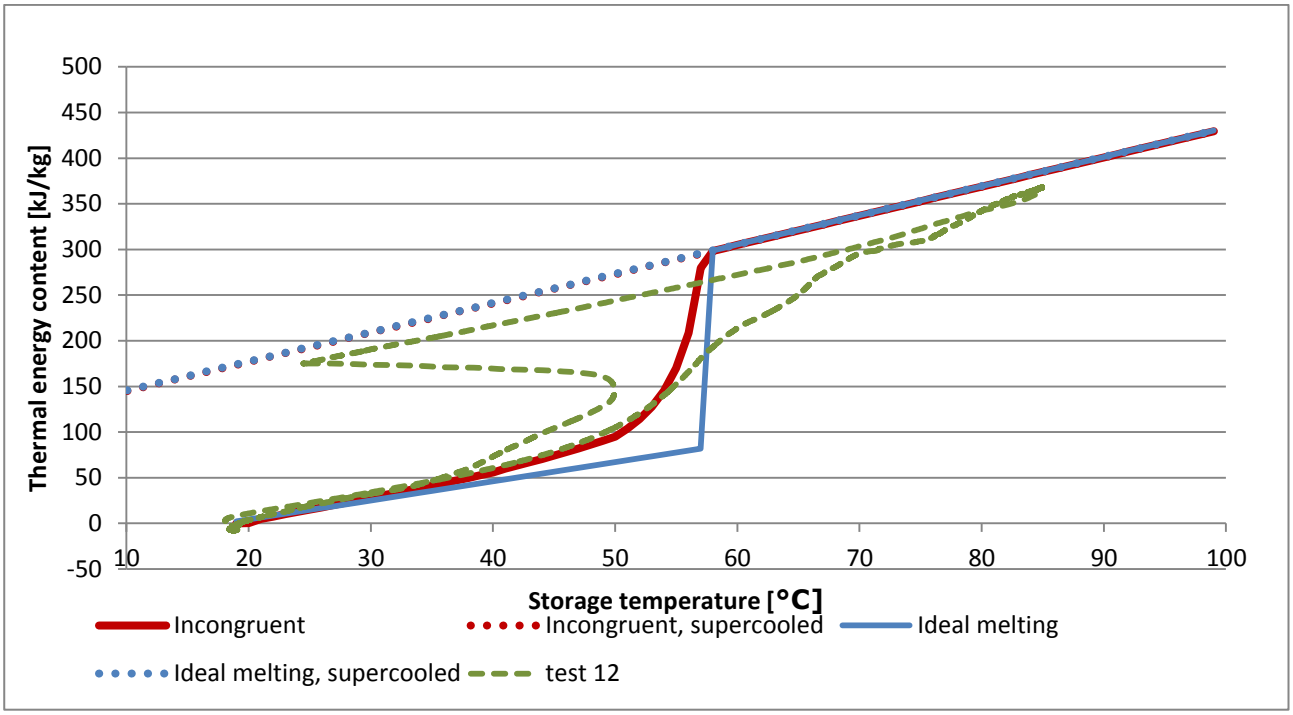

Figure 32. Measured and theoretical energy content of salt water mixture in storage module.

Test cycle 13:

The module was charged with a flow rate of 7.4 l/min for 7 hours with an inlet temperature of 90°C. The module activated during passive discharge with slight subcooling.

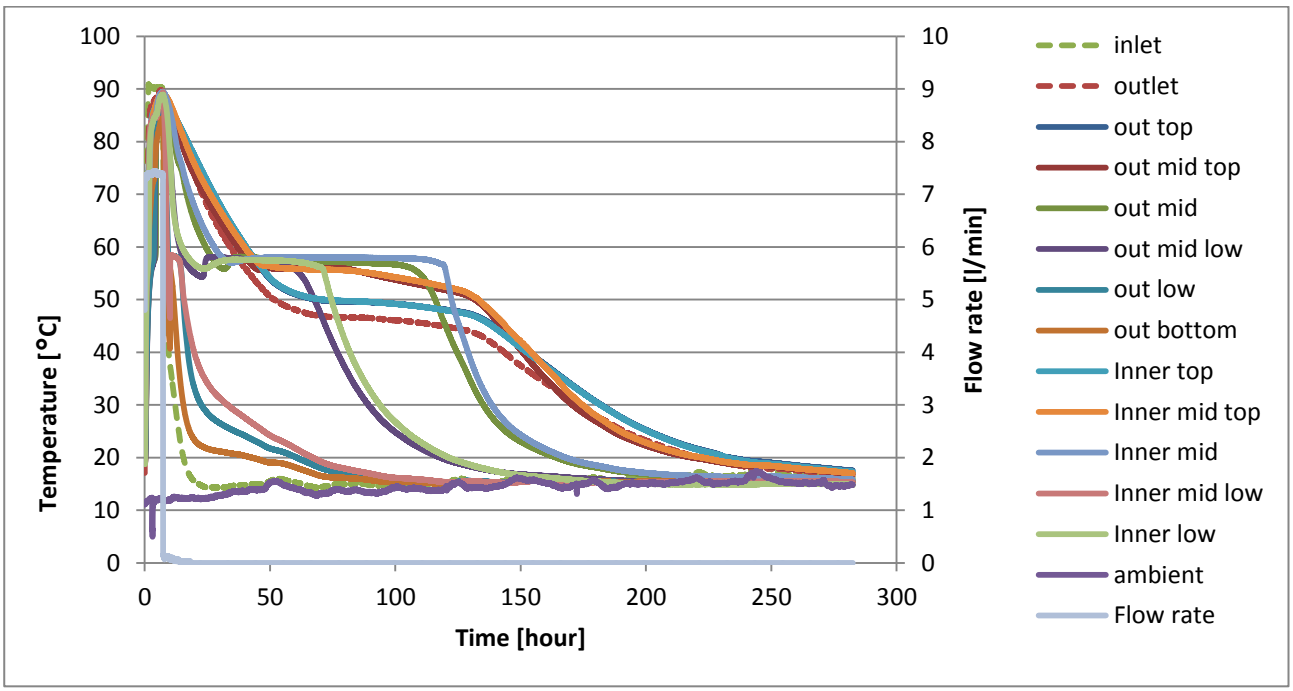

Figure 33. Temperature development over time and flow rate for test cycle 13.

The measured energy content for charging in test cycle 13 was close to theoretical energy content as may be seen is Fig. 34.

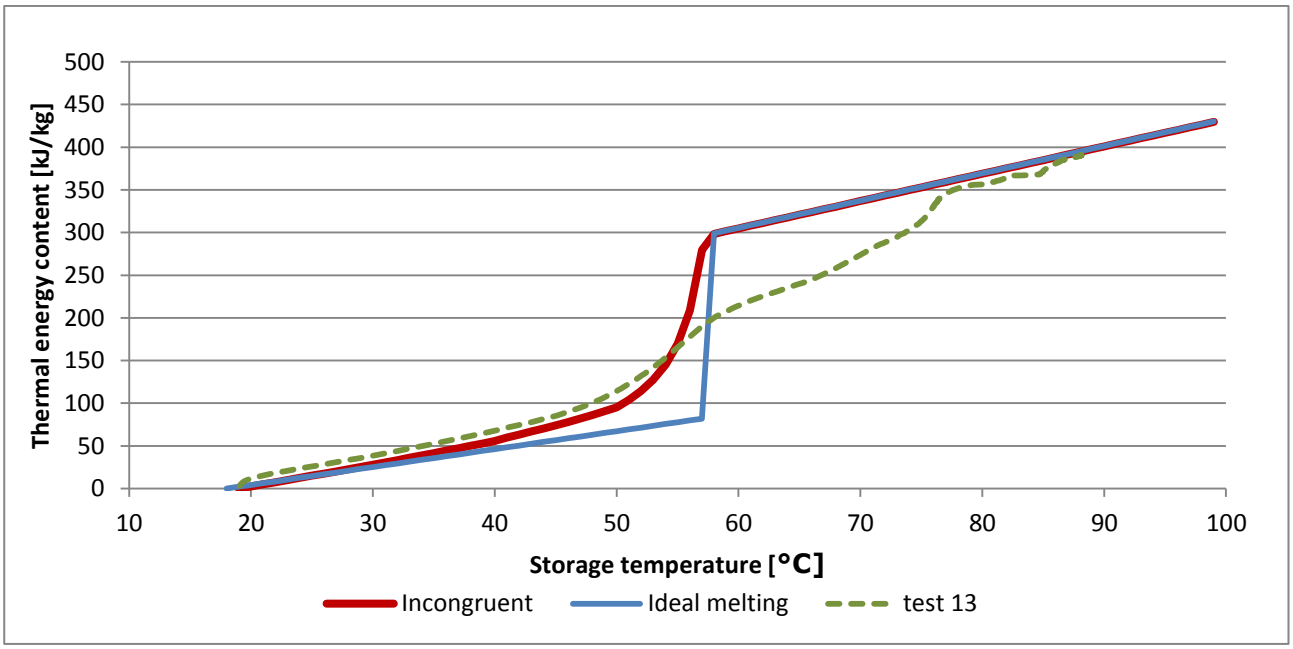

Figure 34. Measured and theoretical energy content of salt water mixture in storage module.

Test cycle 14:

The module was charged for 21 hours with a flow rate of 7.4 l/min with an inlet temperature of 90°C. The module activated during passive discharge after some subcooling in the lower part of the module. Fig. 35 shows the process and development of this test cycle.

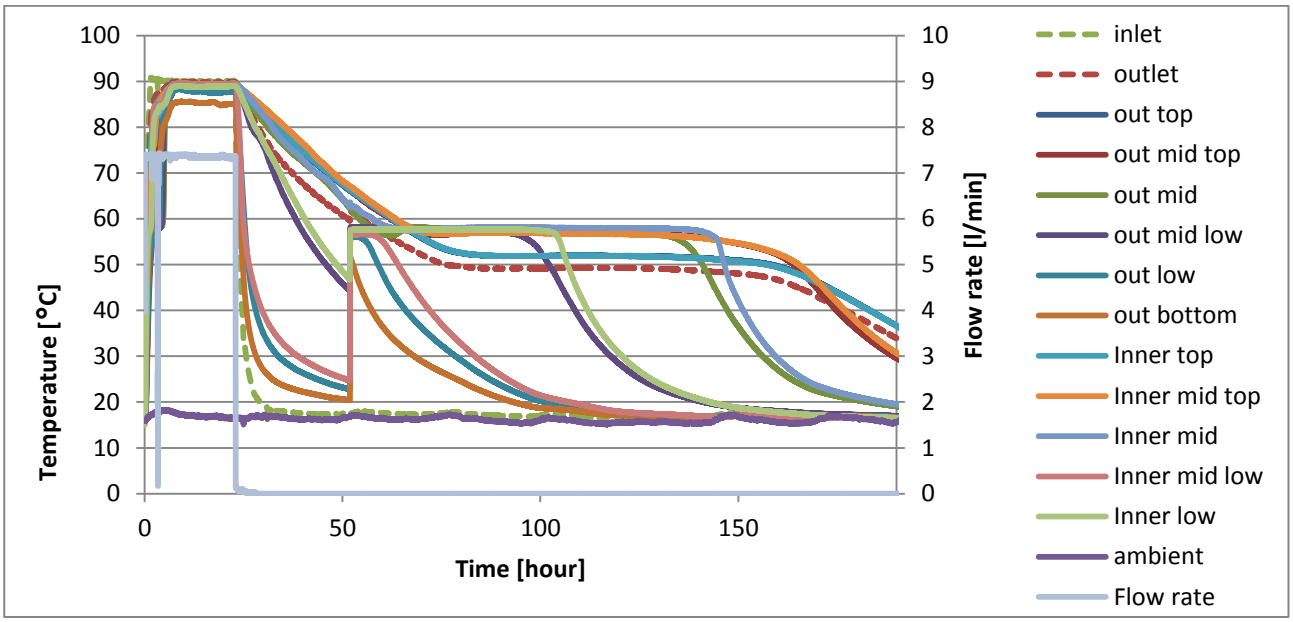

Figure 35. Temperature development over time and flow rate for test cycle 14.

The measured energy content for charging in test cycle 14 was close to theoretical energy content as may be seen is Fig. 36.

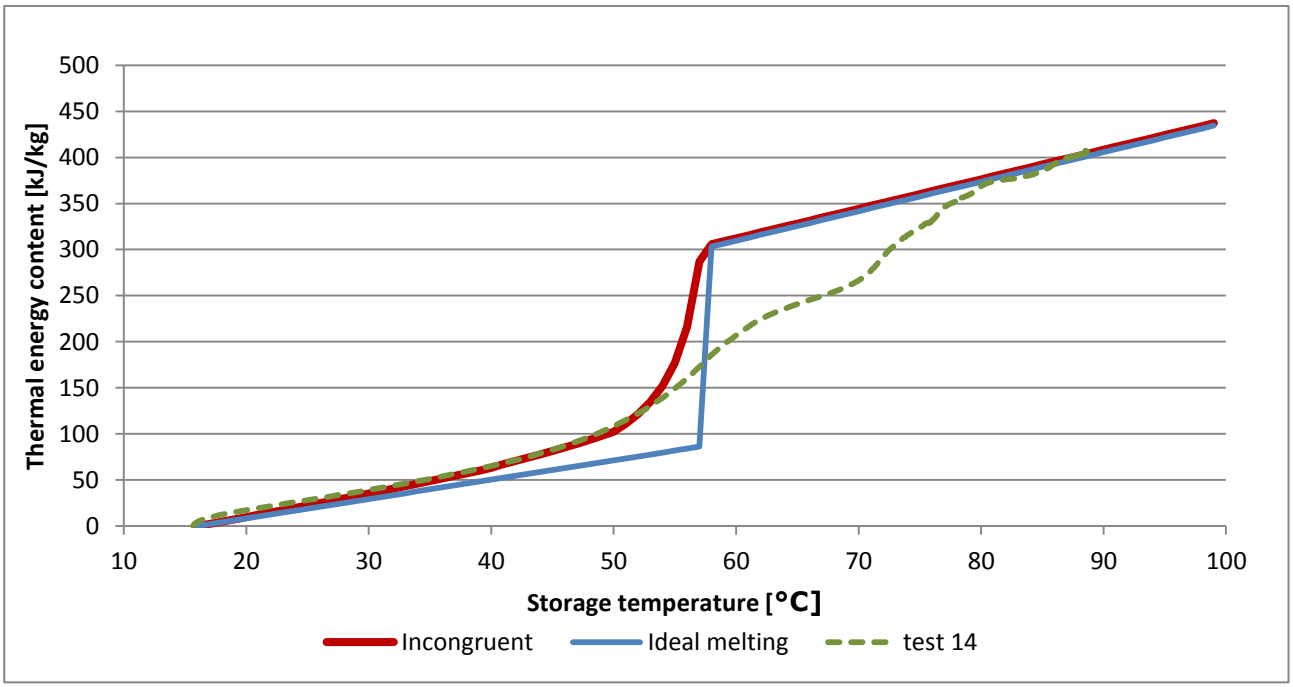

Figure 36. Measured and theoretical energy content of salt water mixture in storage module.

Test cycle 15:

In test cycle 15 the module was charged for 70 hours with a flow rate of 7.4 l/min with an inlet temperature of 90°C. The module was actively discharge to supercooled state where it was stable for 26 hours before manually activated by shaking the module. Fig. 37 shows the process and development of this test cycle.

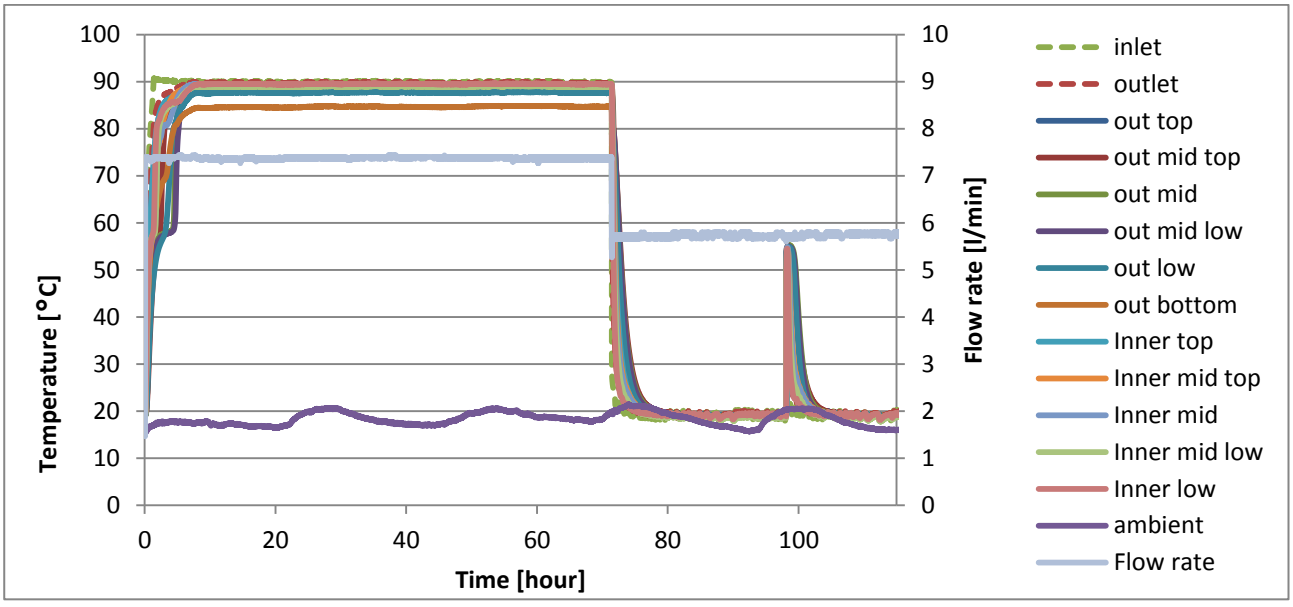

Figure 37. Temperature development over time and flow rate for test cycle 15.

For charge and discharge to supercooled state the measured energy content was coherent with the theoretical energy content but the energy released from the activation is approximately 21 % lower than the theoretical energy content as may be seen in Fig. 38

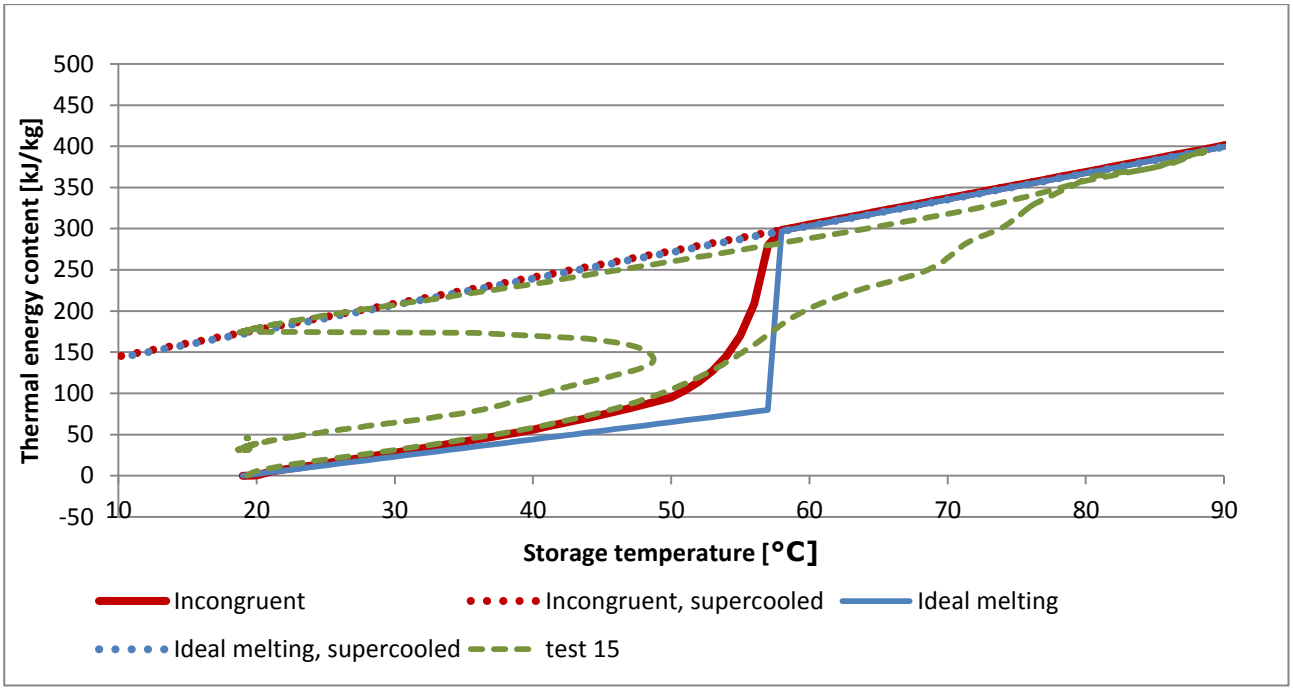

Figure 38. Measured and theoretical energy content of salt water mixture in storage module.

Test cycle 16:

The storage module was charged for 22 hours with a flow rate of 7.4 l/min and an inlet temperature of 90°C. The module was actively discharged. Crystallization started spontaneously during discharge. Fig. 37 shows the process and development of this test cycle.

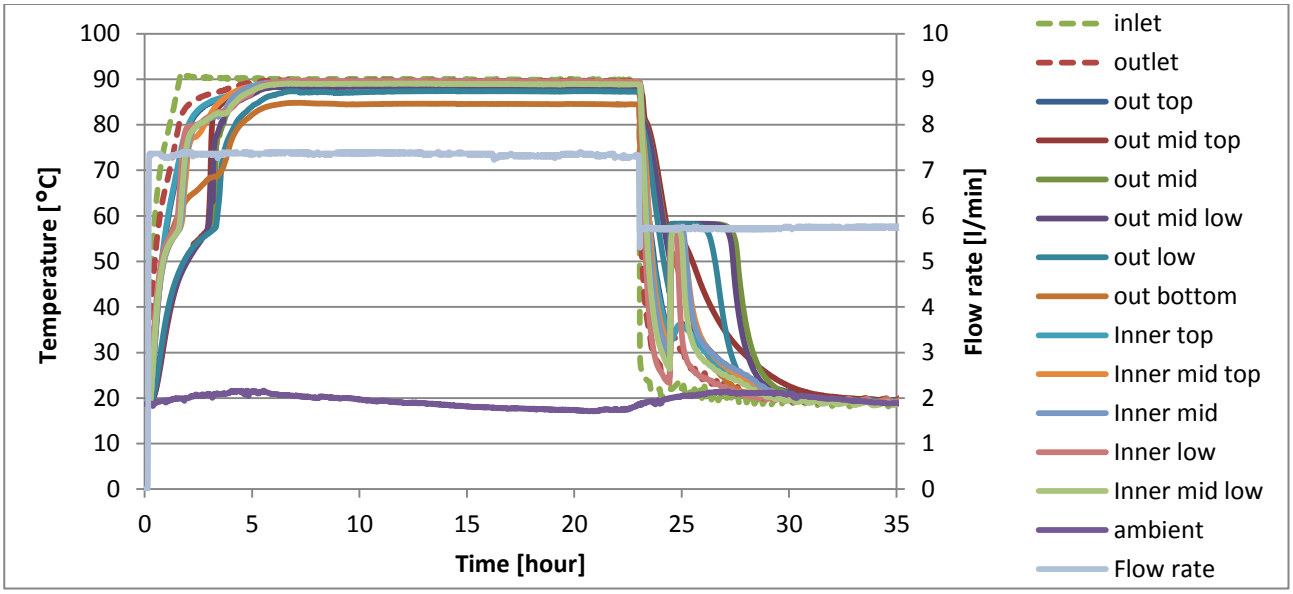

Figure 39. Temperature development over time and flow rate for test cycle 16.

The measured thermal energy charged to the storage module was approximately 26 kJ/kg or 6% lower than the theoretical energy content. For this test cycle 15 kJ//kg more energy is released form the discharge compared to the charge as may be seen in Fig. 40.

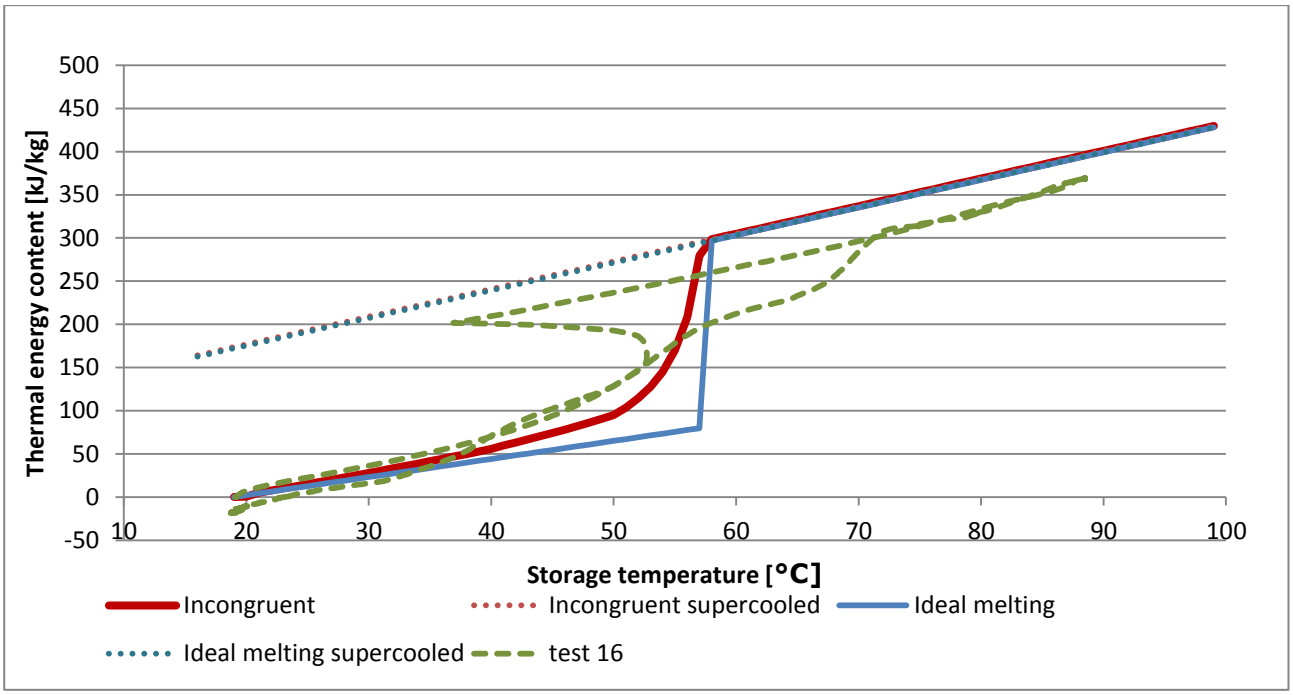

Figure 40. Measured and theoretical energy content of salt water mixture in storage module.

Test cycle 17:

The storage module was charge for 6.5 hours with a flow rate of 7.4 l/min with an inlet temperature of 90°C. The module was actively discharged with a flow rate of 5.7 l/min. Crystallization started spontaneously during discharge. Fig. 37 shows the process and development of this test cycle.

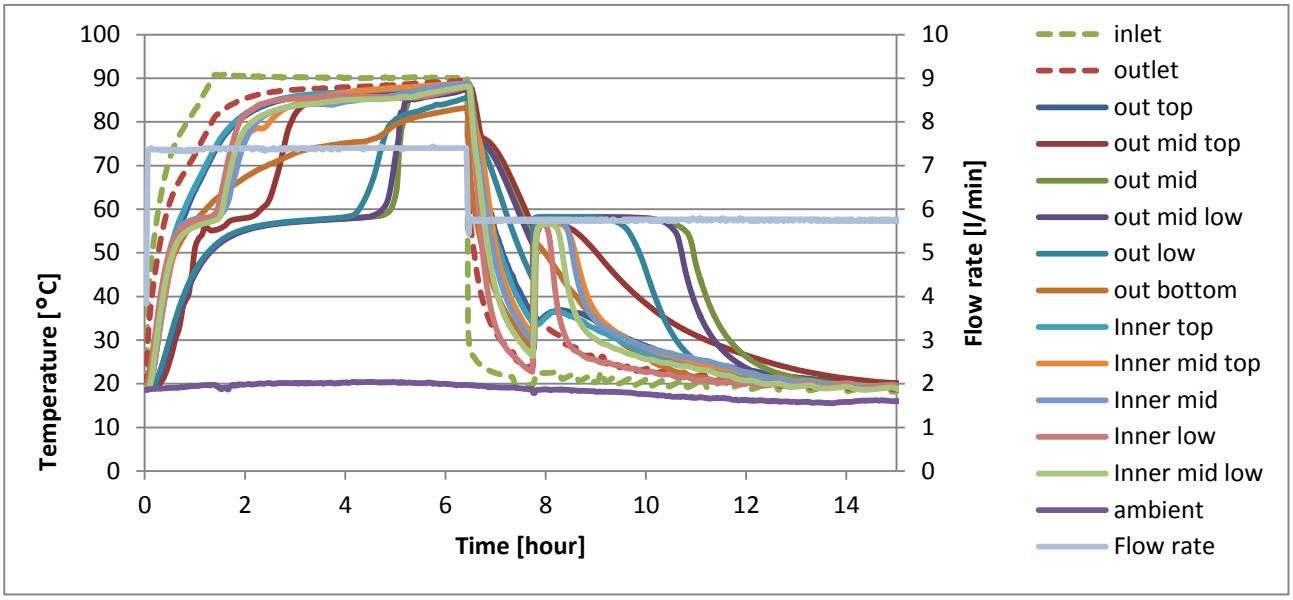

Figure 41. Temperature development over time and flow rate for test cycle 17.

Measured and theoretical energy content was coherent for test cycle 17 as may be seen in Fig. 42.

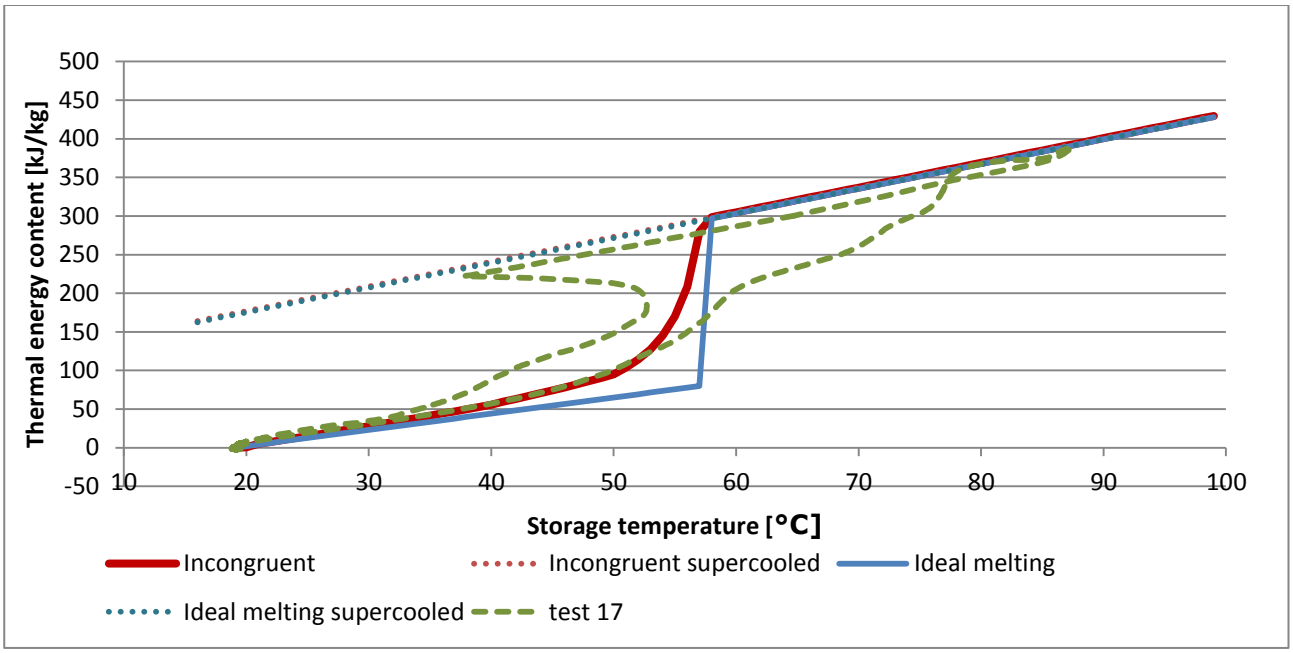

Figure 42. Measured and theoretical energy content of salt water mixture in storage module.

Tests have been carried out to investigate the thermal storage performance of the Thermobatterie developed by H.M. Heizkörper GmbH & Co. KG. The storage utilizes the principle of stable super-cooling of a sodium acetate water mixture for long term heat storage. The tests showed unstable supercooling with spontaneous activation in about half of the test cycles. The thermal energy released from the activated supercooled sodium acetate water mixture was close to the theoretical thermal energy content in the first cycle but was reduced over repeated cycles by up to 20 % in the 15th cycle due to phase separation.

DTU Civil Engineering
Department of Civil Engineering
Technical University of Denmark

Brovej, Building 118
2800 Kgs. Lyngby
Telephone 45 25 17 00

www.byg.dtu.dk

ISBN 9788778773968
ISSN 1601-2917